

University of Nebraska - Lincoln

DigitalCommons@University of Nebraska - Lincoln

Theses, Dissertations, and Student Research from
Electrical & Computer Engineering

Electrical & Computer Engineering, Department of

12-2016

DESIGN AND IMPLEMENTATION OF RECONFIGURABLE PATCH ANTENNAS FOR WIRELESS COMMUNICATIONS

Fei He

University of Nebraska-Lincoln, hefei29000@gmail.com

Follow this and additional works at: <http://digitalcommons.unl.edu/elecengtheses>



Part of the [Electrical and Electronics Commons](#), and the [Systems and Communications Commons](#)

He, Fei, "DESIGN AND IMPLEMENTATION OF RECONFIGURABLE PATCH ANTENNAS FOR WIRELESS COMMUNICATIONS" (2016). *Theses, Dissertations, and Student Research from Electrical & Computer Engineering*. 75.
<http://digitalcommons.unl.edu/elecengtheses/75>

This Article is brought to you for free and open access by the Electrical & Computer Engineering, Department of at DigitalCommons@University of Nebraska - Lincoln. It has been accepted for inclusion in Theses, Dissertations, and Student Research from Electrical & Computer Engineering by an authorized administrator of DigitalCommons@University of Nebraska - Lincoln.

DESIGN AND IMPLEMENTATION OF RECONFIGURABLE PATCH
ANTENNAS FOR WIRELESS COMMUNICATIONS

by

FEI HE

A THESIS

Presented to the Faculty of

The Graduate College at the University of Nebraska

In Partial Fulfillment of Requirements

For the Degree of Master of Science

Major: Telecommunications Engineering

Under the Supervision of Professor Yaoqing Yang

Lincoln, Nebraska

December, 2016

DESIGN AND IMPLEMENTATION OF RECONFIGURABLE PATCH ANTENNAS FOR WIRELESS COMMUNICATIONS

Fei He, M.S.

University of Nebraska, 2016

Advisor: Yaoqing Yang

Reconfigurable patch antennas have drawn a lot of research interest for future wireless communication systems due to their ability to adapt to changes of environmental conditions or system requirements. The features of reconfigurable patch antennas, such as enhanced bandwidths, operating frequencies, polarizations, radiation patterns, etc., enables accommodation of multiple wireless services.

The major objective of this study was to design, fabricate and test two kinds of novel reconfigurable antennas: a dual-frequency antenna array with multiple pattern reconfigurabilities, and a pattern and frequency reconfigurable Yagi-Uda patch antenna. Comprehensive parametric studies were carried out to determine how to design these proposed patch antennas based on their materials dimensions and their geometry. Simulations have been conducted using Advanced Design Systems (ADS) software. As a result of this study, two kinds of novel reconfigurable patch antennas have been designed and validated at the expected frequency bands.

For the new reconfigurable antenna array, the beam pattern selectivity can be obtained by utilizing a switchable feeding network and the structure of the truncated corners. Opposite corners have been slotted on each patch, and a diode on each slot is used for switchable patterns. By controlling the states of the four PIN diodes through the

corresponding DC voltage source, the radiation pattern can be reconfigured. The simulation and measurement results agree well with each other.

For the novel frequency and pattern reconfigurable Yagi-Uda patch antenna detailed in Chapter 4, two slots have been used on driven element to achieve frequency and pattern reconfigurability, and two open-end stubs have been used to adjust working frequency and increase bandwidth. In this design, an ideal model was used to imitate a PIN diode. The absence and presence of a small metal piece has been used to imitate the off-state and on-state of the PIN-diode. Pattern reconfigurability and directivities with an overall 8.1dBi has been achieved on both operating frequencies. The simulation and measurement results agree closely with each other.

Acknowledgments

First of all, I would like to express my sincere thanks and gratitude to Dr. Yaoqing Yang, my advisor and thesis chair, for useful comments, guidance and continuous support through my whole M.S. program. He helped me a lot in all the time of research and writing of this thesis. I could not have imagined having a better advisor and mentor for my M.S study. Besides my advisor, I would like to thank other committee members, Dr. Hamid Sharif, and Dr. Andrew Harms, for their valuable recommendations, encouragement, and hard questions. Deep gratitude goes to my beloved parents, for giving birth to me at the first place, for their continuous encouragement, support and love throughout my life. Last but not the least, I wish to thank my friends in China and United States for all the useful helps and for all the fun during my MS study.

Contents

Chapter 1. Introduction to Reconfigurable Patch Antennas.....	1
1.1 Introduction.....	1
1.2 Objectives	5
1.3 Outline of the Thesis.....	6
Chapter 2. Theory of Microstrip Patch Antenna.....	7
2.1 Introduction.....	7
2.2 Basic Characteristics of a Microstrip Patch Antenna.....	7
2.2.1 Radiation Pattern of a Patch Antenna	11
2.2.2 Polarization of a Patch Antenna.....	12
2.2.3 Bandwidth of a Patch Antenna.....	13
2.3 Feeding Method	13
2.4 Method of Analysis.....	15
2.4.1 Fringing Effects	16
2.4.2 Effective Length and Resonant Frequency	17
2.4.3 Effective Width.....	19
Chapter 3. A Proposed Novel Dual-Frequency Array Antenna with Multiple Pattern Reconfigurabilities.....	21
3.1 Introduction.....	21
3.2 Basic single patch antenna design.....	21
3.3 Dual-frequency pattern reconfigurable antenna array design	26
3.3.1 Switchable feeding network.....	26
3.3.2 Antenna array design	27
3.4 Fabrication and measurement of proposed antenna array.....	43
3.4 Summary	47
Chapter 4. A Proposed Pattern and Frequency Reconfigurable Yagi-Uda Patch Antenna.....	48
4.1 Introduction.....	48
4.2 Design of the Proposed Reconfigurable Yagi-Uda Patch Antenna.....	49
4.2.1 Antenna Schematic	49
4.2.2 Design of Proposed Frequency Reconfigurable Antenna	51
4.2.3 Pattern reconfigurable of proposed Yagi-Uda antenna.....	68
4.2.4 Using of stubs for 2.41GHz	74
4.3 Fabrications and Measurements of the Proposed Reconfigurable Yagi-Uda patch Antenna	78

4.4 Discussions	86
4.5 Summary of the Proposed Yagi-Uda Antenna.....	93
Chapter 5. Conclusions	94
References.....	96

List of Figures

Figure 2.1: Microstrip antenna.....	9
Figure 2.2: Different shapes of patch antenna.....	10
Figure 2.3: Radiation pattern for half-wave square patch antenna.....	11
Figure 2.4: The nearly square antenna for circular polarization.....	13
Figure 2.5: Typical feeds for microstrip antennas.....	14
Figure 2.6: Microstrip antenna and its electric filed lines.....	16
Figure 2.7: Physical and effective lengths of rectangular microstrip patch antenna.....	19
Figure 3.1: Layout simulation for Basic Antennas.....	24
Figure 3.2: Return loss for two basic antenna elements.....	25
Figure 3.3: Schematic of a single-feed switchable feed network.....	26
Figure 3.4: Geometry of built array antenna.....	27
Figure 3.5: Configuration (a): Basic antenna array with short lines of a quarter waveguide length.....	29
Figure 3.6: Configuration (b): Antenna array with short lines of a quarter waveguide length and truncated corners on 1.92GHz antenna element.....	29
Figure 3.7: Configuration (c): Antenna array with short lines of a quarter waveguide length and truncated corners on 2.11GHz antenna element.....	30
Figure 3.8: Configuration (d): Antenna array with short lines of a quarter waveguide length and truncated corners on both antenna elements.....	30
Figure 3.9: Simulated surface current distribution at 1.92 GHz for configuration (d).....	31
Figure 3.10: Simulated surface current distribution at 2.11 GHz for configuration (d).....	31

Figure 3.11: Axial Ratio for antenna array of Configuration (d) at working frequency of 1.92 GHz (left) and 2.11 GHz (right).....	32
Figure 3.12: Return loss for configuration (d)	32
Figure 3.13: Configuration (d) with additional ports.....	33
Figure 3.14: Detail of two additional added ports.....	34
Figure 3.15: Creating a new EM Model.....	35
Figure 3.16: Introduce new EM Model to schematic design.....	35
Figure 3.17: A pin-diode that has been added to the schematic simulation.....	36
Figure 3.18: Co-simulation for configuration (d) with all pin-diodes at off-state.....	36
Figure 3.19: Return loss of Co-simulation for configuration (d) with all pin-diodes at off-state.....	37
Figure 3.20: Co-simulation for configuration (d) with all pin-diodes at on-state.....	37
Figure 3.21: Detail of DC voltage.....	38
Figure 3.22: Return loss of Co-simulation for configuration (d) with all pin-diodes at on-state.....	38
Figure 3.23: Return loss for the antenna array when operating in different configurations in simulation.....	40
Figure 3.24 (1) (2): The simulated radiation pattern of Configuration (a) and Configuration (d).....	41
Figure 3.25: T tech mill machine used to fabricate proposed antenna array.....	43
Figure 3.26: Photograph of the proposed antenna array.....	44
Figure 3.27: Agilent network analyzer used to measure the proposed antenna array.....	44

Figure 3.28: Comparison of measured return losses of configuration (d) with and without PIN diodes.....	46
Figure 3.29: Return loss for the antenna array in different working Configurations between simulation and measurement.....	46
Figure 4.1: Geometry of Proposed Reconfigurable Yagi-Uda Patch Antenna.....	50
Figure 4.2: The geometry of a patch antenna with a switchable slot.....	52
Figure 4.3 (a): Relative electric currents on the patch antennas at their resonant frequencies with the switch OFF.....	53
Figure 4.3 (b): Relative electric currents on the patch antennas at their resonant frequencies with the switch ON.....	53
Figure 4.4: Layout design for the patch antenna with resonant frequency at 2.495GHz..	54
Figure 4.5: Return loss of the proposed 2.495GHz single patch antenna.....	54
Figure 4.6: Basic antenna design with a slot.....	55
Figure 4.7: Return loss of a basic patch antenna with a slot.....	55
Figure 4.8: Basic antenna design with a metal piece in the center of slot.....	56
Figure 4.9: Return loss of a basic patch antenna with a metal piece in the center of slot.	56
Figure 4.10: Basic patch antenna with parasitic elements.....	58
Figure 4.11: Return loss of the antenna proposed in Figure 4.10.....	59
Figure 4.12: Antenna proposed in Figure 4.8 with increased-size director elements.....	59
Figure 4.13: Return loss of antenna proposed in Figure 4.10.....	60
Figure 4.14: Antenna proposed in Figure 4.8 with increased-size reflector elements.....	61
Figure 4.15: Return loss of antenna proposed in Figure 4.12.....	61

Figure 4.16: Geometry of Proposed Reconfigurable Yagi-Uda Patch Antenna.....	63
Figure 4.17: Layout simulation for proposed antenna with four metal pieces.....	64
Figure 4.18: Simulated return loss for proposed antenna with four metal pieces.....	64
Figure 4.19: Layout simulation for proposed antenna without four metal pieces.....	65
Figure 4.20: Simulated return loss for proposed antenna without four metal pieces.....	66
Figure 4.21: Surface Current Distribution for Antenna Working at 2.41 GHz.....	67
Figure 4.22: Surface Current Distribution for Antenna Working at 1.90 GHz.....	67
Figure 4.23: Early design of the proposed 2.41 GHz antenna.....	68
Figure 4.24: Return loss of early 2.41 GHz design.....	69
Figure 4.25: Pattern for the early 2.41 GHz design.....	69
Figure 4.26: Early design of the proposed 1.90 GHz antenna.....	70
Figure 4.27: Return loss of early 1.90 GHz design.....	70
Figure 4.28: Pattern for the early 1.90 GHz design.....	71
Figure 4.29: Radiation patterns of 2.41 GHz and 1.90 GHz for proposed antenna.....	72
Figure 4.30: Radiation intensity for two working frequencies.....	73
Figure 4.31: Stub connected to driven element by using metal piece at 2.41GHz	75
Figure 4.32: Stub disconnected to driven element at 1.90 GHz.....	75
Figure 4.33: Return loss for proposed antenna working at 2.41GHz	76
Figure 4.34: Without two pieces of metal used to connect stubs and driven element.....	76
Figure 4.35: Return loss for proposed antenna with 2 metal pieces that used to connect stubs and driven pieces have been removed.....	77
Figure 4.36: The T Tech mill machine used to build the proposed antenna.....	78

Figure 4.37: The T Tech mill machine controlled by a computer.....	79
Figure 4.38: Milling device of T Tech Mill Machine	79
Figure 4.39: Antenna layout structure in control software of mill machine.....	80
Figure 4.40: Antenna layout structure with a new added outline.....	80
Figure 4.41: Prototype of the proposed 1.90GHz Yagi-Uda patch antenna.....	81
Figure 4.42: Measurement of prototype 1.90GHz Yagi-Uda patch antenna (1).....	82
Figure 4.43: Measurement of prototype 1.90GHz Yagi-Uda patch antenna (2).....	82
Figure 4.44: Measurement result for 1.90GHz Yagi-Uda patch antenna.....	83
Figure 4.45: Prototype of the proposed 2.41GHz Yagi-Uda Patch Antenna.....	83
Figure 4.46: Measurement of the prototype 2.41GHz Yagi-Uda patch antenna (1).....	84
Figure 4.47: Measurement of the prototype 2.41GHz Yagi-Uda patch antenna (2).....	84
Figure 4.48: Measurement result for 2.41 GHz Yagi-Uda patch antenna.....	85
Figure 4.49: Simulation and Measurement results for proposed antenna without all four metal pieces (Design working frequency is 1.90 GHz).....	86
Figure 4.50: Simulation and Measurement results for proposed antenna with all four metal pieces (Design working frequency is 2.41 GHz).....	87
Figure 4.51: The layout structure for proposed antenna.....	88
Figure 4.52: The proposed antenna with the metal piece loaded in the right slot has been moved up 1mm.....	88
Figure 4.53: The resonant point shift to 2.434 GHz based on the change has been made in figure 4.52.....	89
Figure 4.54: The proposed antenna with the metal piece loaded in the right slot has been moved down for 1mm.....	90

Figure 4.55: The resonant point shift to 2.385 GHz based on the change has been made in figure 4.54.....	90
Figure 4.56: The proposed antenna with the height of metal pieces loaded in slots has been increased by 0.2 mm.....	91
Figure 4.57: The resonant point shift to 2.424 GHz based on the change has been made in figure 4.56.....	91
Figure 4.58: The proposed antenna with the height of metal pieces loaded in slots has been decreased by 0.2 mm.....	92
Figure 4.59: The resonant point shift to 2.393 GHz based on the change has been made in figure 4.58.....	92

Chapter 1. Introduction to Reconfigurable Patch Antennas

1.1 Introduction

Patch antennas are widely used today. They are used for satellite communications and various military purposes such as GPS, mobile, missile systems, etc., due to their light weight, simple structure and easy implementation. The main advantages of patch antennas are as follows:

- (1) Low cost to fabricate.
- (2) Easy to manufacture.
- (3) Efficient radiation.
- (4) Support both linear and circular polarization.
- (5) Light weight.
- (6) Integrate easily with microwave integration circuits.

The increasing demand for modern mobile, satellite and wireless communication systems have driven many researchers to work on improving performance and enhancing applications of patch antennas. Reconfigurable antennas have drawn much attention for future wireless communication systems due to their ability to modify their geometry to adapt to changes in environmental conditions or system requirements such as enhanced bandwidths, operating frequencies, polarizations, radiation patterns, etc. [1]. Microstrip antenna is one of the most popular choices in designing the reconfigurable antenna because of their advantages we introduced above. Reconfigurable antennas can be roughly classified into three main types: reconfigurable frequency, reconfigurable polarization and reconfigurable radiation pattern antennas. Usually, a reconfigurable antenna is realized by

using many kinds of RF switches, such as PIN diodes, Micro-electro-mechanical systems (MEMs) and GaAs field-effect transistors (GaAs FETs).

A reconfigurable radiation pattern antenna reduces the effects of noisy environments by changing the null positions, and it saves energy by adjusting the main beam signal towards the intended user to improve the overall system performance. In [2], a single-feed switchable feed network, which replaces the traditional PIN diode or MEM, was used to obtain pattern diversity. In [3], a wide-band L-probe circular patch antenna was presented with dual feeds and an integrated matching network with switches. In order to reconfigure the radiation pattern electrically, the structure of this matching system is relatively complex. In [4], the method of switching load to reconfigure the pattern of antenna is used. A MEMs-switched parasitic antenna array providing radiation pattern diversity with a novel modeling method was proposed in [5]. A novel equilateral triangular patch antenna with two diverse patterns working at nearly the same resonant frequency was proposed in [6]. In [7], a pattern reconfigurable antenna based on a two-element dipole array model with a new structure is introduced by this author. In [8], they explored a very compact planar radiation pattern reconfigurable antenna using metasurface. In [9], they proposed a compact, low-profile, high impedance surface (HIS)-based, pattern reconfigurable antenna generating a broad and tilted beam. In [10], a new method to reconfigure the radiation pattern of a simple circular patch antenna with shorting pins located at the edge of the patch was presented. Genetic Algorithm (GA) and Finite Element software was used to simulate and optimize the impact of the shorting pins on this antenna.

Compared to traditional broadband antennas, frequency reconfigurable antennas have a relatively smaller size and higher isolation [11]. In [12], a frequency reconfigurable patch

was proposed that used 19 reed switches, which replace bias and control circuits, to connect the patch with the ground plane. [13] was introduced a compact frequency-reconfigurable patch antenna capable of switching between three operating bands, with the feature of shorting load. In [14] frequency agility was achieved by integrating a varactor diode between the patch and the ground to make a frequency reconfigurable antenna. This method also reduced the antenna size. Presented in [15] was a frequency reconfigurable microstrip patch antenna using Defected Ground Structure (DGS) with aperture coupled feed line. In [16], a multilayer frequency reconfigurable patch antenna for high frequency was proposed. In [17], a novel frequency-reconfigurable antenna based on a circular monopole patch antenna was presented. The proposed antenna consists of a center-fed circular patch and four sector-shaped patches surrounding it. By controlling eight varactor diodes, which are introduced to bridge the gaps between the circular patch and the sector-shaped patches, different working frequencies can be achieved. A novel design of frequency-reconfigurable antenna by using an aperture-coupled feeding technique and stacked patch structure was introduced [18]. An octagonal-shaped frequency reconfigurable patch antenna was designed and studied in [19]. In this antenna design, open ended L-slots have been used on both sides of the patch and four PIN diodes are used for the operation of this antenna. In [20] is a design for a frequency reconfigurable antenna with conical-beam radiation. The design is based on a coplanar annular-ring microstrip antenna that works on the TM_{02} mode, and several shorting strips that are symmetrically placed along the circumference of the radiating patch and are used to vary its resonant frequency.

Polarization reconfigurable antennas have drawn increasing attention because they have some desirable advantages for modern wireless communications, such as avoiding fading loss caused by multipath effects in wireless local area networks, providing a powerful modulation scheme in active read/write microwave tagging systems, realizing frequency reuse to expand the capability in satellite communication systems, and being a suitable candidate in multiple-input-multiple-output (MIMO) systems [21]. The study in [22] proposed a polarization reconfigurable patch antenna with polarization states that can be switched among linear polarization (LP), left-hand (LH) and right hand (RH) circular polarizations (CPs). The CP waves of this antenna are caused by two perturbation elements of loop slots in the ground plane. In [23], a new polarization reconfigurable-agile antenna, which is based on a quad-mode reconfigurable feeding network with four dynamic transmission modes, was proposed. This antenna can be switched between four different polarizations. [24] introduced a new quadri-polarization reconfigurable circular patch antenna which is composed of a circular radiating patch and a switchable feed network. A stub-loaded microstrip patch antenna with both frequency and polarization selectivity was proposed in [25].

We will focus on pattern and frequency reconfigurable antennas in this thesis. There is a developmental trend in wireless communication systems that requires the use of antennas capable of accessing services in various frequency bands, sometimes with the use of a single antenna. So far, most of the reported pattern reconfigurable antennas can only switch the beam in a limited range. And there are few antenna designs concerned with both radiation pattern and dual-frequency. A pattern reconfigurable antenna that has multiband characteristics improves the whole system performance.

1.2 Objectives

The objective of this thesis is to design, fabrication and testing of two different reconfigurable patch antennas.

The first antenna proposed in this thesis is a novel dual-frequency antenna array with multiple pattern diversities. The desired resonant frequencies of two microstrip patch antenna elements are 1.92 GHz and 2.11 GHz, respectively. These frequencies can be used in wideband code division multiple access (WCDMA) communication systems. According to [2], a single-feed switchable feed network can be used as a basic beam pattern reconfigurable antenna system, and it also introduced dual-frequency features of the antenna system. We use the structure demonstrated in [26] to create more pattern selectivity and investigate the impact of this structure on the pattern of the antenna array. This array antenna has been constructed on a RO4350B substrate with 1.52-mm thickness that has a dielectric constant of 3.48 and size 208mm ×135mm.

The second antenna proposed in this thesis is a pattern and frequency reconfigurable Yagi-Uda patch antenna. The proposed working frequencies for this antenna are 1.90 GHz and 2.41 GHz. which are suitable for LTE and Wi-Fi networks, respectively. The proposed Yagi-Uda patch antenna consists of two reflectors, a driven element and six director elements. The reflector elements and director elements are tuned properly in frequency compared to the driven element when using ADS. Two slots were used in the driven element to introduce frequency and pattern reconfigurabilities to this antenna system. Two stubs, which were used to improve the return loss performance and adjust working frequency, were connected to the driven element when working in the 2.41GHz mode. Four metal pieces were used to imitate PIN-diodes in simulation and measurement. In order to

validate the effectiveness of our design, we built two antennas – one with and one without these metal pieces (2.41GHz mode and 1.90 GHz mode, respectively). The two antennas with different modes were fabricated on RO4350B substrate with 1.52-mm thickness. The measured and simulated results agree very well.

The proposed antennas were simulated using Advanced Design System [ADS], and fabricated using a new model of a T Tech Mill machine. Aglient network Analyzer is used to measure the return losses of proposed antennas.

1.3 Outline of the Thesis

This thesis consists of five chapters. The overview of each chapter follows.

Chapter 1: Provides the introduction, motivation and objective of this master thesis and includes the literature review on reconfigurable patch antennas.

Chapter 2: Presents the fundamentals of Microstrip Patch Antennas (MSAs), including the fundamental geometries and characteristics of the MSA, feeding technology, and the methods of analysis used for the MSA design.

Chapter 3: Presents the design, fabrication and testing of a novel dual-frequency patch array antenna with multiple pattern reconfigurabilities. The beam pattern selectivity can be obtained by utilizing a switchable feeding network and the special structure used in this array antenna. There are two opposite corners which have been slotted on each patch and a diode on the slot which is used as a switch to control multiple patterns. By controlling four PIN diodes through the corresponding DC voltage source, the radiation pattern can be changed. The simulation and measurement results agree nearly with each other.

Chapter 4: Presents the design, fabrication and testing of a novel pattern and frequency reconfigurable Yagi-Uda patch antenna. This Yagi-Uda patch antenna consists of two

reflectors, a driven element and six director elements. The reflector elements and director elements are tuned properly in frequency compared to the driven element. Two slots were used in the driven element to introduce frequency and pattern selectivity to this antenna system. Two stubs have been connected to the driven element when it's working in 2.41 GHz so as to improve the returnloss performance and adjust working frequency. The simulated and measured return loss results agree nearly with each other.

Chapter 5: Presents the conclusions of this thesis.

Chapter 2. Theory of Microstrip Patch Antenna

2.1 Introduction

Low profile antennas have drawn much attention because they are suitable for high-performance aircraft, spacecraft and satellite and missile applications, where size, weight, cost, performance, ease of installation, and aerodynamic profile are significant constraints. For today's rapidly-developing mobile or personal communication devices, there exists same need for compact and low profile antennas. Microstrip antennas (also referred to as patch antennas or microstrip patch antennas) can be used in a wide range of applications from commercial communication systems to satellites, and even biomedical applications [27]. Chapter 14 of *Antenna Theory: Analysis and Design* [27] contributes greatly to the fundamentals of patch antenna addressed in this chapter of the thesis.

2.2 Basic Characteristics of a Microstrip Patch Antenna

The history of patch antenna can be traced back to 1953, when G.A. Deschamps first proposed this kind of antenna. However, patch antennas didn't become practical until the

1970s. In that time, it was developed further by researchers such as Robert E. Munson and others by using low-loss soft substrate materials that were just becoming available during that time.

Based on [27], a microstrip antenna (Patch antenna), as shown in Figure 2.1, normally consists of a very thin ($t \ll \lambda_0$ where λ_0 is the free-space wavelength) metallic patch placed a small fraction of a wavelength ($h \ll \lambda_0$, usually $0.003\lambda_0 \leq h \leq 0.05\lambda_0$) above a ground plane. The distance between the patch and the ground plane – the substrate or dielectric height h – determines the bandwidth of antenna. A relatively thicker substrate can increase the gain, but it may result in some undesired effects such as surface wave excitation. Surface waves can decrease efficiency and perturb the radiation pattern. The patch antenna is designed so its pattern maximum is normal to the patch (broadside radiator). This is accomplished by properly choosing the mode (field configuration) of excitation beneath the patch. In general, modes are designated as TM_{nmp} . The ‘p’ value is mostly omitted because the electric field variation is considered negligible in the z-axis since only a phase variation exists in the z axis. So, TM_{nm} represents the field variations in the x and y directions. The field variation in the y direction (impedance width direction) is negligible and so m is considered 0. The field has one minimum-to-maximum variation in the x direction (resonance length direction and a half-wave long), thus n is 1 in this case, and we say that this patch operates in the TM_{10} mode [28].

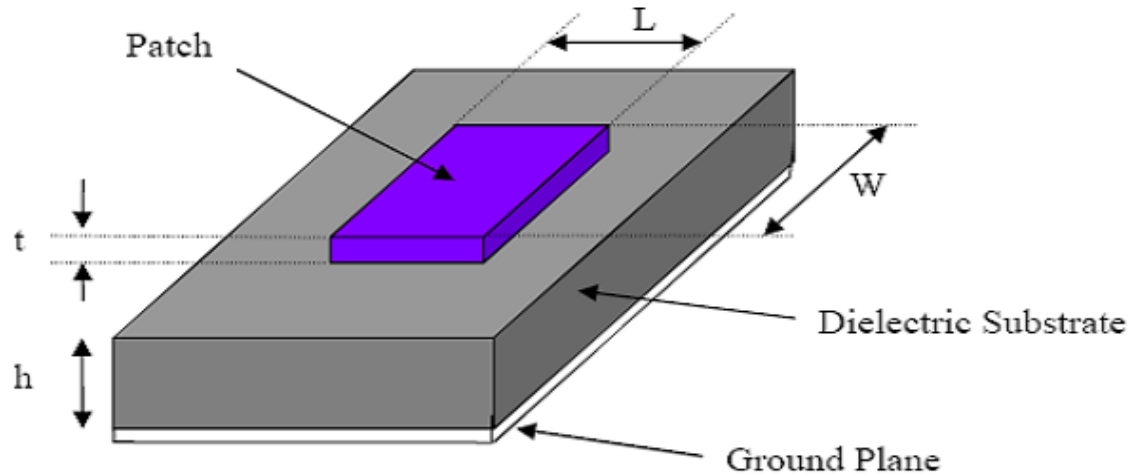


Figure 2.1 Microstrip antenna

For a rectangular patch, the length L of the element is usually $\frac{\lambda_0}{3} < h < \frac{\lambda_0}{2}$. The patch and the ground are separated by a dielectric sheet (usually referred to as the substrate), also as shown in Figure 2.1.

There are numerous substrates that can be used for the design of microstrip antennas, and their dielectric constants, ϵ_r , are usually in the range of $2.2 \leq \epsilon_r \leq 12$. The most desirable ones for antenna performance are thick substrates with dielectric constants at the lower end of the range because they provide better efficiency, larger bandwidth, and loosely bound fields for radiation into space, but at the cost of large element size [29]. Thin substrate with higher dielectric constants are suitable for microwave circuitry because they require tightly bound fields to minimize undesired radiation and coupling, and result in smaller element size. However, they are less efficient and have a relatively smaller bandwidth because of their great losses [29]. Since microstrip antennas are often integrated with other microwave circuits, a compromise has to be made between good antenna performance and circuit design.

Basically, microstrip antennas are also referred to as patch antenna. Usually, the radiating elements and feed lines of microstrip antennas are photoetched on the dielectric substrate. The radiating patch is generally made of conducting material such as copper or gold and can be any possible shape, such as rectangular, thin strip (dipole), circular, elliptical, triangular, etc. These and others are illustrated in Figure 2.2. Among the possible shapes, the square, rectangular, dipole, and circular are the most common because they are easy to analyze and fabricate. As well, they have other attractive characteristics, especially low cross-polarization radiation. Microstrip dipoles are attractive because they inherently possess a larger bandwidth and occupy less space, which makes them very suitable for arrays [30], [31], [32], [33]. Linear and circular polarization patch antennas can be obtained with either single elements or arrays of microstrip antennas. An array of microstrip elements, with single or multiple feeds, can also be used to introduce scanning capabilities and achieve greater directivities.

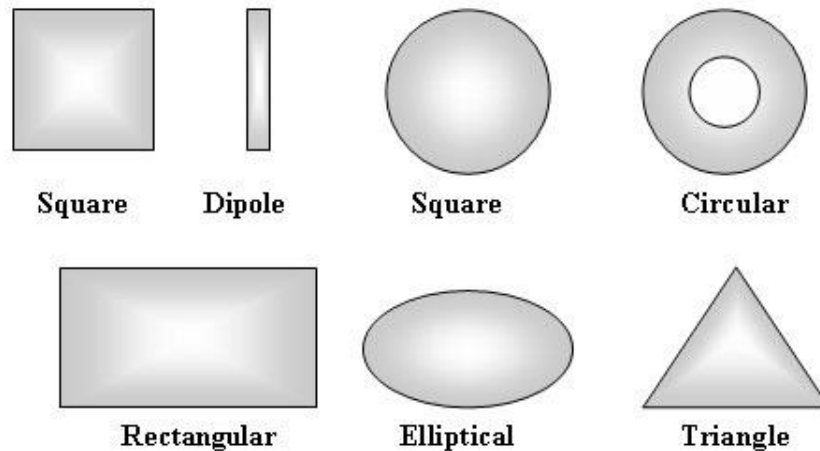


Figure 2.2 Different shapes of patch antenna

2.2.1 Radiation Pattern of a Patch Antenna

A patch antenna radiates energy in certain directions and we say that the antenna has directivity (usually expressed in dBi). So far, the directivity usually has been defined relative to an isotropic radiator. An isotropic radiator emits an equal amount of power in all directions and it has no directivity. If the antenna has a 100% radiation efficiency (meaning the energy delivered to the antenna can be 100% radiated from antenna), all directivity would be converted to gain. The typical rectangular patch excited in its fundamental mode has a maximum directivity in the direction perpendicular to the patch (z-axis). The directivity decreases when moving away from zenith direction towards lower elevations. Figure 2.3 shows a typical radiation pattern for half-wave square patch antenna [28].

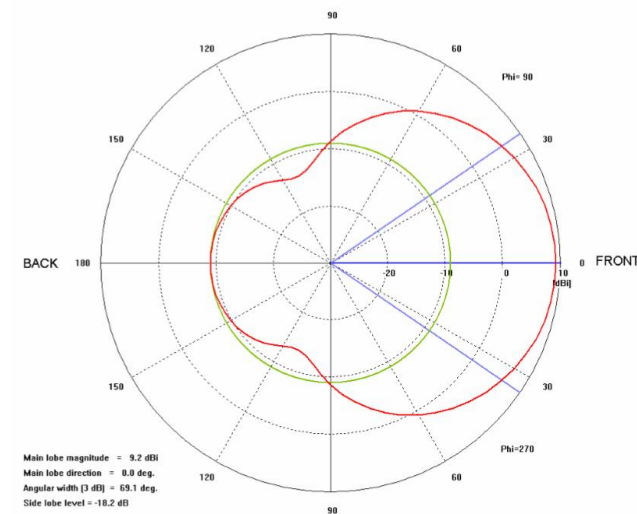


Figure 2.3 Radiation pattern for half-wave square patch antenna [28]

2.2.2 Polarization of a Patch Antenna

The plane in which the electric field varies is also known as the polarization plane. The basic patch antenna is linearly polarized since the electric field varies in only one direction. However, a large number of applications such as satellite communications, do not work well with linear polarization because, due to the moving antenna platform, the relative orientation of the antenna is unknown. In these applications, circular polarization is useful since it is not sensitive to antenna orientation. Basic antennas do not generate circular polarization; hence some changes have to be made to the patch antenna to enable it to generate circular polarization. For a circularly polarized patch antenna, the electric field varies in two orthogonal planes (x and y directions) with the same magnitude but a 90° phase difference, as shown in Figure 2.4. Necessary to generate circular polarization for a patch antenna is the simultaneous excitation of two modes, i.e. the TM₁₀ mode (x direction) and the TM₀₁ mode (y direction). One of the modes is excited with a 90° phase delay to the other mode. A circularly polarized antenna can either be right-hand circular polarized (RHCP) or left-hand circular polarized (LHCP). The antenna is RHCP when the phases are 0° and -90° for the antenna in Figure 2.4, and the signal radiates towards the reader. It is LHCP when the phases are 0° and $+90^\circ$, and the signal radiates away [28].

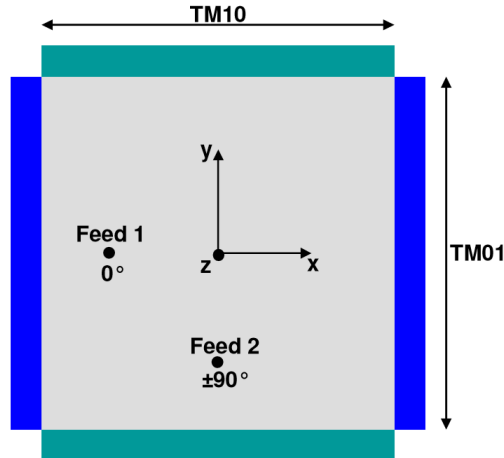


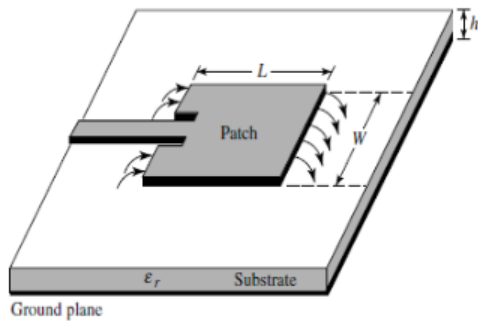
Figure 2.4 The nearly square antenna for circular polarization [28]

2.2.3 Bandwidth of a Patch Antenna

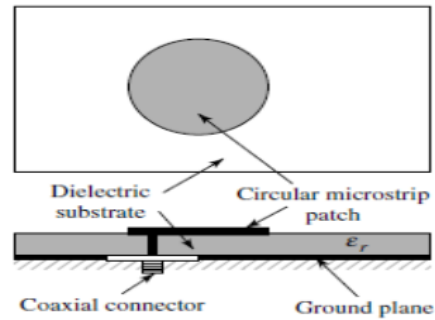
The impedance bandwidth depends on a large number of parameters related to the patch antenna element itself like quality factor, Q , and the type of feed technology used. Usually, the impedance bandwidth of a square, half-wave patch antenna is typically limited to 1 to 3%, which is a major disadvantage of this type of patch antenna. [28]

2.3 Feeding Method

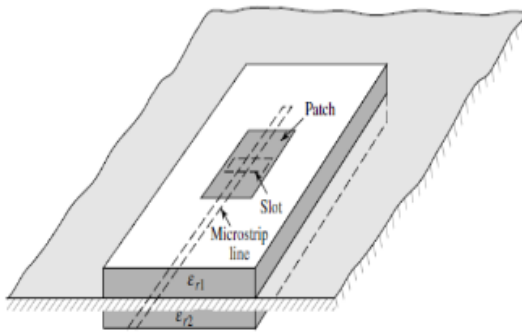
There are many configurations that can be used to feed microstrip antennas. The four most popular are the microstrip line, coaxial probe, aperture coupling and proximity coupling [27]. These are all displayed in Figure 2.5.



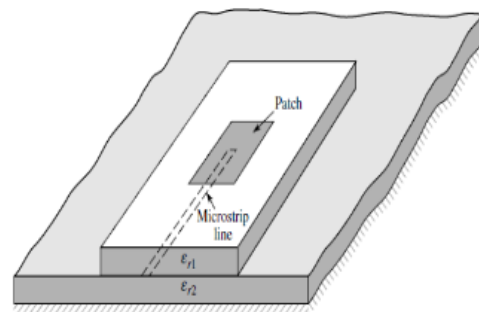
(a) Microstrip line feed



(b) Probe feed



(c) Aperture-coupled feed



(d) Proximity-coupled feed

Figure 2.5 Typical feeds for microstrip antennas [27]

The microstrip line feed is easy to fabricate, simple to match by controlling the inset position and rather simple to model. However, as the substrate thickness increases, surface waves and spurious feed radiation increase, which for practical uses, limit the bandwidth (typically 2-5%).

Coaxial-line feeds, where the inner conductor of coax is attached to the radiation patch while the outer conductor is connected to the ground plane, are also widely used. The coaxial feed is easy to fabricate and match with low spurious radiation. However, it also has a narrow band and it is more difficult to model, especially for thick substrates ($h > 0.02\lambda_0$).

Both the microstrip feed line and the probe possess inherent asymmetries which generate higher order modes which produce cross-polarized radiation. Non-contacting aperture coupling feeds, as shown in Figures 2.5 (c) and (d), have been introduced to overcome some of these problems mentioned above. For a basic aperture coupled patch antenna, shown in Figure 2.5 (c), the radiating microstrip patch element is etched on the top of the antenna substrate, and the microstrip feed line is etched on the bottom of the feed substrate. The thickness and dielectric constants of these two substrates may thus be chosen independently to optimize the distinct electrical functions of radiation and circuitry. Although the original prototype antenna used a circular coupling aperture, it was quickly realized that the use of a rectangular slot would improve the coupling, for a given aperture area, due to its increased magnetic polarizability. Most aperture coupled microstrip antennas now use rectangular slots, or variations thereof. Proximity coupling, shown in Figure 2.5 (d), has the largest bandwidth among these four feeding methods, and has low spurious radiation. However, fabrication is difficult. Length of feeding stub and width-to-length ratio of patch can be used to control the match performance.

In general, the input feed point for the antenna must be placed in such a point along the transmission line where the input impedance match is 50Ω , and the antenna reactance must be minimized as much as possible.

2.4 Method of Analysis

There are many methods of analysis for microstrip antenna. Comparing to other methods, the transmission line method is the easiest method. It gives good physical insight, representing the rectangular patch as a pair of two radiating slots, separated by a

low-impedance (Z_c) transmission line of certain length L . However, this method is less accurate and it is more difficult to model coupling [27].

2.4.1 Fringing Effects

Because the dimensions of the patch are finite along the length and width, the fields at the edges of the patch undergo fringing. It is the fringing fields that are responsible for the radiation. This is illustrated along the length in Figure 2.6 for the two radiating slots of the microstrip antenna. The amount of fringing is a function of the dimensions of the patch and the height of the substrate. For the principal E-plane, fringing is a function of the ratio of the length of the patch L to the height h of the substrate (L/h) and the dielectric constant ϵ_r of the substrate. Since for microstrip antennas $L/h \gg 1$, fringing is reduced. However, it must be taken into account because it influences the resonant frequency of the antenna. Because of the fringing effect, in which some of the waves travel in the substrate and some in air, an effective dielectric constant ϵ_{reff} is introduced to account for this effect.

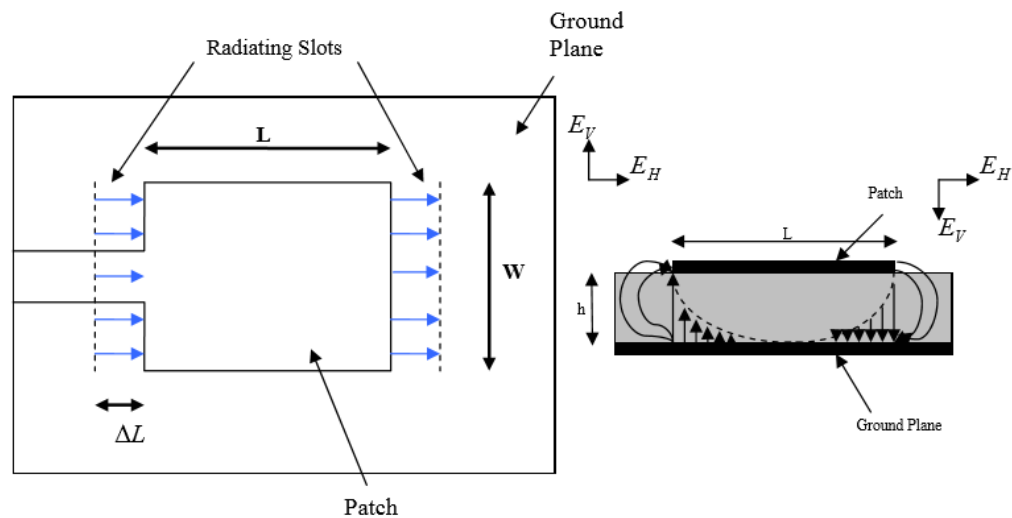


Figure 2.6 Microstrip antenna and its electric field lines

The effective dielectric constant is defined as the dielectric constant of the uniform dielectric material so that the electric field lines have identical electrical characteristics, particularly the propagation constant, as the actual field line.

The value of the effective dielectric constant is essentially constant at low frequencies, then increasing monotonically as the frequency increases, and ends up approaching the value of the dielectric constant of the substrate at higher frequencies. The initial values (at low frequencies) of the effective dielectric constant are referred to as the static values, and they are given by [34]:

$$W/h > 1$$

$$\epsilon_{reff} = \frac{\epsilon_r + 1}{2} + \frac{\epsilon_r - 1}{2} \left[1 + 12 \frac{h}{W} \right]^{-\frac{1}{2}} \quad (2-1)$$

Where ϵ_{reff} = Effective dielectric constant

ϵ_r = Dielectric constant of substrate

h = Height of dielectric substrate

W = Width of the Patch

2.4.2 Effective Length and Resonant Frequency

In the transmission line model, the antenna is represented by two radiating slots ($W \times h$) separated by a low impedance transmission line (Z_c) of length L. The slots represent very high-impedance terminations from both sides of the transmission line (almost an open circuit). Thus, we expect this structure to have highly resonant characteristics depending mainly on its length L. Due to the fringing effect, the resonant length of the patch is not exactly equal to the physical length. The fringing effect makes the physical length of

antenna shorter than the effective electrical length of the patch. The dimensions of the patch along its length have been elongated on each end by a length of ΔL , which is a function of the effective dielectric constant ϵ_{reff} and the width-to-height ratio (W/h). A well-known and practical approximate relation for the normalized extension of the length show as follows:

$$L_{eff} = L + 2\Delta L \quad (2-2)$$

$$L_{eff} = \frac{1}{2f_r \sqrt{\mu_0 \epsilon_0 \sqrt{\epsilon_{reff}}}} = \frac{v_0}{2f_r \sqrt{\epsilon_{reff}}} \quad (2-3)$$

$$\Delta L = 0.412h \frac{(\epsilon_{reff} + 0.3) \left(\frac{W}{h} + 0.264\right)}{(\epsilon_{reff} - 0.258) \left(\frac{W}{h} + 0.8\right)} [35] \quad (2-4)$$

For dominant TM_{010} mode f_r is:

$$f_{r010} = \frac{1}{2L \sqrt{\mu_0 \epsilon_0 \sqrt{\epsilon_r}}} = \frac{v_0}{2L \sqrt{\epsilon_r}} \quad (2-5)$$

Where v_0 is the speed of light in free space. The resonant frequency of a patch depends highly on L . Because (2-5) does not account for fringing, it must be modified to include edge effects and when the fringing effect is taken into account, (2-5) becomes

$$\begin{aligned} f_{r010} &= \frac{1}{2L_{eff} \sqrt{\mu_0 \epsilon_0 \sqrt{\epsilon_{reff}}}} = \frac{1}{2(L + 2\Delta L) \sqrt{\mu_0 \epsilon_0 \sqrt{\epsilon_{reff}}}} \quad (2-6) \\ &= q \frac{1}{2L \sqrt{\mu_0 \epsilon_0 \sqrt{\epsilon_r}}} = q \frac{v_0}{2L \sqrt{\epsilon_r}} \end{aligned}$$

Where

$$q = \frac{f_{rc010}}{f_{r010}} \quad (2-6a)$$

The q factor is referred to as the fringe factor (length reduction factor). As the substrate height increases, fringing also increases and results in larger separations between the radiating edges and lower resonant frequencies.

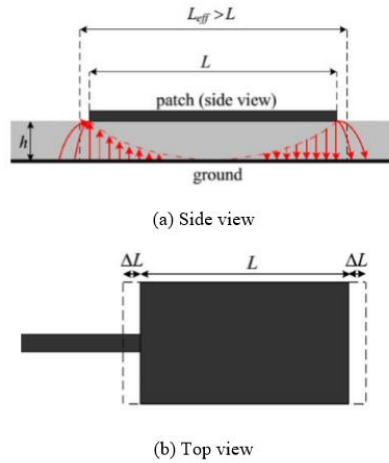


Figure 2.7 Physical and effective lengths of rectangular microstrip patch antenna

2.4.3 Effective Width

For an effective radiator, a practical width that leads to good radiation efficiencies is:

$$W = \frac{1}{2f_r \sqrt{\mu_0 \epsilon_0}} \sqrt{\frac{2}{\epsilon_r + 1}} = \frac{v_0}{2f_r} \sqrt{\frac{2}{\epsilon_r + 1}} \quad (2-7)$$

Where v_0 is the free-space velocity of light [36].

The procedure of designing a rectangular patch using the transmission line model is as follows:

- (1) Input data: ϵ_r , f_r (in Hz), and h
- (2) Calculate W using (2-7),

$$W = \frac{1}{2f_r \sqrt{\mu_0 \epsilon_0}} \sqrt{\frac{2}{\epsilon_r + 1}} = \frac{v_0}{2f_r} \sqrt{\frac{2}{\epsilon_r + 1}}$$

- (3) Calculate $\epsilon_{r_{eff}}$ using (2-1),

$$\epsilon_{r_{eff}} = \frac{\epsilon_r + 1}{2} + \frac{\epsilon_r - 1}{2} \left[1 + 12 \frac{h}{W} \right]^{-\frac{1}{2}}$$

- (4) Calculate the actual (physical) length of the patch using (2-2), (2-3) and (2-4)

$$\begin{aligned} L &= \frac{1}{2f_r \sqrt{\mu_0 \epsilon_0} \sqrt{\epsilon_{reff}}} 2\Delta L \\ &= \frac{v_0}{2f_r \sqrt{\epsilon_{reff}}} 2\Delta L \end{aligned}$$

Chapter 3. A Proposed Novel Dual-Frequency Array Antenna with Multiple Pattern Reconfigurabilities

3.1 Introduction

This chapter presents the design, fabrication and testing of a novel dual-frequency array antenna with multiple pattern reconfigurabilities. The transmission line model is implemented to calculate the basic dimensions of the conventional MSA. The Advanced Design System [ADS] software is used in modeling and simulating the designed antennas. The beam pattern selectivity can be obtained by utilizing a switchable feeding network and the special structure used in this array antenna. Opposite corners have been slotted on each patch and a diode placed on the slot, which is used as a switch to control multiple patterns. By controlling four PIN diodes through the corresponding DC voltage source, the radiation pattern can be changed. The simulation and measurement results closely agree.

3.2 Basic single patch antenna design

In this section, a novel dual-frequency antenna array with multiple pattern diversities is proposed. The desired resonant frequencies of two microstrip patch antennas are 1.92 GHz and 2.11 GHz, respectively. The proposed antenna array consists of two different patch antenna elements. The first step of designing the proposed antenna array is designing its two patch antenna elements.

To design two conventional rectangular patch antenna elements with operating frequencies of 1.92GHz and 2.11GHz respectively, we should follow the method discussed in chapter 2. The width of patch antenna elements can be found using (2-7):

$$W_{1.92} = \frac{1}{2f_{r1.92}\sqrt{\mu_0\epsilon_0}} \sqrt{\frac{2}{\epsilon_r+1}} = \frac{v_0}{2f_{r1.92}} \sqrt{\frac{2}{\epsilon_r+1}} \quad (3-1)$$

$$\begin{aligned}
&= \frac{3 \times 10^8}{2 \times 1.92 \times 10^9} \sqrt{\frac{2}{1+3.6}} \\
&= 51.5 \text{ mm} \\
W_{2.11} &= \frac{1}{2f_{r2.11} \sqrt{\mu_0 \epsilon_0}} \sqrt{\frac{2}{\epsilon_r + 1}} = \frac{v_0}{2f_{r2.11}} \sqrt{\frac{2}{\epsilon_r + 1}} \quad (3-2) \\
&= \frac{3 \times 10^8}{2 \times 2.11 \times 10^9} \sqrt{\frac{2}{1+3.6}} \\
&= 46.8 \text{ mm}
\end{aligned}$$

To find the effective dielectric constant, ϵ_{reff} , and when $W/h > 1$, we can use (2-1):

$$\begin{aligned}
\epsilon_{reff1.92} &= \frac{\epsilon_r + 1}{2} + \frac{\epsilon_r - 1}{2} \left[1 + 12 \frac{h}{W_{1.92}} \right]^{-\frac{1}{2}} \quad (3-3) \\
&= \frac{3.6+1}{2} + \frac{3.6-1}{2} \left[1 + 12 \frac{1.524}{51.5} \right]^{-\frac{1}{2}} \\
&= 2.3 + 1.3 \left[1 + 0.355 \right]^{-\frac{1}{2}} \\
&= 3.421
\end{aligned}$$

$$\begin{aligned}
\epsilon_{reff2.11} &= \frac{\epsilon_r + 1}{2} + \frac{\epsilon_r - 1}{2} \left[1 + 12 \frac{h}{W_{2.11}} \right]^{-\frac{1}{2}} \quad (3-4) \\
&= \frac{3.6+1}{2} + \frac{3.6-1}{2} \left[1 + 12 \frac{1.524}{46.8} \right]^{-\frac{1}{2}} \\
&= 2.3 + 1.3 \left[1 + 0.399 \right]^{-\frac{1}{2}} \\
&= 3.399
\end{aligned}$$

This value for ϵ_{reff} is reasonable, because $1 \leq \epsilon_{reff} \leq \epsilon_r$.

The effective length can be found using (2-2), (2-3) and (2-4):

$$\begin{aligned}
L_{eff1.92} &= \frac{c}{2f_{1.92} \sqrt{\epsilon_{reff1.92}}} \quad (3-5) \\
&= \frac{3 \times 10^8}{2 \times 1.92 \times 10^9 \sqrt{3.421}} \\
&= \frac{3}{38.4 \times 1.85}
\end{aligned}$$

$$= \frac{3}{71.04}$$

$$= 42.2 \text{mm}$$

$$L_{eff2.11} = \frac{c}{2f_{2.11}\sqrt{\epsilon_{reff2.11}}} \quad (3-6)$$

$$= \frac{3 \times 10^8}{2 \times 2.11 \times 10^9 \sqrt{3.399}}$$

$$= \frac{3}{42.2 \times 1.845}$$

$$= \frac{3}{77.859}$$

$$= 38.5 \text{mm}$$

$$\Delta L_{1.92} = 0.412h \frac{(\epsilon_{reff1.92} + 0.3) \left(\frac{W_{1.92}}{h} + 0.264 \right)}{(\epsilon_{reff1.92} - 0.258) \left(\frac{W_{1.92}}{h} + 0.8 \right)} \quad (3-7)$$

$$= 0.412 \times 1.524 \times 10^{-3} \times \frac{(3.421 + 0.3) \left(\frac{51.5}{1.524} + 0.264 \right)}{(3.421 - 0.258) \left(\frac{51.5}{1.524} + 0.8 \right)}$$

$$= \frac{(3.721)(33.79 + 0.264)}{(3.163)(33.79 + 0.8)} \times 0.628 \times 10^{-3}$$

$$= \frac{126.71}{109.41} \times 0.628 \times 10^{-3}$$

$$= 0.00073 \text{m}$$

$$= 0.73 \text{mm}$$

$$L_{1.92} = L_{eff1.92} - 2\Delta L_{1.92}$$

$$= 42.2 - 1.46$$

$$= 40.74 \text{mm}$$

$$\Delta L_{2.11} = 0.412h \frac{(\epsilon_{reff2.11} + 0.3) \left(\frac{W_{2.11}}{h} + 0.264 \right)}{(\epsilon_{reff2.11} - 0.258) \left(\frac{W_{2.11}}{h} + 0.8 \right)} \quad (3-8)$$

$$= 0.412 \times 1.524 \times 10^{-3} \times \frac{(3.399 + 0.3) \left(\frac{46.8}{1.524} + 0.264 \right)}{(3.399 - 0.258) \left(\frac{46.8}{1.524} + 0.8 \right)}$$

$$\begin{aligned}
&= \frac{(3.699)(30.71+0.264)}{(3.141)(30.71+0.8)} \times 0.628 \times 10^{-3} \\
&= \frac{114.57}{98.97} \times 0.628 \times 10^{-3} \\
&= 0.000727 \text{ m} \\
&= 0.727 \text{ mm} \\
L_{2.11} &= L_{eff} - 2\Delta L_{2.11} \\
&= 38.5 - 1.454 \\
&= 37.05 \text{ mm}
\end{aligned}$$

We used the side line feeding method, with the width of the feeding line being determined by ADS simulation.

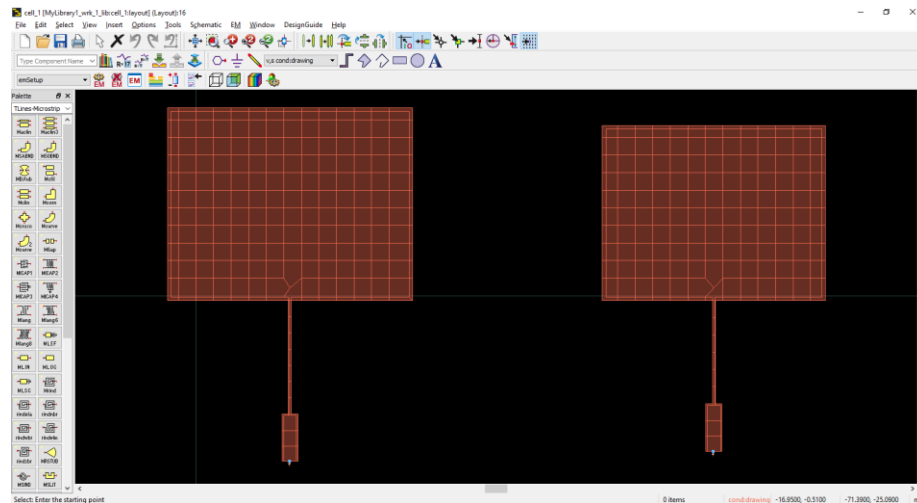


Figure 3.1 Layout simulation for Basic Antennas

Figure 3.1 shows the layout simulation for two basic antennas. Many simulation and optimization works based on the basic parameters were developed from the equations. After the optimization works, the dimensions of two antenna elements were set to 51.8 mm × 40.72 mm (1.92GHz) and 47.12 mm × 36.98 mm (2.11 GHz), respectively. In the future work, we will design our desired antenna array based on these two basic elements.

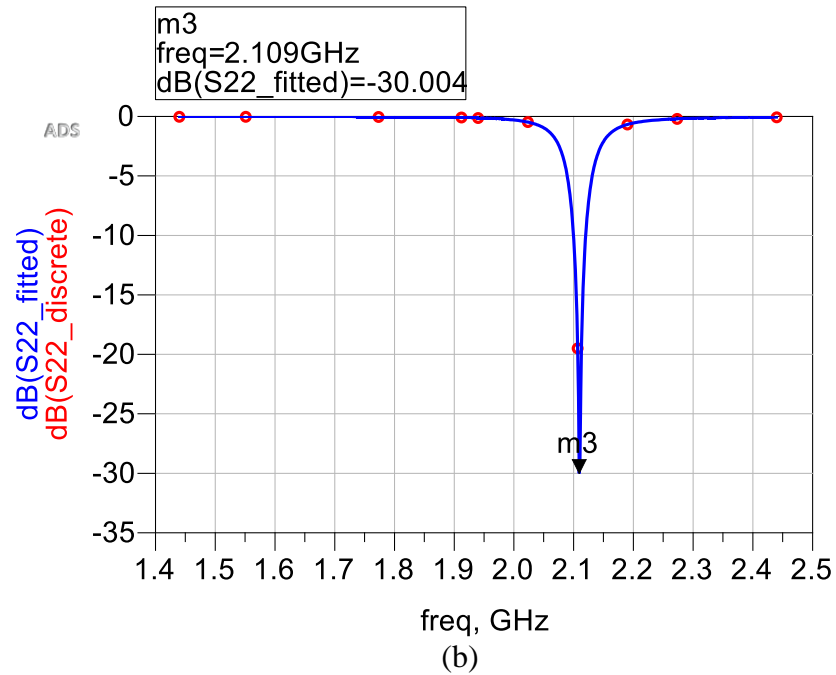
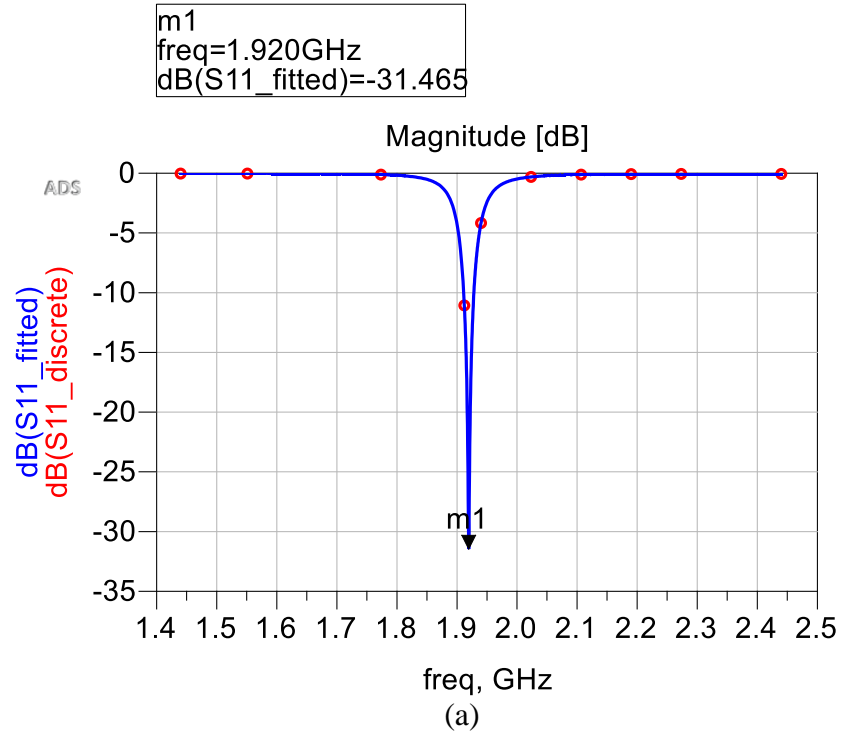


Figure 3.2 Return loss for two basic antenna elements

Based on Figure 3.2 we can conclude that these two patch antenna worked well at the expected frequencies.

3.3 Dual-frequency pattern reconfigurable antenna array design

In this section, the design of the dual-frequency pattern reconfigurable array antenna based on those two antenna elements from Section 3.2 above is discussed. According to [2], a single-feed switchable feed network can be used as a basic beam pattern reconfigurable antenna system that also introduces dual-frequency features to the antenna system. We use the structure discussed in [26] to create more pattern selectivity and investigate the impact of this structure to the pattern of the antenna array.

3.3.1 Switchable feeding network

The two antenna elements were connected by a single-feed switchable network. The basic schematic of the single-feed switchable feed network is shown in Figure 3.3. According to [2], the principle of operation of this switchable feed network is based on the assumption that the resonant frequency ratio of the two micro-strip patch antennas is very close to 1.4:1. It basically consists of two quarter-wavelength branch lines with characteristic impedances of Z_1 and Z_2 and lengths of L_1 and L_2 . Two different rectangular micro-strip patch antennas of different size were connected to output ports 2 and 3. Under this particular condition, the single-feed switchable feed network can be worked as an ideal switch.

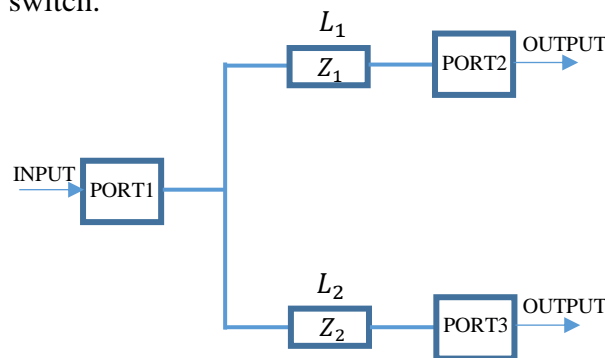


Figure 3.3 Schematic of a single-feed switchable feed network.

The diode used is equivalent to a resistor of 1.2Ω when it is forward-biased and to a capacitor of 0.21pF when it is reverse-biased. The optimized geometrical parameters are shown in Table 1. Two rectangular patch antennas of different sizes are connected to the corresponding outputs of the switchable feed network.

The following figures (3.5) – (3.8) are four different simulated designs of this array antenna that were developed using Advance Design System (ADS) software in order to determine how the truncated corners impact the performance of the antenna array. Configuration (a) is the basic antenna array with short lines of quarter waveguide length, shown in Figure 3.5; Configuration (b) is the antenna array with short lines of quarter waveguide length and truncated corners on the 1.92GHz antenna element, shown in Figure 3.6; Configuration (c) shows the antenna array with short lines of quarter waveguide length and truncated corners on the 2.11GHz antenna element, shown in Figure 3.7 and; Configuration (d) shows the antenna array with short lines of quarter waveguide length and truncated corners on both antenna elements, shown in Figure 3.8. To easily validate the effectiveness of our design, we built and measured Configuration (d). However, by incorporating four PIN-diodes and a DC voltage into Configuration (d), we can investigate properties between different configurations such as (a) (Figure 3.5) and (d) (Figure 3.8.).

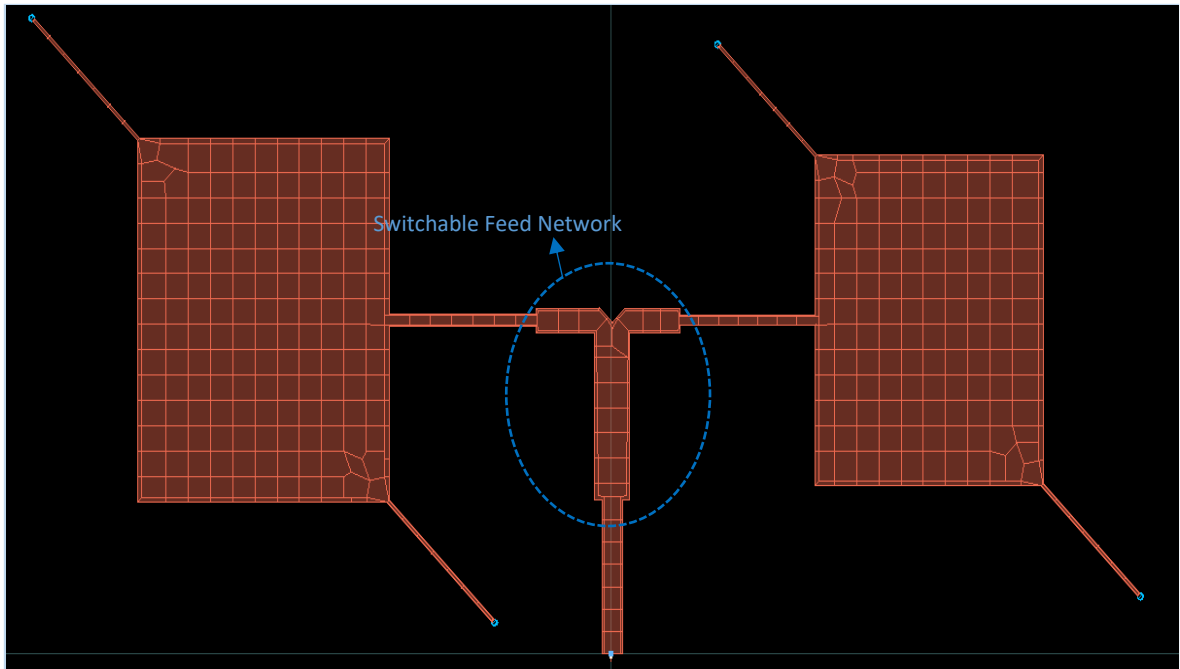


Figure 3.5 Configuration (a): Basic antenna array with short lines of quarter waveguide length

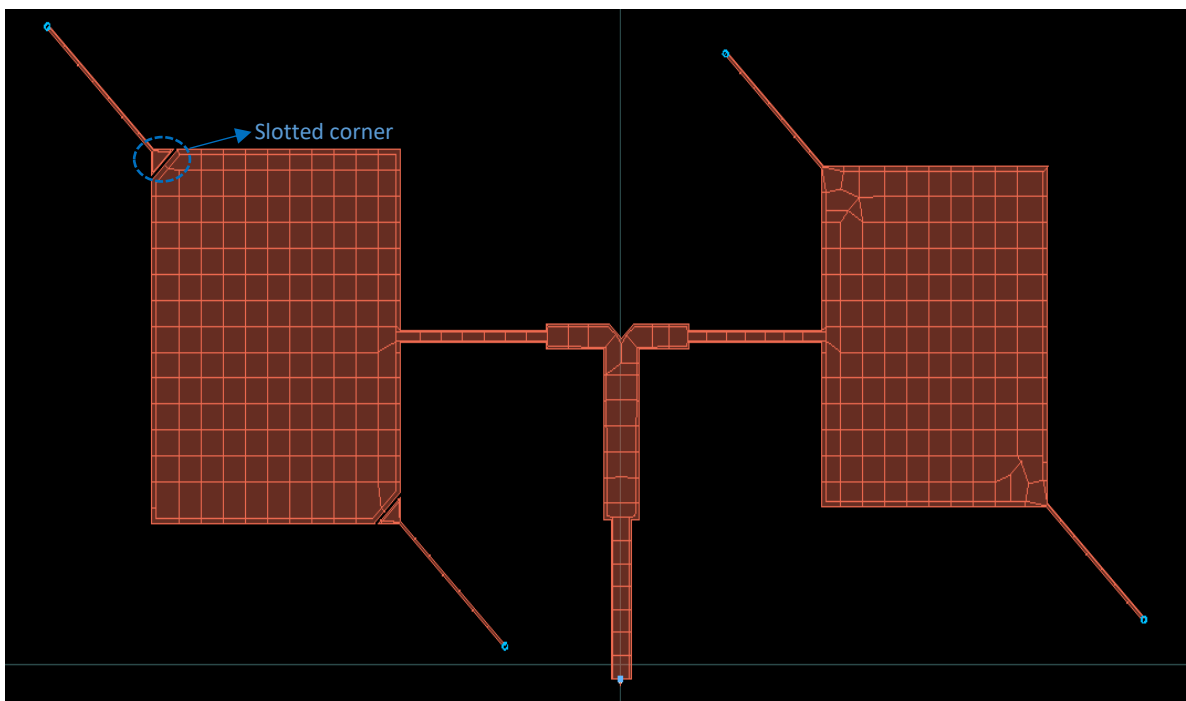


Figure 3.6 Configuration (b): Antenna array with short lines of quarter waveguide length and truncated corners on the 1.92GHz antenna element

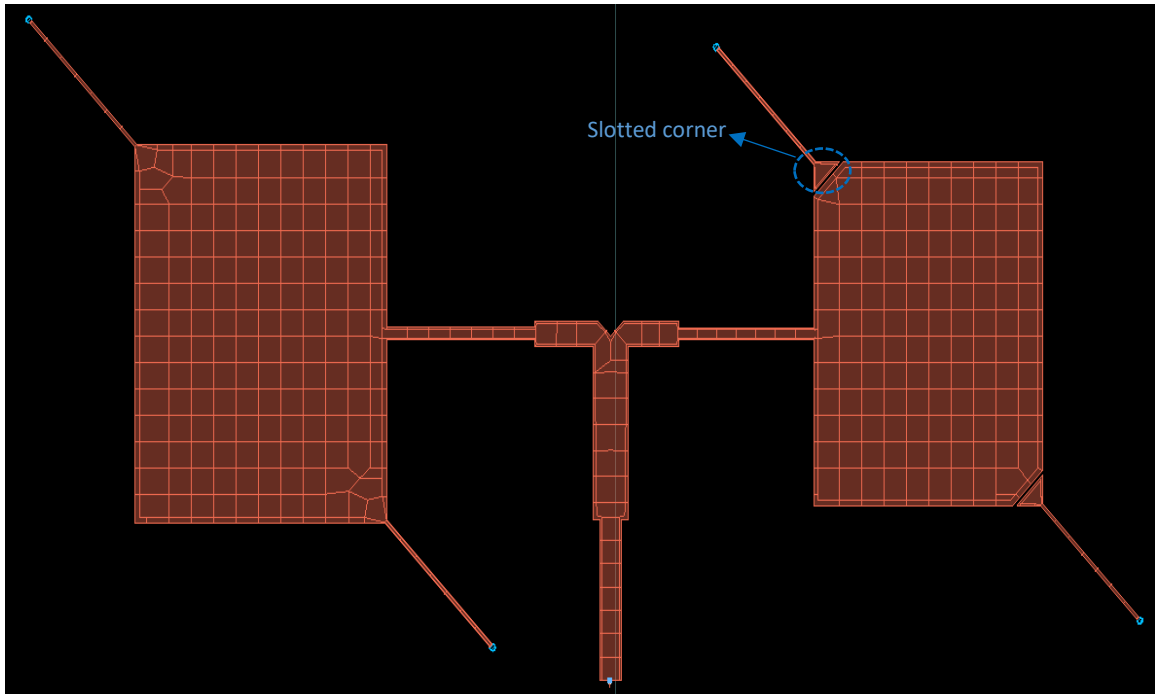


Figure 3.7 Configuration (c): Antenna array with short lines of quarter waveguide length and truncated corners on the 2.11GHz antenna element

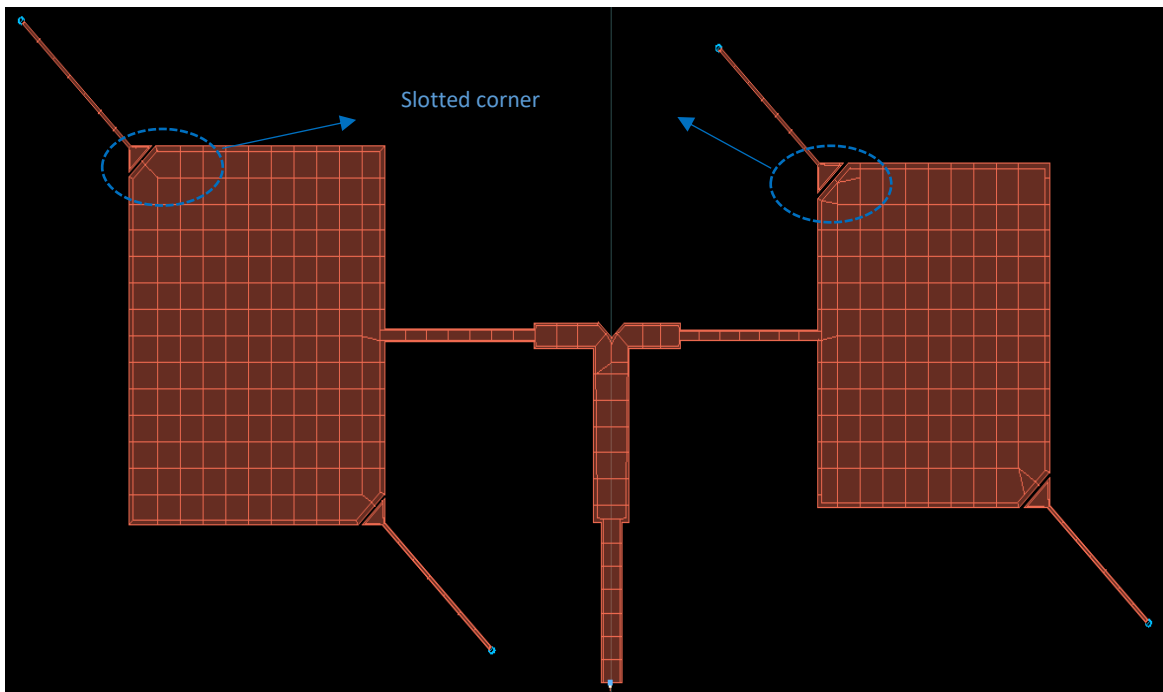


Figure 3.8 Configuration (d): Antenna array with short wires of quarter waveguide length and truncated corners on both antenna elements

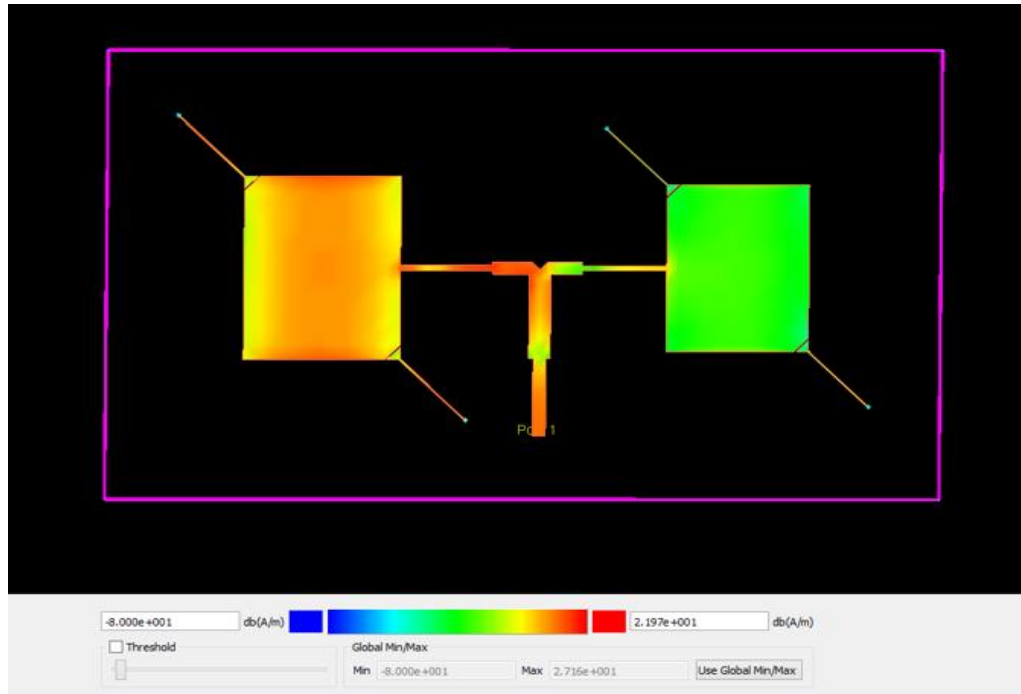


Figure 3.9 Simulated surface current distribution at 1.92 GHz for Configuration (d)

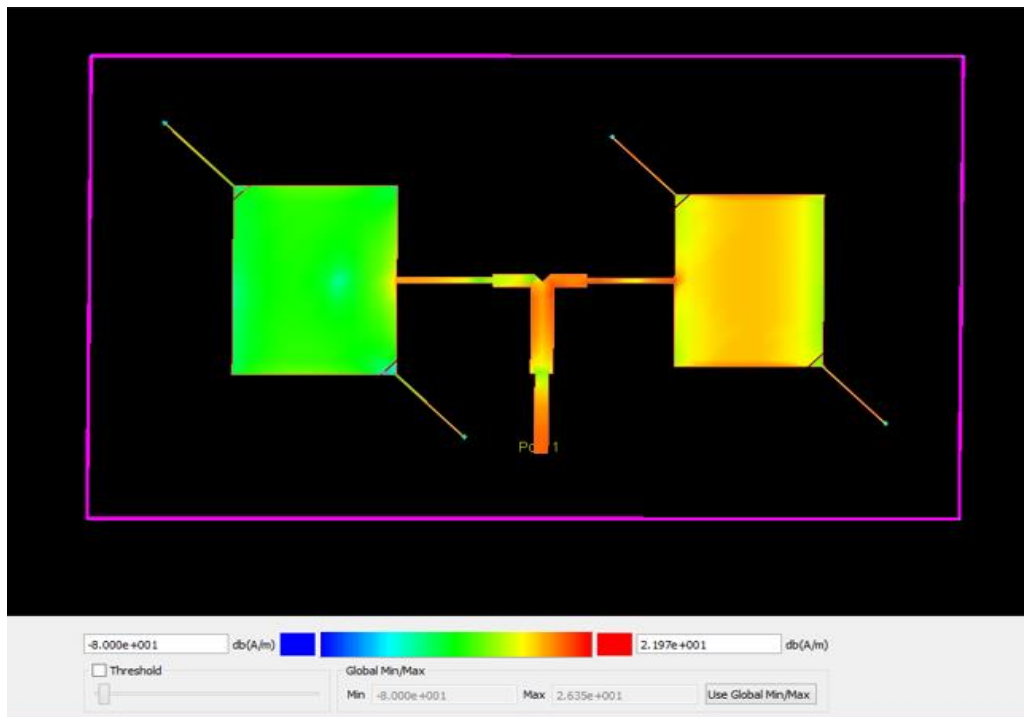


Figure 3.10 Simulated surface current distribution at 2.11 GHz for Configuration (d)

Figure 3.9 and Figure 3.10 show the simulated surface current distribution around the designed resonant frequency, proving the effectiveness of the switchable network used in the antenna system.

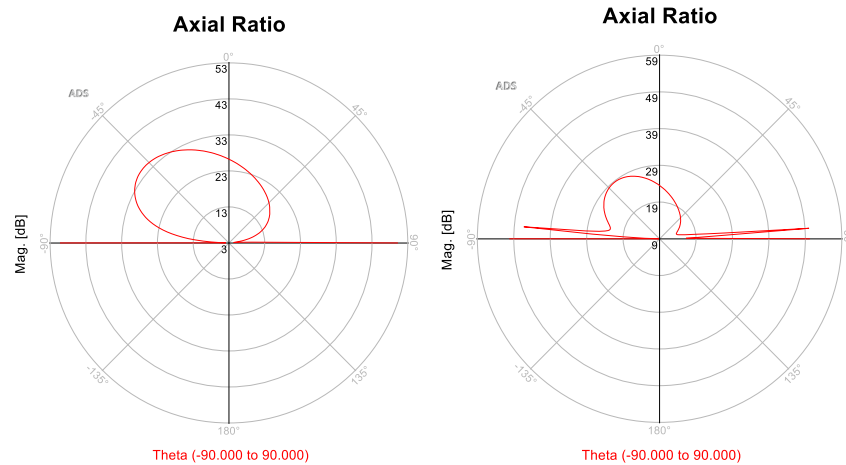


Figure 3.11 Axial Ratio for antenna array of configuration (d) at working frequency of 1.92 GHz (left) and 2.11 GHz (right)

As can be seen from Figure 3.11, the axial ratio of this antenna array at each working center frequency of Configuration (d) in the main lobe direction are all greater than 10 dB. This means the antenna array of Configuration (d) works in linear polarization mode for two different working frequencies.

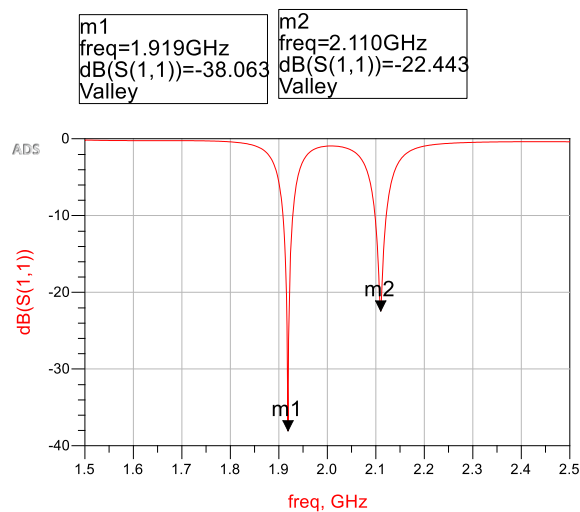


Figure 3.12 Return loss for configuration (d)

Figure 3.12 shows the return loss performance is very good at two working frequencies after many simulation and optimization works have been done. After the Configuration (d) had been built, we added four PIN diodes and a DC voltage into the antenna system. These changes have impacts on the antenna system. In order to determine the impact on antenna return loss performance, we used the co-simulation function of ADS. Figure 3.13-3.22 show how to use the co-simulation function and the return loss performance for co-simulation work.

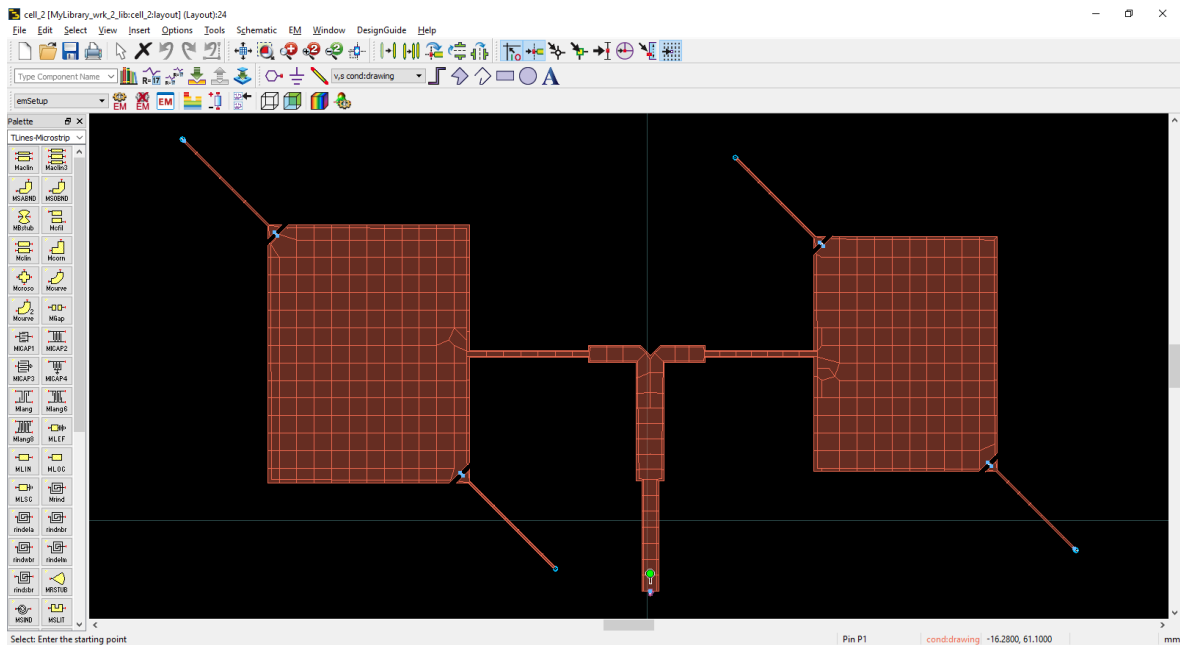


Figure 3.13 Configuration (d) with additional ports

To begin to do co-simulation, many ports need to be added into the design, shown in Figure 3.13. The detail of two ports can be observed in Figure 3.14. These ports are the positions where PIN diodes and DC voltage will be brought into the schematic simulation. After all the ports were added to the system, a new simulation can be run.

Next, an EM model needs to be created by selecting EM > Component > Create EM Model and Symbol in the layout window, shown in Figure 3.15.

Finally, the newly created EM model is introduced to a new schematic simulation, shown in Figure 3.16. Then many schematic items, such as PIN diodes, DC voltage, wire and S-parameter simulation control, were added into the antenna system. Figure 3.17 shows a PIN diode that has been added into the antenna system to control the pattern of the proposed antenna.

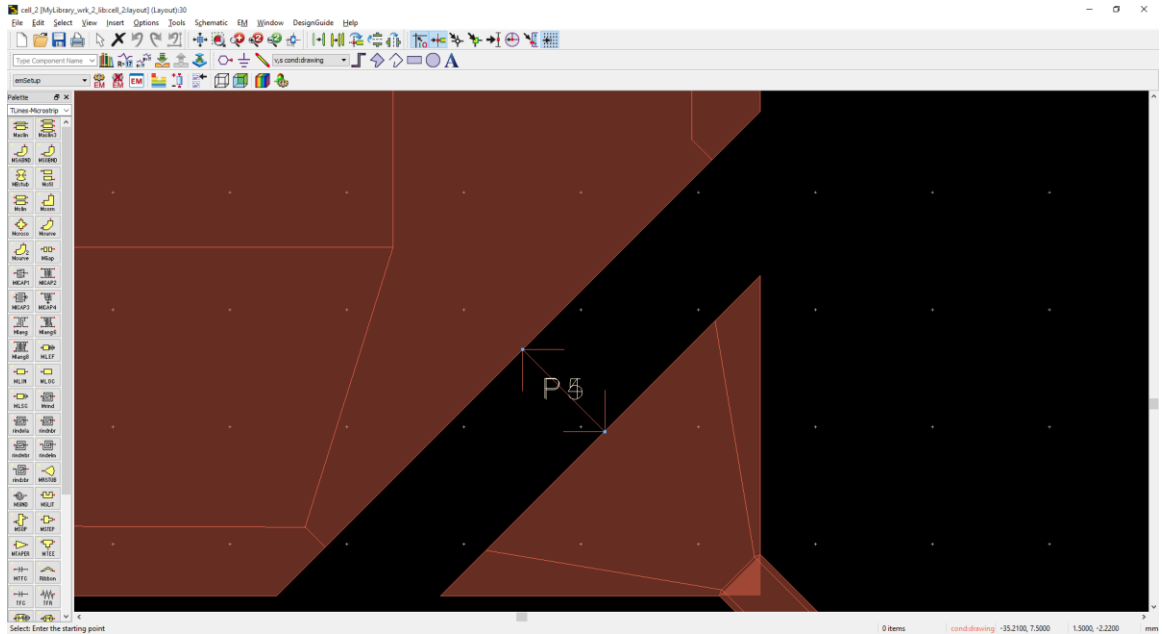


Figure 3.14 Detail of two additional added ports

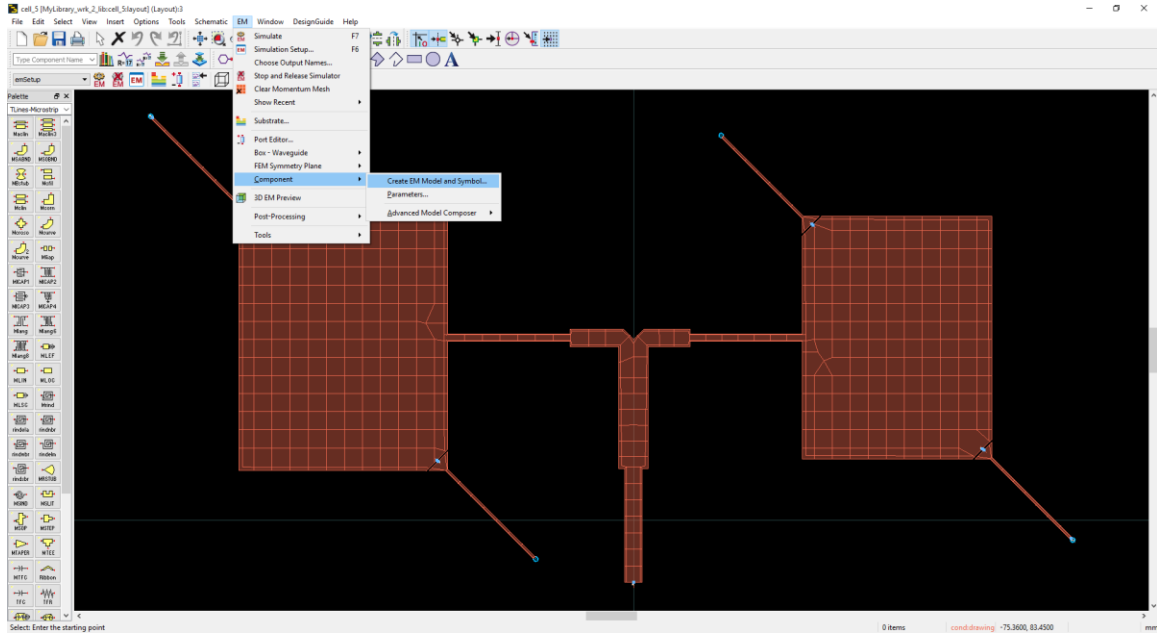


Figure 3.15 Creating a new EM Model

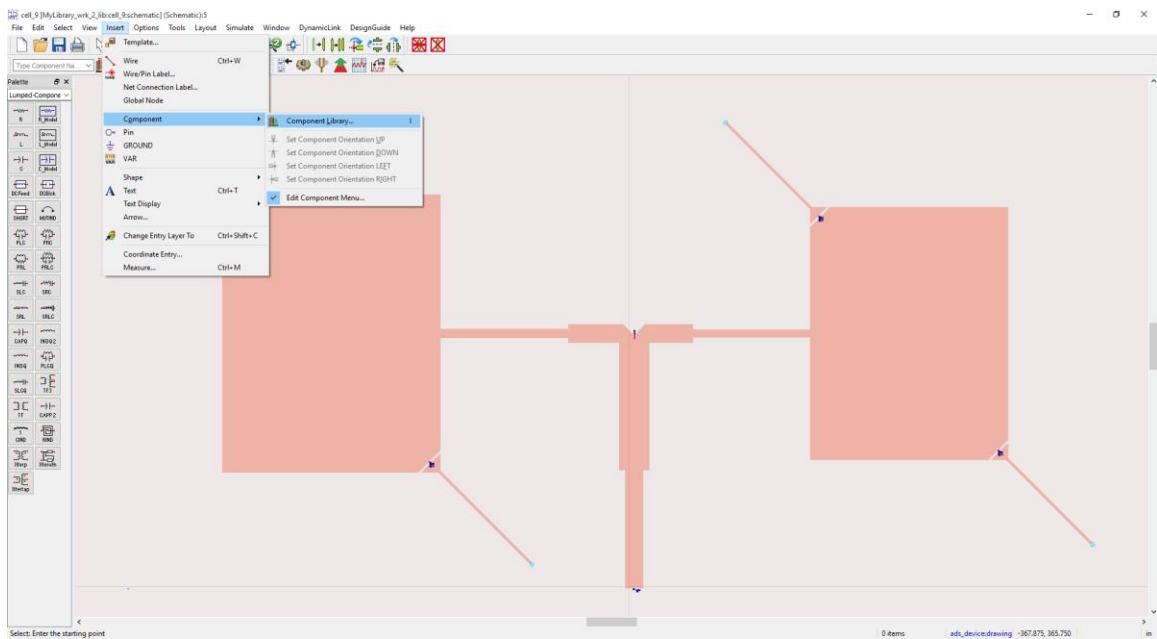


Figure 3.16 Introducing new EM Model to schematic design

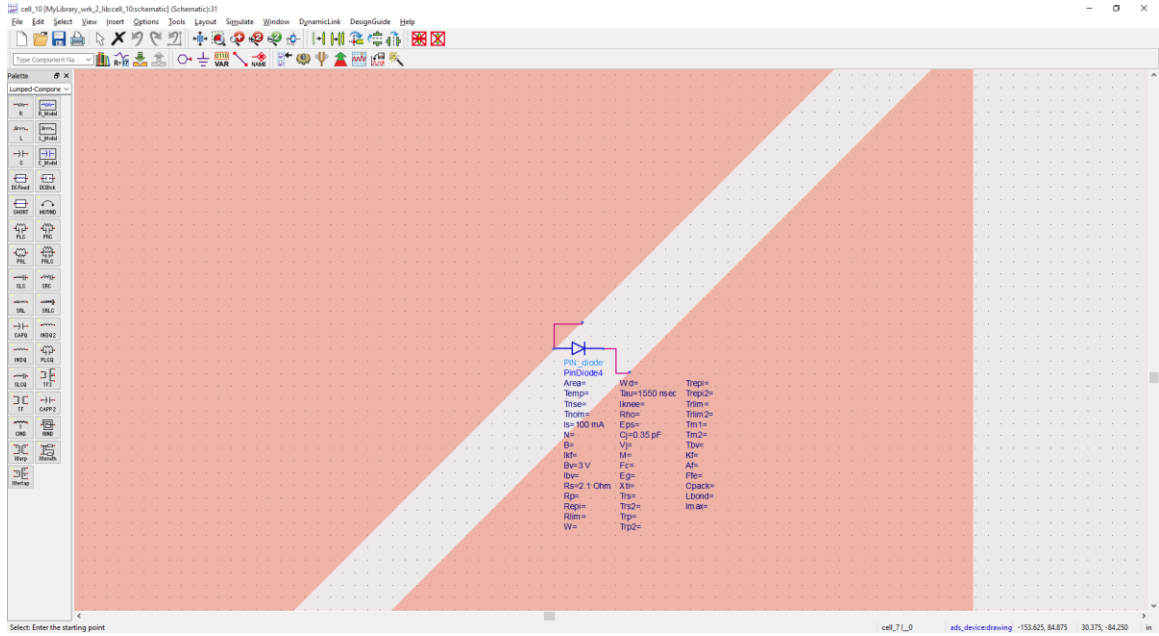


Figure 3.17 A PIN diode that has been added to the schematic simulation

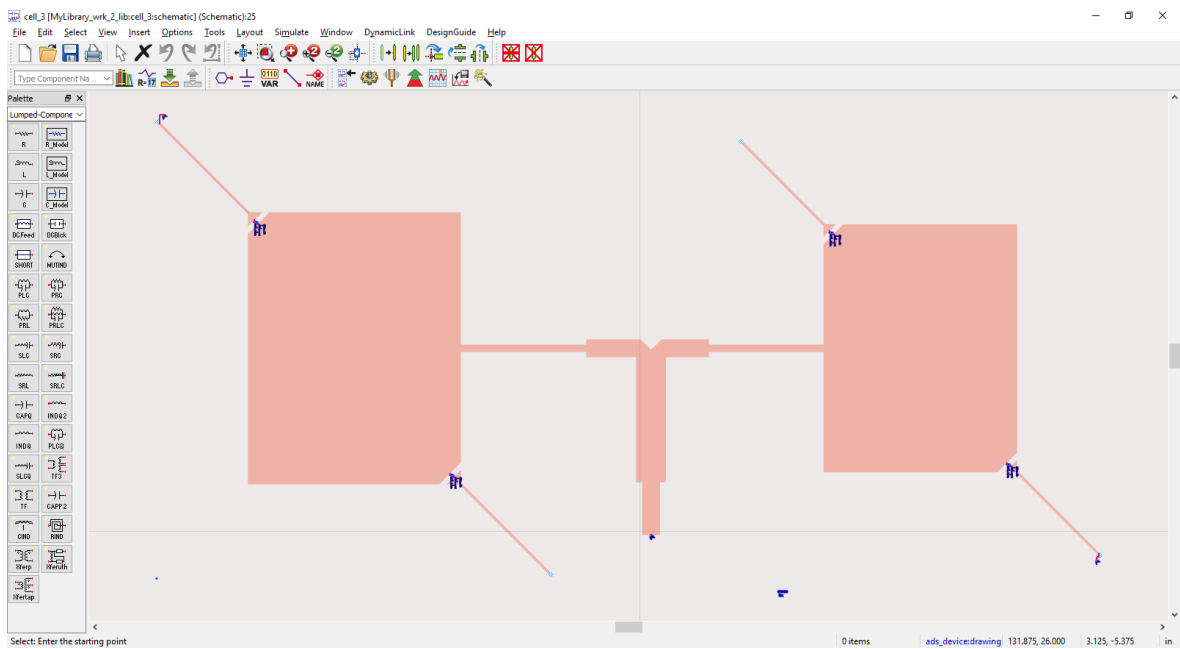


Figure 3.18 Co-simulation for Configuration (d) with all PIN diodes at off-state

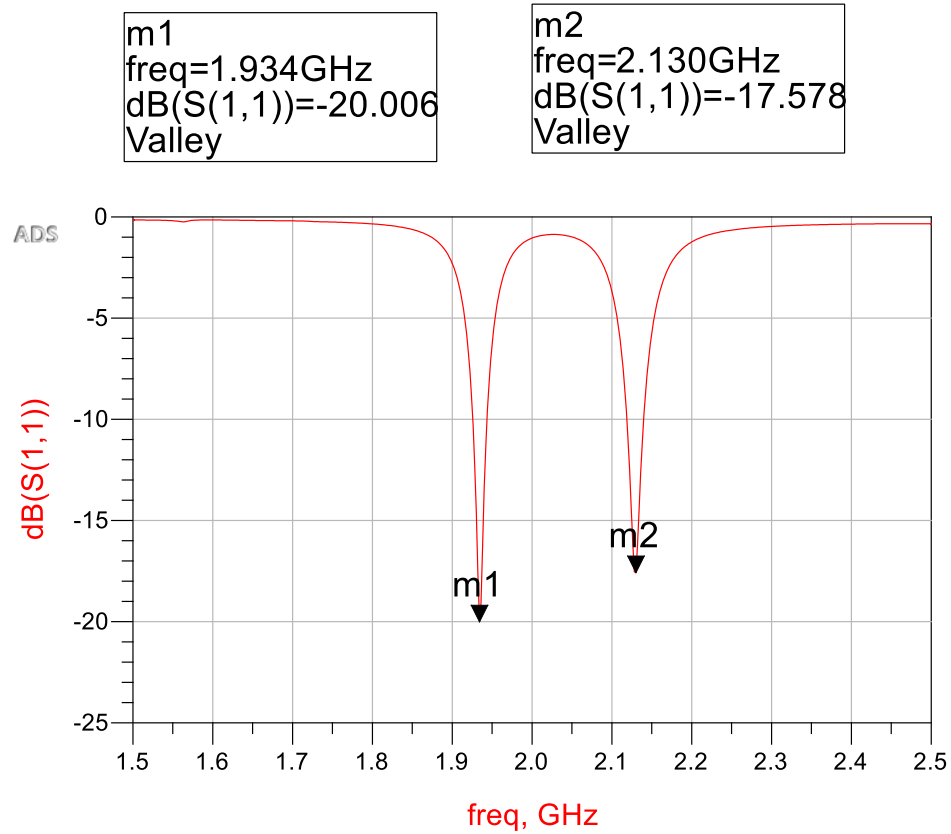


Figure 3.19 Return loss of co-simulation for Configuration (d) with all PIN diodes at off-state

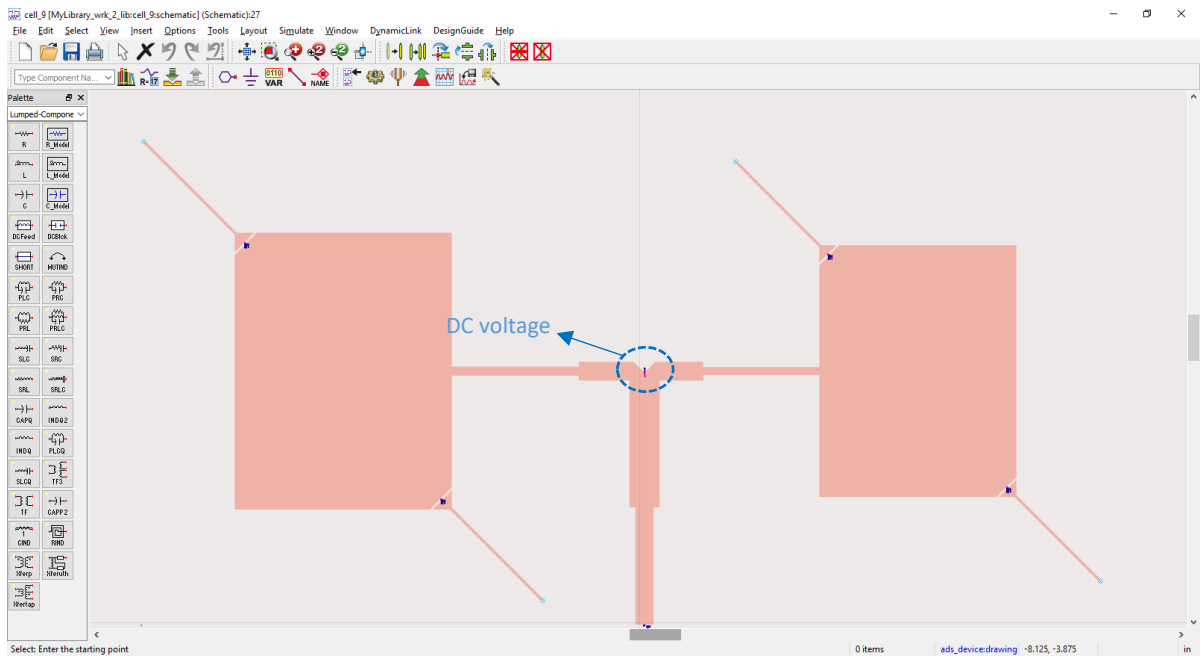


Figure 3.20 Co-simulation for Configuration (d) with all PIN diodes at on-state

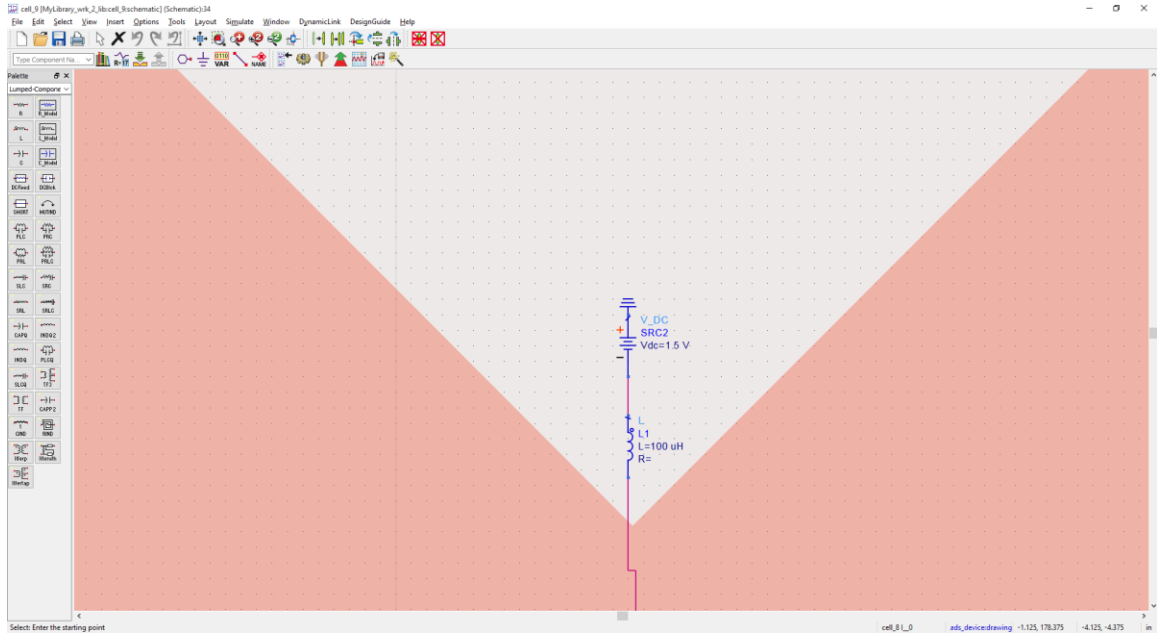


Figure 3.21 Detail of the DC voltage

The forward voltage of our PIN diode is 1.2 V, thus a 1.5 V DC-voltage is sufficient to control the PIN diodes.

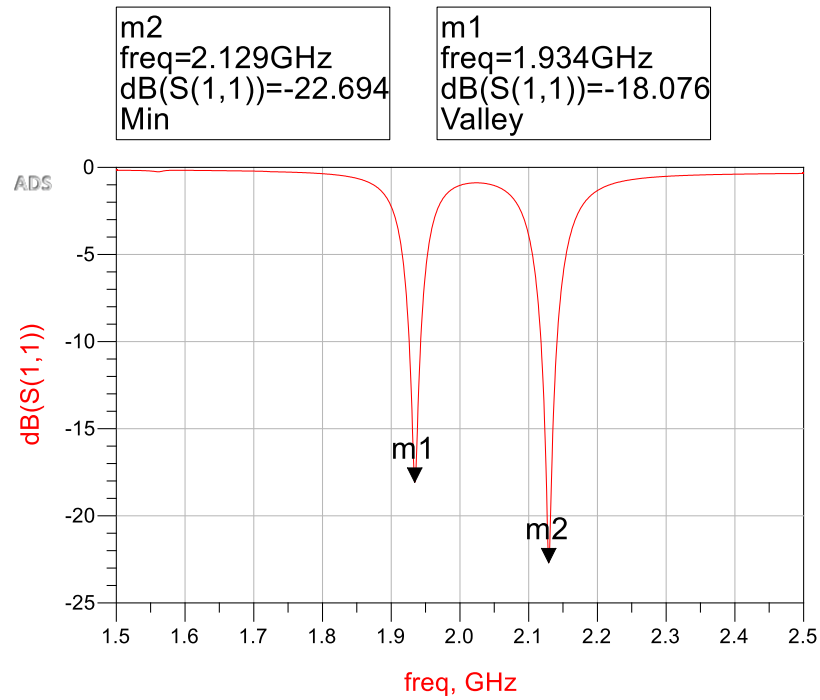


Figure 3.22 Return loss of co-simulation for Configuration (d) with all PIN diodes at on-state

Comparing Figures 3.19 and 3.22 with Figure 3.12, we find that the added PIN diodes and DC voltage impacted both values and frequency of return loss of this antenna array.

Figure 3.23 compares the return loss parameters of four different configurations at two different working frequencies in the simulation. For the simulated return loss of Configuration (b), because it has been slotted on the 1.92 GHz element (which causes a small change of radiation area), the red curve has a tiny frequency shift at around 1.92 GHz when compared to the Configuration (a) curve, but overlapped at the 2.11 GHz compared to the Configuration (a) curve. For the simulated return loss of Configuration (c), because it has been slotted on the 2.11 GHz element (which causes a small change of radiation area), the black curve has a tiny frequency shift at around 2.11 GHz compared to the Configuration (a) curve, but overlapped at the 1.92 GHz compared to the Configuration (a) curve. For the simulated return loss of Configuration (d), because it has been slotted on both the 1.92 GHz element and the 2.11 GHz element, the green curve has a tiny frequency shift both at around 1.92 GHz and at the 2.11 GHz compared to the Configuration (a) curve. From Figure 3.23, it can also be observed that there is about a 10 MHz shift of working frequency between the antenna array of Configuration (a) and Configuration (d) in simulation.

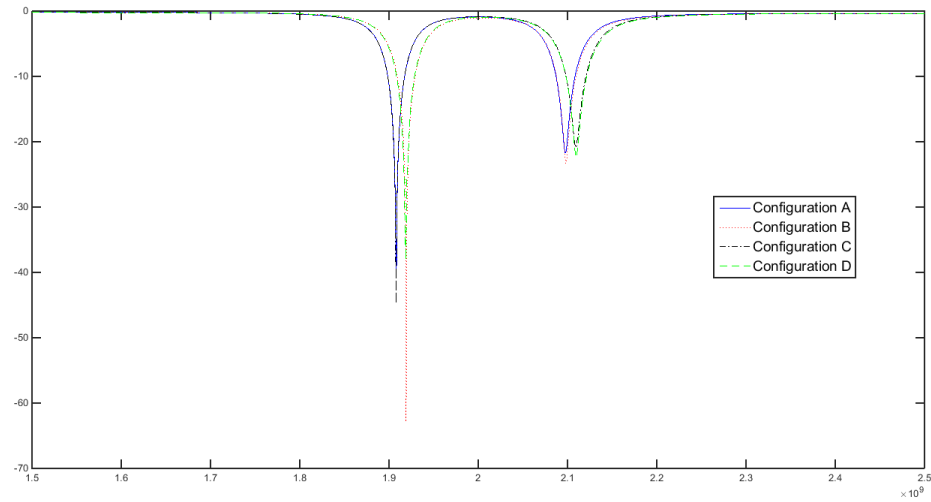
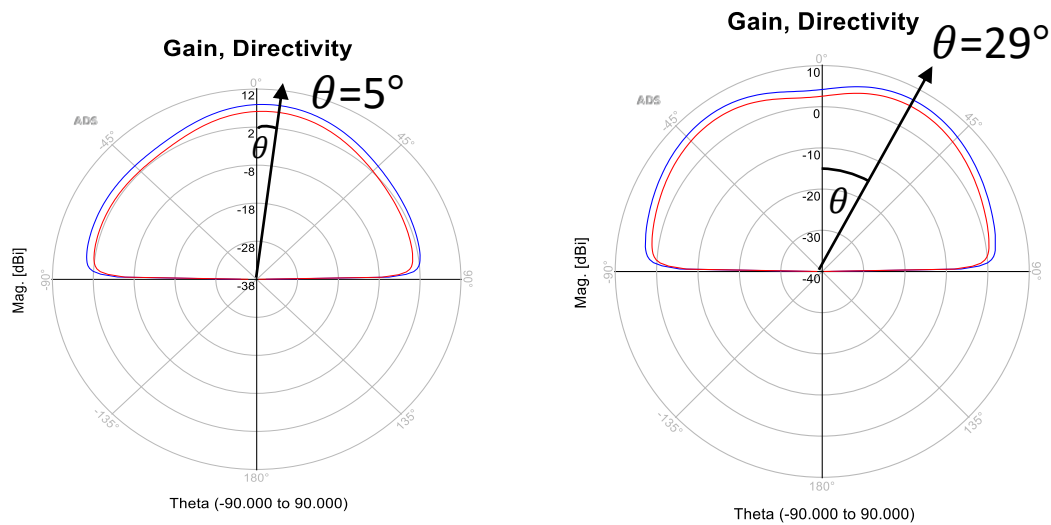
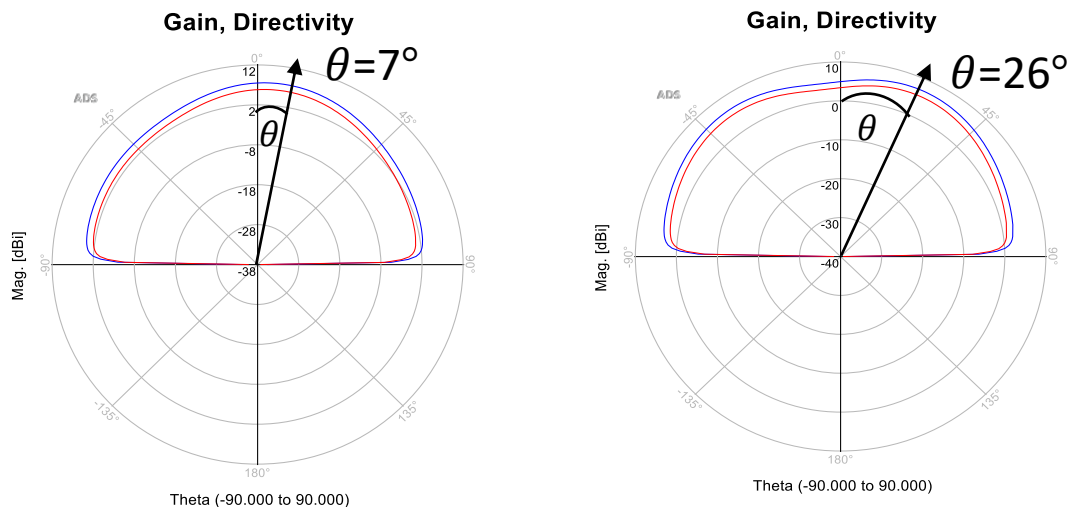


Figure 3.23 Return loss for the antenna array when operating in different configurations in simulation

Because the proposed antenna array is supposed to work between configuration (a) and (d) by controlling the different states of PIN diodes, we investigate the patterns of configurations (a) and (d). Figure 3.24 (1) and (2) show the simulated radiation patterns of Configuration (a) and Configuration (d), respectively. The black arrow line represents the maximum radiation direction. Table 3.2 shows all the related parameters at the two resonant frequencies of 1.92 GHz and 2.11 GHz in simulations for all four antenna configurations. It can be seen from Figure 3.24 that the patterns of different working frequencies for the same configuration are different and the patterns of different configurations are different. Table 3.2 shows the difference of main beam direction steering (azimuth angle- ϕ , elevation angle- θ) for all four different configurations. It demonstrates that the multi pattern reconfigurability goal has been achieved.



(1) Gain and Directivity of Configuration (a) at 1.92 GHz and 2.11GHz



(2) Gain and Directivity of Configuration (d) at 1.92 GHz and 2.11GHz

Figure 3.24 (1)(2) The simulated radiation pattern of Configuration (a) and Configuration (d)

Generally, in all four configurations, the efficiencies of the antenna array are more than 66.0%. In Configuration (a), the directivity and gain at 1.92GHz are 7.925dB and 6.118 dB, respectively, and at 2.11GHz are 6.994dB and 5.386dB, respectively. In Configuration (d), the directivity and gain change to 7.518dB and 5.848dB at 1.92GHz and are 6.955dB and 5.411dB at 2.11GHz. Also as can be seen from Table 2, the maximum radiation

direction changed for different configurations at the same working frequency after corners are slotted on the patch.

TABLE 3.2 PARAMETER VALUES OF THE RADIATION PATTERN OF PORPOSED ANTENNA

	E_MAX	Theta_max	Phi_max
Configuration (a) 1.92GHz	0.722	5	357
Configuration (a) 2.11GHz	0.672	29	357
Configuration (b) 1.92GHz	0.757	7	358
Configuration (b) 2.11GHz	0.687	29	357
Configuration (c) 1.92GHz	0.718	5	356
Configuration (c) 2.11GHz	0.696	23	358
Configuration (d) 1.92GHz	0.758	7	358
Configuration (d) 2.11GHz	0.720	26	358
	D_MAX	Gain_MAX	Efficiency
Configuration (a) 1.92GHz	7.925	6.118	66%
Configuration (a) 2.11GHz	6.994	5.386	68.8%
Configuration (b) 1.92GHz	7.492	5.821	68.1%
Configuration (b) 2.11GHz	7.089	5.476	69%
Configuration (c) 1.92GHz	7.873	6.077	66.1%
Configuration (c) 2.11GHz	6.804	5.285	70%
Configuration (d) 1.92GHz	7.518	5.848	68.1%
Configuration (d) 2.11GHz	6.955	5.411	70.1%

3.4 Fabrication and measurement of the proposed patch antenna array

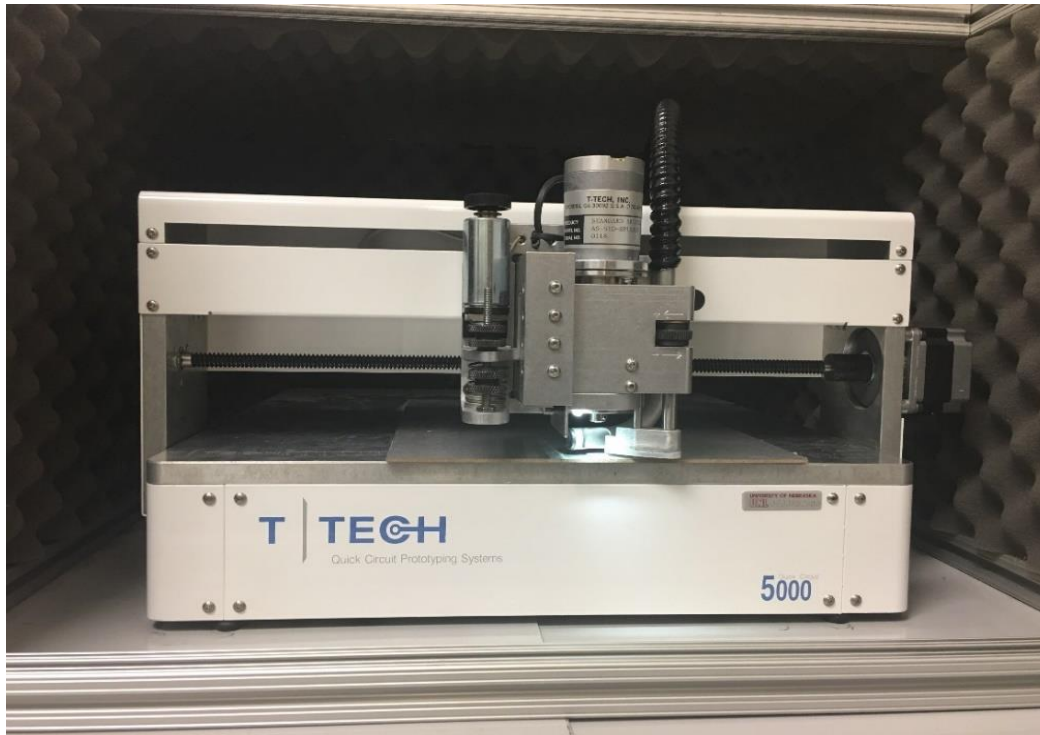


Figure 3.25 T Tech Mill Machine used to fabricate proposed antenna array

Figure 3.25 shows the mill machine used to build the proposed patch antenna array. The system was built based on Configuration (d). Figure 3.26 shows the photo of array antenna we built based on Configuration (d) with four PIN diodes and a RF choke. It is constructed on an RO4350B substrate with 1.52-mm thickness and dielectric constant of 3.48 and sized 208mm \times 135mm.

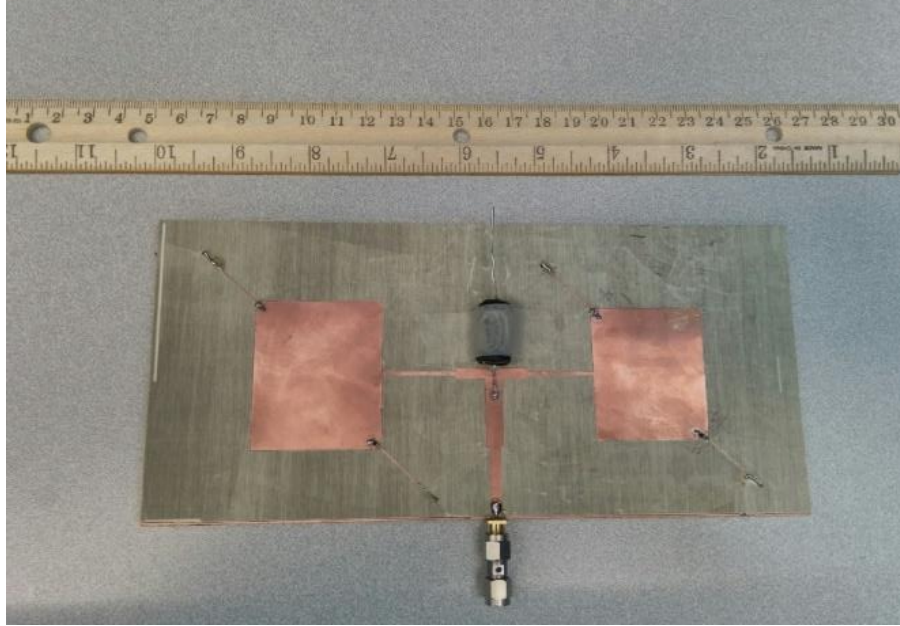


Figure 3.26 Photograph of the proposed antenna array

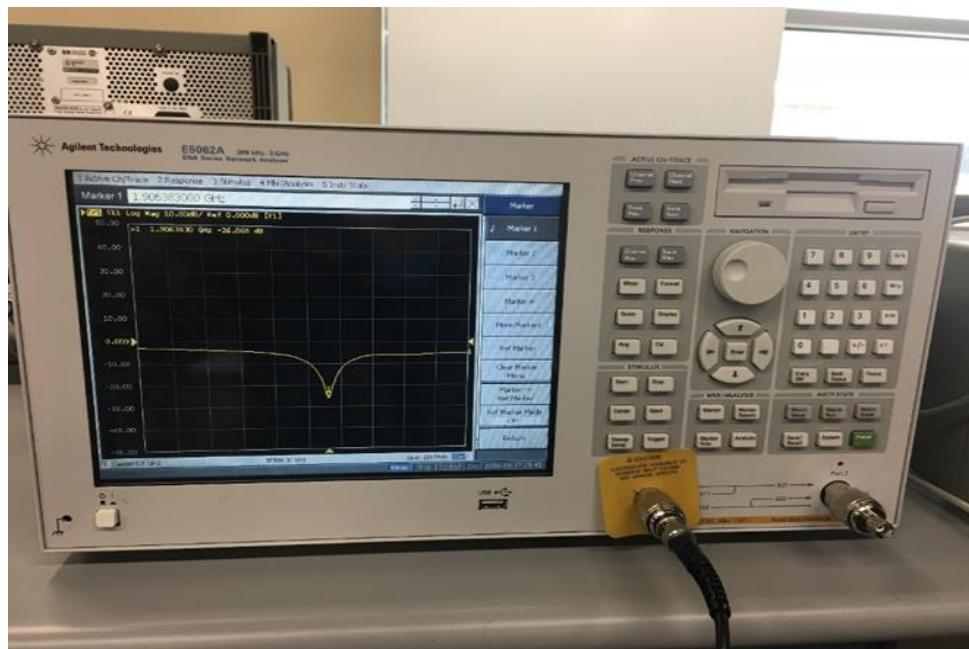


Figure 3.27 Agilent network analyzer used to measure the proposed antenna array

Figure 3.27 shows the measurement process of return loss of the proposed antenna array. To determine how the added PIN diodes with soldering residue and DC voltage impact the return loss of our array antenna, this proposed Configuration (d) array antenna was

measured with and without PIN diodes and DC voltage, shown in Figure 3.28. The blue, dashed line represents the measured return loss of Configuration (d) without PIN diodes and DC voltage. When all the diodes are at on-state, the antenna array works like Configuration (a), and when all the diodes work at off-state, the antenna array works like Configuration (d). The red curve of Figure 3.28 represents the measured return loss of Configuration (d) with all the PIN diodes at off-state, at that moment, the whole antenna system was supposed to work like configuration d. There is almost no frequency shift between the blue, dashed line and the red line, which matches well with theory. The black line of Figure 3.28 represents the measured return loss of Configuration (d) with all the PIN diodes at on-state, at that moment, the whole antenna system was supposed to work like configuration a. Because at this moment all four truncated corners have been connected to the antenna system, the radiation area has been increased and the resonant frequency shifted to a lower value, which also matches well with theory.

In order to investigate the differences of return loss of the proposed antenna between measurement and simulation, the measured and simulated return losses of proposed antenna array were compared, as shown in Figure 3.29. Based on Figure 3.29, it is observed that the antenna array performs well in both working frequencies. The measured return losses for PIN diodes in the on-state are -23.7dB and -18.26dB, corresponding to their resonant frequencies of 1.855GHz and 2.049GHz, respectively. The measured return losses for PIN diodes in the off-state are -24.8dB and -17.89dB, corresponding to their resonant frequencies of 1.865GHz and 2.060GHz, respectively. The discrepancies in frequency (about 50 Mhz) between simulation and measurement are largely attributed to fabrication errors and soldering residue. Regarding the measurements of Configuration (d) without all

PIN diodes soldered-on and with all PIN diodes at off-state, there is about 10 dB difference of return loss, but the working frequency remains nearly the same. Further research in the near future is called for in order to determine if this has an impact on antenna pattern.

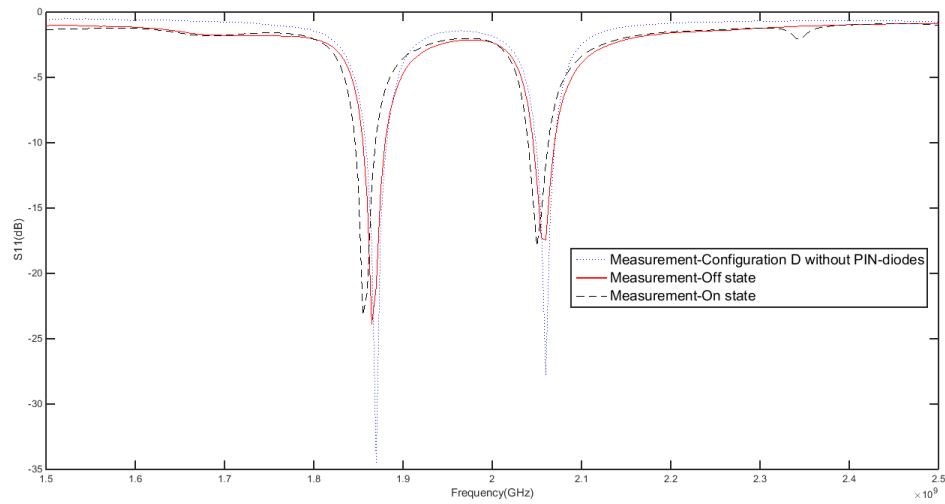


Figure 3.28 Comparison of measured return loss of Configuration (d) with and without PIN diodes

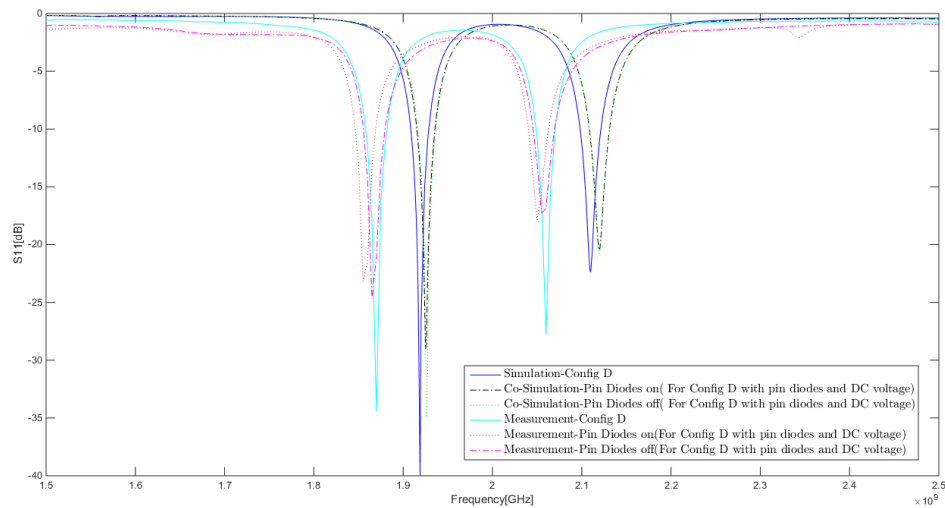


Figure 3.29 Return loss for the antenna array in different working Configurations between simulation and measurement

3.4 Summary

In this chapter, a novel dual-frequency antenna array with multiple pattern selectivities is proposed. A single-feed switchable network was used as a basic beam pattern reconfigurability structure for this dual-frequency antenna array. The slotted corners on the patch, together with the states of the PIN diodes give this antenna array more freedom of pattern changeability. The measured bandwidth of the return loss below -10 dB for on-state is about 25 MHz and for the off-state is also nearly 25 MHz at two different working frequencies. This pattern reconfigurable patch antenna array can be applied in the wideband code division multiple access system.

Chapter 4. A Proposed Pattern and Frequency Reconfigurable Yagi-Uda Patch Antenna

4.1 Introduction

Currently, for particular applications, directional antennas such as log periodic and Yagi-Uda antennas are needed. These types of antennas have been widely used in applications such as industrial, medical, radar, wireless communications and even bioscience. The single microstrip Yagi-Uda antenna was first developed by J. Huang at Jet Propulsion Laboratory [37]. His proposed antenna consisted of four patches that were electromagnetically coupled to each other, and had the maximum gain of 8dBi while the front to back (F/B) ratio was low. The microstrip Yagi-Uda array usually consists of a driven microstrip antenna element, along with many parasitic microstrip elements which are placed on the same substrate surface in such a way to enhance the overall antenna characteristics [38] [39]. In [39] a design of Wide-Band Microstrip Yagi-Uda antenna with high gain and high F/B ratio is presented. This design is interesting and inspiring. In [40], a slot-loaded Yagi patch antenna with dual-band and pattern reconfigurable characteristics was proposed. It consists of one driven patch and four parasitic patches with special slots, and by controlling 12 switches which have been placed in the slots, the reconfigurable characteristics of the proposed microstrip Yagi antenna can be obtained. In [41], a linearly polarized Yagi-Uda patch antenna that consists of rectangular parasitic elements is presented. In that study, the impact of shorting location or switching location on the performance of beam tilt angle and return loss performance was investigated. In [42], a linear phased array with reconfigurable dynamic Yagi-Uda patch antenna (RDYPA) elements is proposed. For this design, three array modes can be obtained by adjusting the

states of array elements. Presented in [43] is a low-profile, broadly steerable, and reconfigurable array antenna with parasitic patches. This design used only a single-layered substrate and six switches to introduce five directive beam patterns with the maximum beam tilt angle of 50 degrees in its steering mode, and high gain. This kind of antenna configuration shows many advantages over a single patch antenna, which in particular increases the directivity. The Yagi-Uda configuration makes the beam peak away from vertical direction and tilt in the end-fire direction. Unlike traditional phase arrays, there are no additional circuit elements such as power dividers or switchable phase delay transmission elements that introduce additional loss.

In this chapter, we present a novel design of Yagi-Uda patch antenna with frequency and pattern selectivity. The proposed antenna is designed to operate around the 1.9 GHz band and 2.41 GHz band, which is used in LTE and Wi-Fi networks respectively. Our proposed antenna consists of two reflector elements, a driven element and six director elements. We used four metal pieces to replace PIN diodes in simulation and measurement works in order to easily validate our design. Two stubs connected to the driven element were used to improve the return loss performance when working at 2.41 GHz. The simulation and measurement results closely agree.

4.2 Design of the Proposed Reconfigurable Yagi-Uda Patch Antenna

4.2.1 Antenna Schematic

Figure 4.1 shows the proposed microstrip Yagi-Uda antenna that consists of nine patches with its feeding structure. There are two reflectors, each with dimensions $W4 \times L3$, six directors, each with dimensions $W5 \times L4$ and one driven patch with dimensions $W1 \times L1$.

Four metal pieces, which were used to replace PIN diodes, all with same dimensions (0.9mm×1mm) are shown as small brown rectangles in Figure 4.1. The optimized values for our design to get the best performance are shown in Table 4.1

TABLE 4.1 PARAMETER VALUES OF THE PROPOSED ANTENNA

W1	29.5mm	W2	22.3mm	W3	2.72mm	W4	18mm	W5	30.5 mm
L1	48.5mm	L2	6.5mm	L3	10.5mm	L4	40mm	H1	2.21mm
H2	7.73mm	H3	13.24mm	G1	1mm	G2	0.8mm		

4.2.2 Design of Proposed Frequency Reconfigurable Antenna

(1) Concept of Patch Antennas with Switchable Slots

A basic patch antenna with a switchable slot (PASS) structure is shown in Figure 4.2. The patch dimensions are $L \times W$. The antenna was fabricated on a dielectric substrate with dielectric permittivity ϵ_r , and thickness h . A probe was located at (X_f, Y_f) as the feeding port to excite the TM_{10} mode. A slot with length L_s , width W_s , and position P_s , was incorporated into the patch. A switch was placed in the center of the slot to control its configuration. The switch can be either a PIN diode, or a MEMs-based switch [44].

The frequency shift for the basic PASS structure can be explained by investigating the surface electric currents of the patch antennas. When the switch is in the OFF mode, the surface electric currents on the patch have to flow around the slot, as shown in Figure 4.3 (a), resulting in a relatively greater length of the current path. Therefore, the antenna resonates at a lower frequency. In contrast, when the switch is in the ON mode, part of the electric current can go directly through the switch, and part of the electric current will still flow around the slot, as shown in Figure 4.3 (b). In this case, the average length of the current path is relatively shorter, so that the antenna has a higher resonant frequency. As

the result, PASS show different resonant features based on different states of the switch. It needs to be pointed out that when the switch is in the ON mode, a PASS structure still has a longer current-path length than the patch antenna without a slot. Thus, its resonant frequency should be lower than the patch antenna without a slot [44]. Because the higher working frequency of this frequency reconfigurable design is 2.41GHz, and we also know the resonant frequency of an antenna with slot is lower than the same antenna without slot anyway, we designed a basic patch antenna (Figure 4.4) with the resonant frequency 2.495GHz (Figure 4.5). The 2.495 GHz frequency allows us to insert a slot. For the basic design, the radiation patch has dimensions of 30.5 mm× 30.5 mm and the return loss is -23.523 dB at 2.495 GHz.

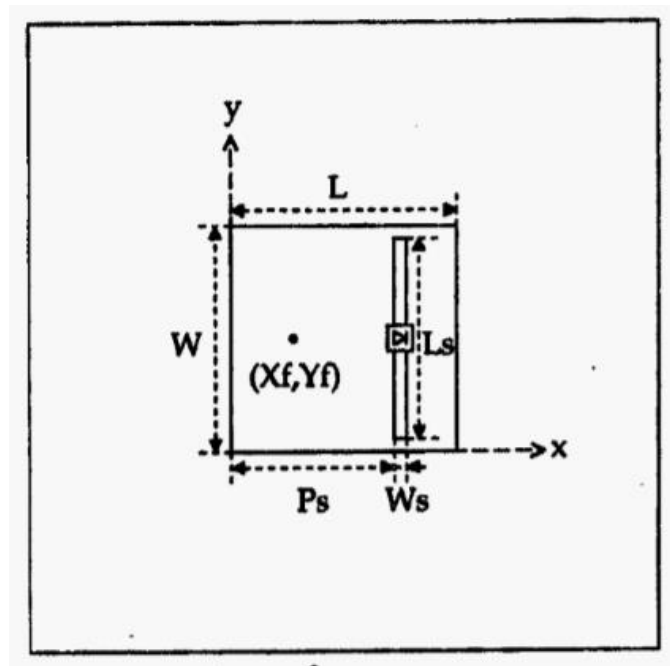


Figure 4.2 Geometry of a patch antenna with a switchable slot [44]

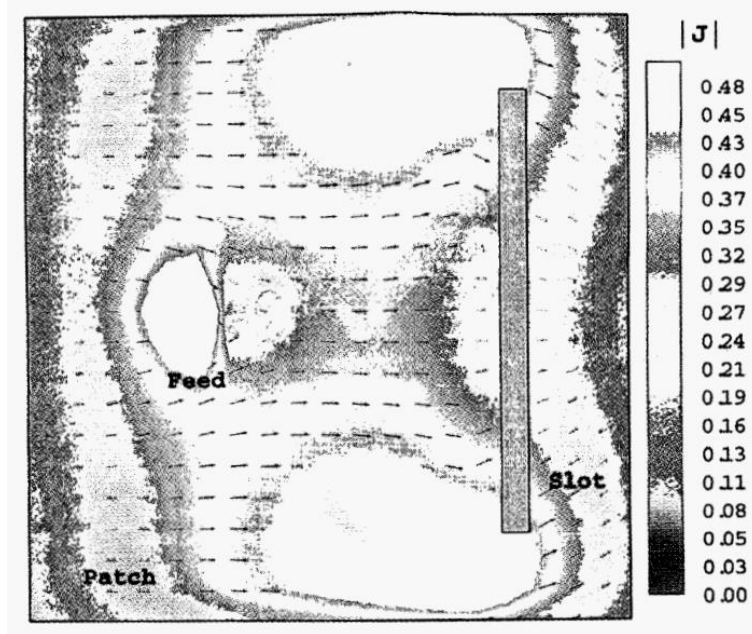


Figure 4.3 (a) Relative electric currents on patch antennas at their resonant frequencies with the switch OFF [44]

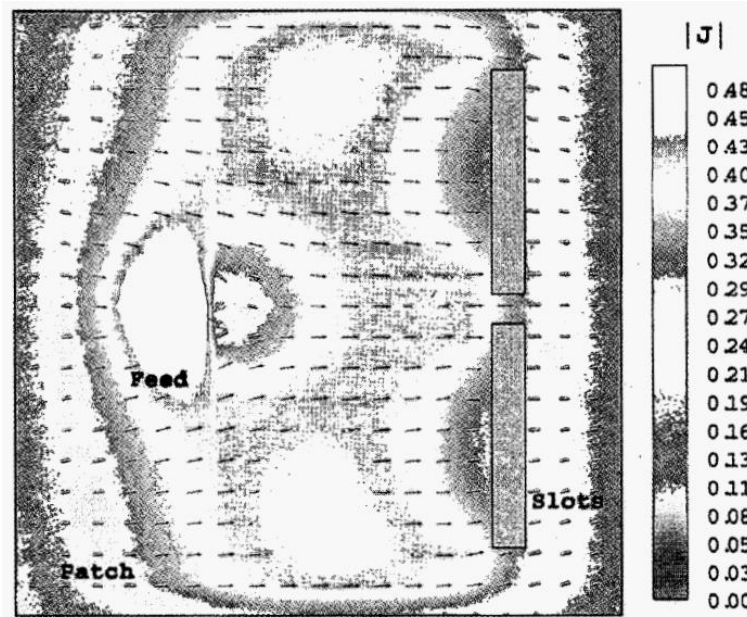


Figure 4.3 (b) Relative electric currents on patch antennas at their resonant frequencies with the switch ON [44]

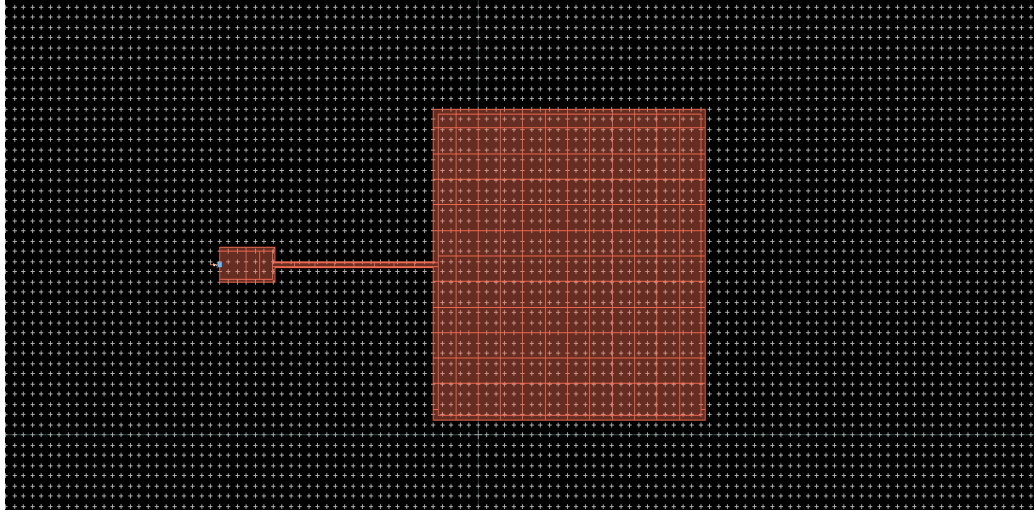


Figure 4.4 Layout design for the patch antenna with resonant frequency at 2.495GHz

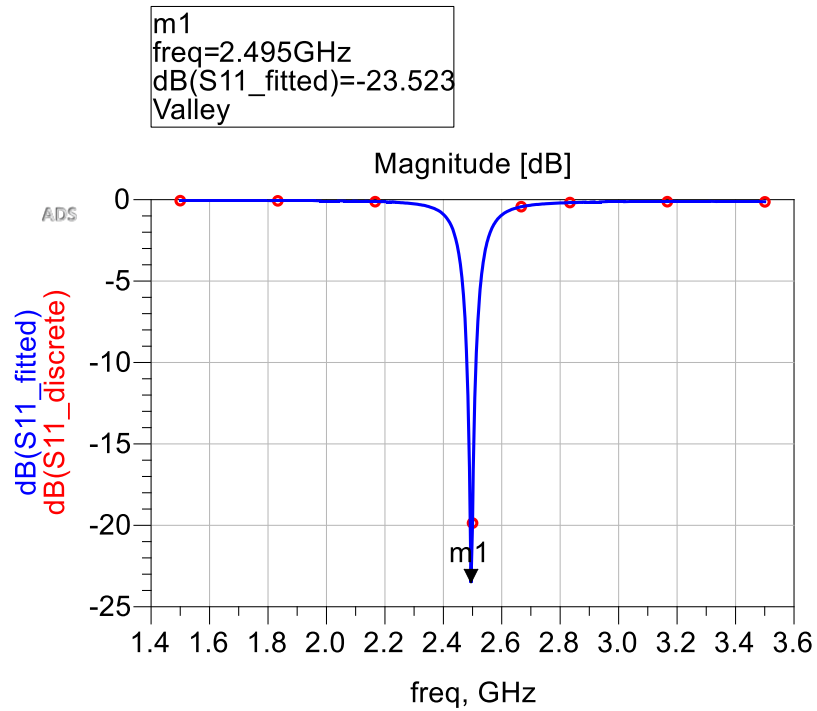


Figure 4.5 Return loss of the proposed 2.495GHz patch antenna

Then a slot was added to the basic 2.495GHz patch antenna design, as shown in Figure 4.6. The slot we added into this antenna is with the dimension of 26mm×1mm and it's 2.25mm to top and bottom side of the antenna, 7.75mm to the right side, 21.75mm to the left side.

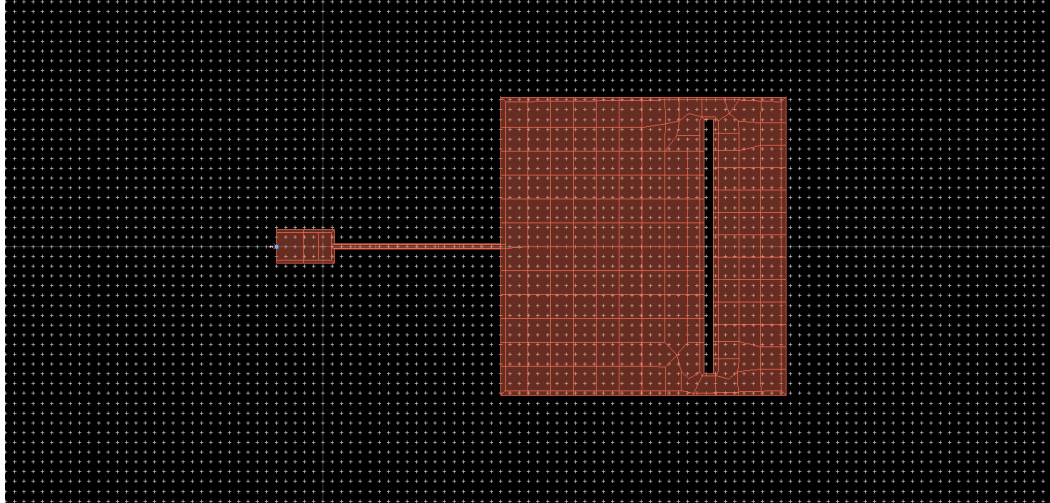


Figure 4.6 Basic antenna design with a slot

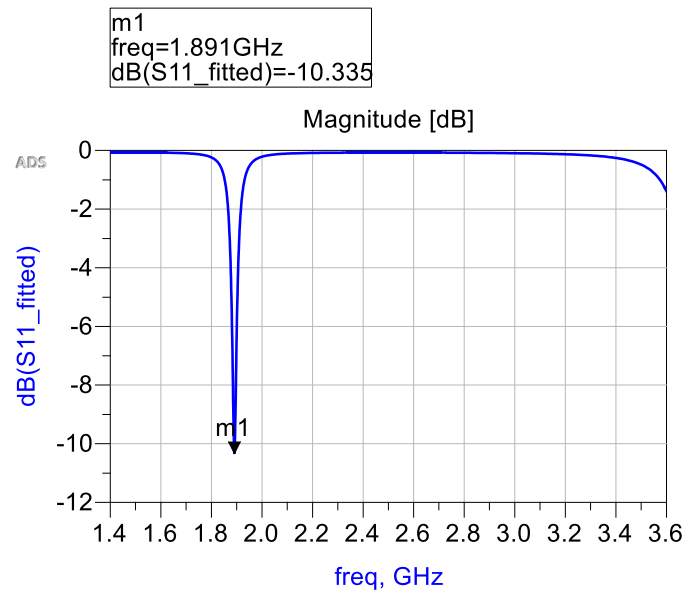


Figure 4.7 Return loss of a basic patch antenna with a slot

After the slot has been added into this single patch antenna, it can be observed from Figure 4.5 and 4.7 that the resonant frequency shifted from 2.495 GHz to 1.891 GHz. The added slot impacted a lot on the working frequency of patch antenna.

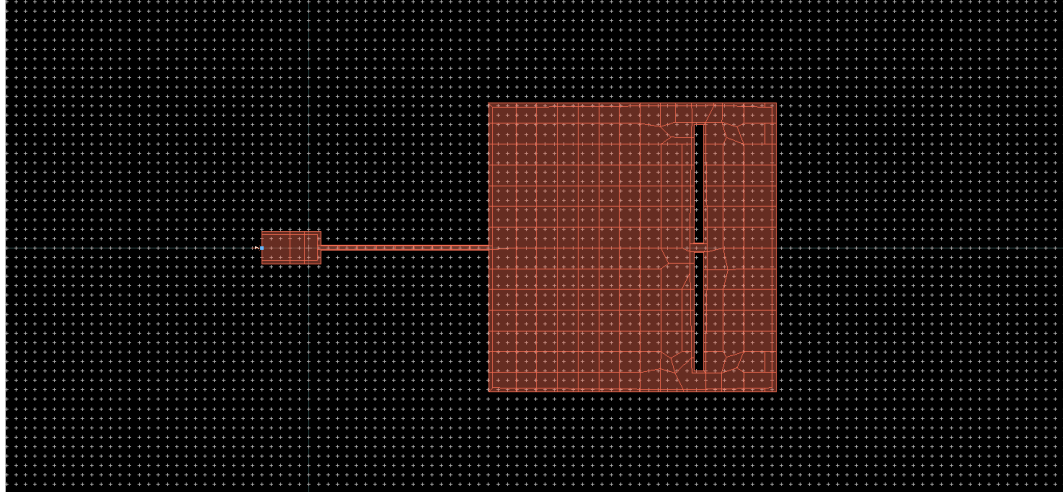


Figure 4.8 Basic antenna design with a metal piece in the center of slot

Then we inserted a metal piece to imitate on-state of PIN diode, shown in Figure 4.8. It can be observed in Figure 4.9 that the resonant frequency shifted to 2.256 GHz from 1.891 GHz with a return loss of -14.422 dB. This closely matched theory.

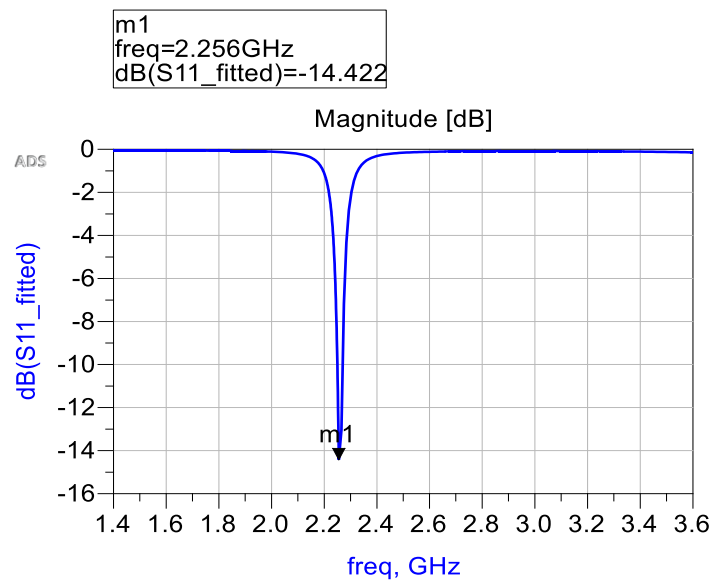


Figure 4.9 Return loss of a basic patch antenna with a metal piece in the center of slot.

Basically, when the slot length was increased, the resonant frequencies of the antenna decreased for both the ON and OFF modes of the switch.

For a PASS design, since the current distributions in the ON and OFF switch modes are different, the input impedances in the ON and OFF switch modes are different at the same feeding location. When the frequency ratio is small, the impedance difference is not significant. However, if the frequency ratio becomes larger, the PASS design may not get a good common match for both modes [44]. For this proposed Yagi-Uda patch antenna, the two expected working frequencies are 1.9 GHz and 2.41 GHz, so the frequency ratio is $2.4/1.9 = 1.26$. It's difficult to find a good common match point for two modes by using only one slot.

According to [44], this problem can be solved by balancing the currents to find a common matching position for both modes.

(2) The Impact of Parasitic Elements on Resonant Frequency of a Patch Antenna

The microstrip Yagi-Uda array usually consists of a driven microstrip antenna along with several parasitic elements which are arranged on the same substrate surface in such a way as to enhance the overall antenna characteristics. For our design, we planned to use two reflector elements, a driven element and six director elements. The parasitic elements, which includes all of the reflector and director elements, have impacts on the resonant frequency of this antenna system. Figure 4.10 shows the basic patch antenna with many parasitic elements.

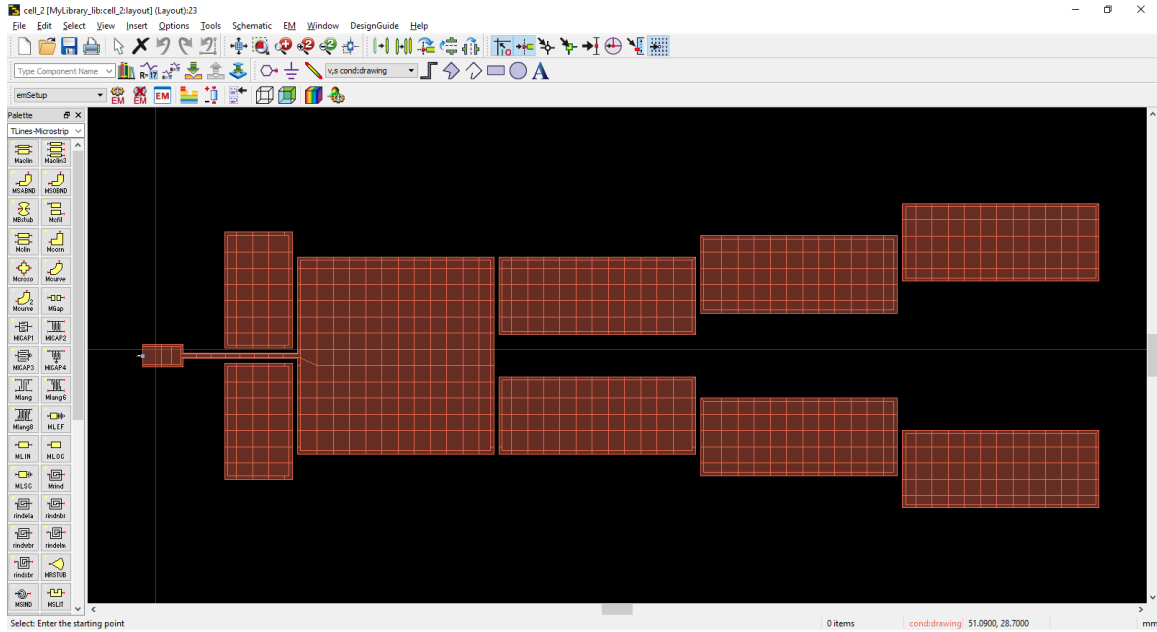


Figure 4.10 Basic patch antenna with parasitic elements

In Figure 4.10, the two reflector elements on the left of the driven element have the dimensions $18 \text{ mm} \times 10.5 \text{ mm}$, and the six director elements each have the dimensions $0.5 \text{ mm} \times 12 \text{ mm}$. The return loss of the antenna proposed in Figure 4.10 is shown in Figure 4.11, which shows a resonant frequency shift to 2.460 GHz from 2.495 GHz.

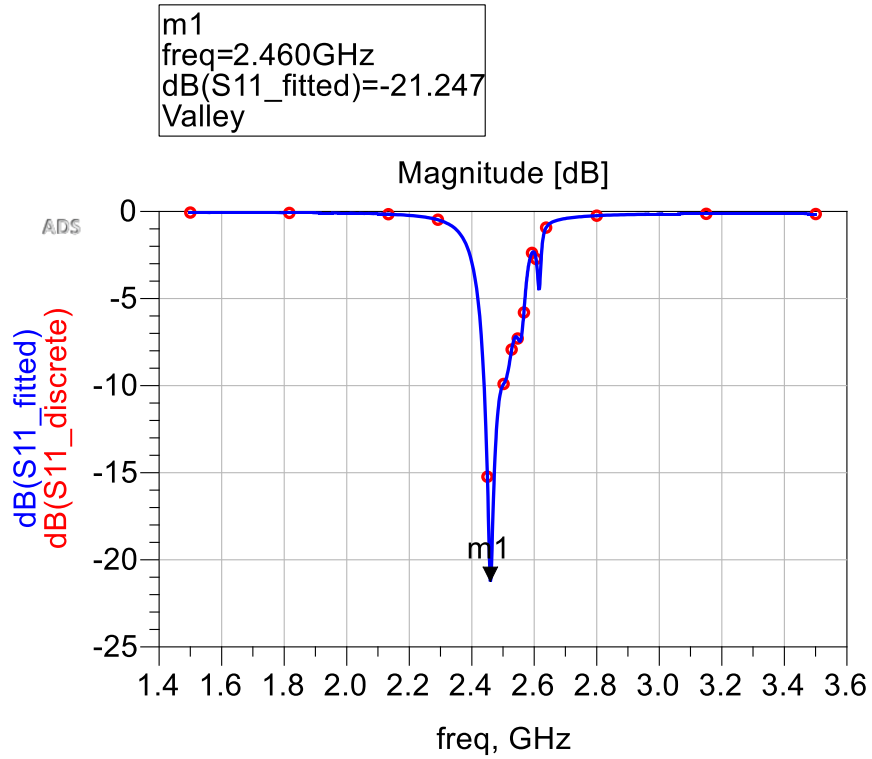


Figure 4.11 Return loss of the antenna proposed in Figure 4.10

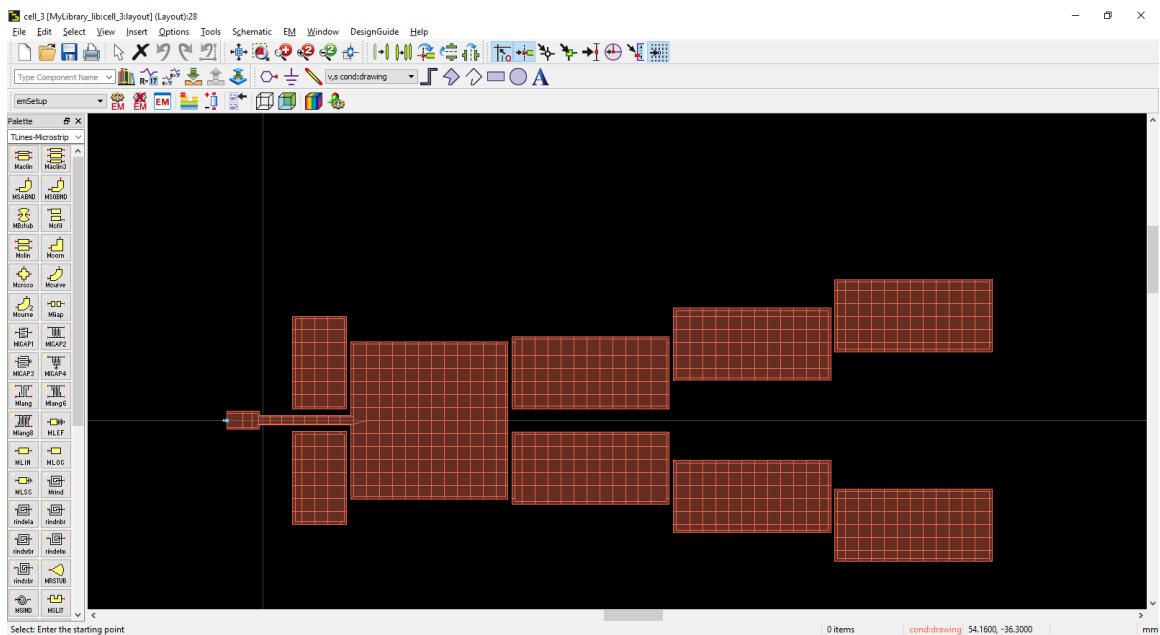


Figure 4.12 Antenna proposed in Figure 4.8 with increased-size director elements

Figure 4.12 shows the antenna which has been proposed in Figure 4.10 with increased size of director elements. The six director elements in Figure 4.12 each have the dimensions 30.5 mm \times 14 mm.

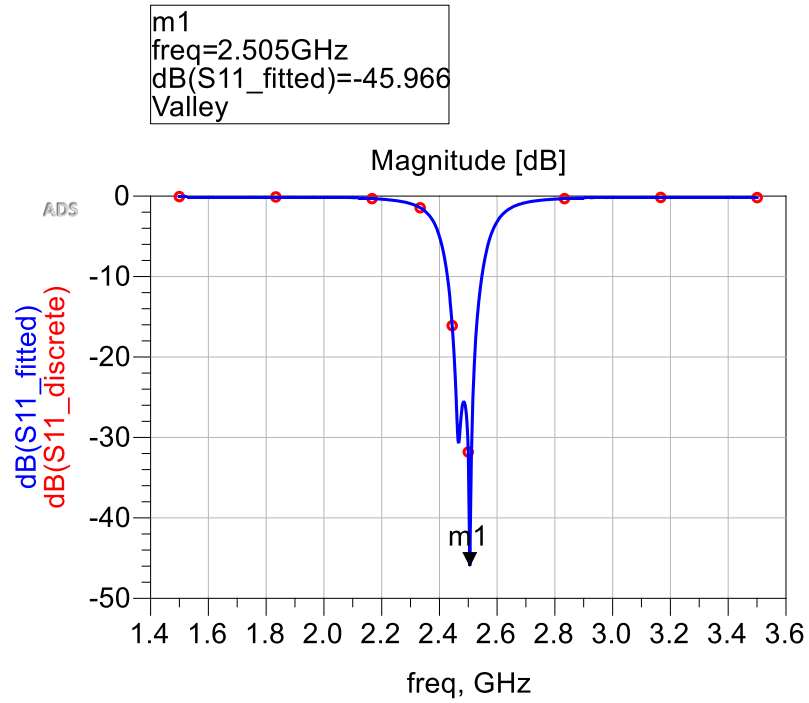


Figure 4.13 Return loss of antenna proposed in Figure 4.10

As can be observed from Figure 4.13, with the increased size of director elements, the resonant frequency shifts to 2.505 GHz from 2.460 GHz.

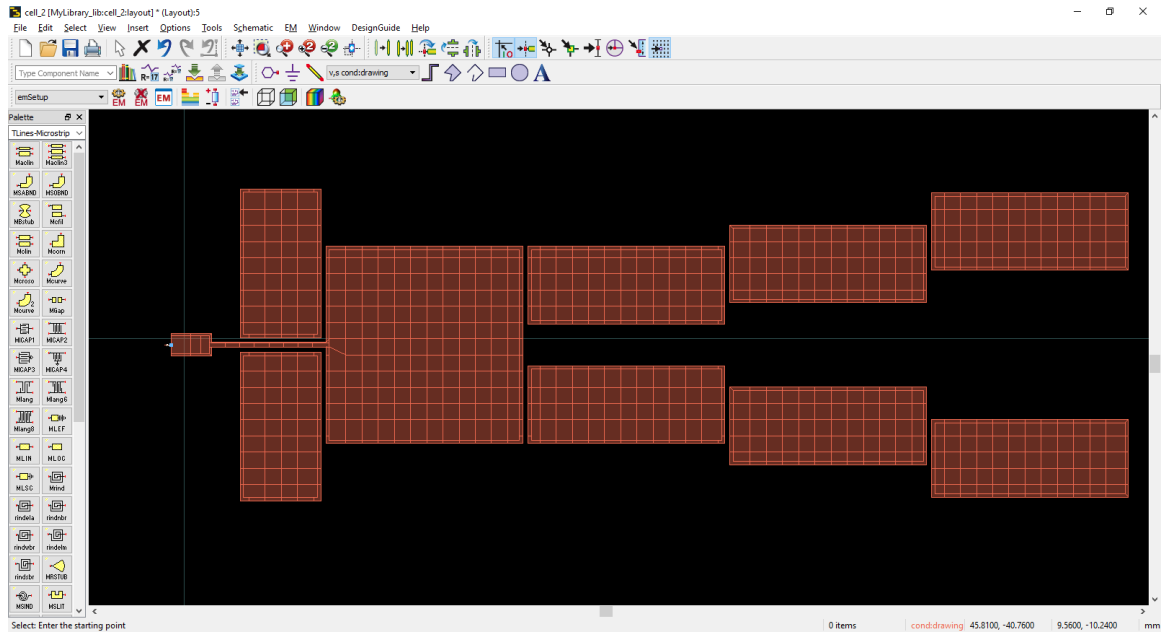


Figure 4.14 Antenna proposed in Figure 4.8 with increased-size reflector elements

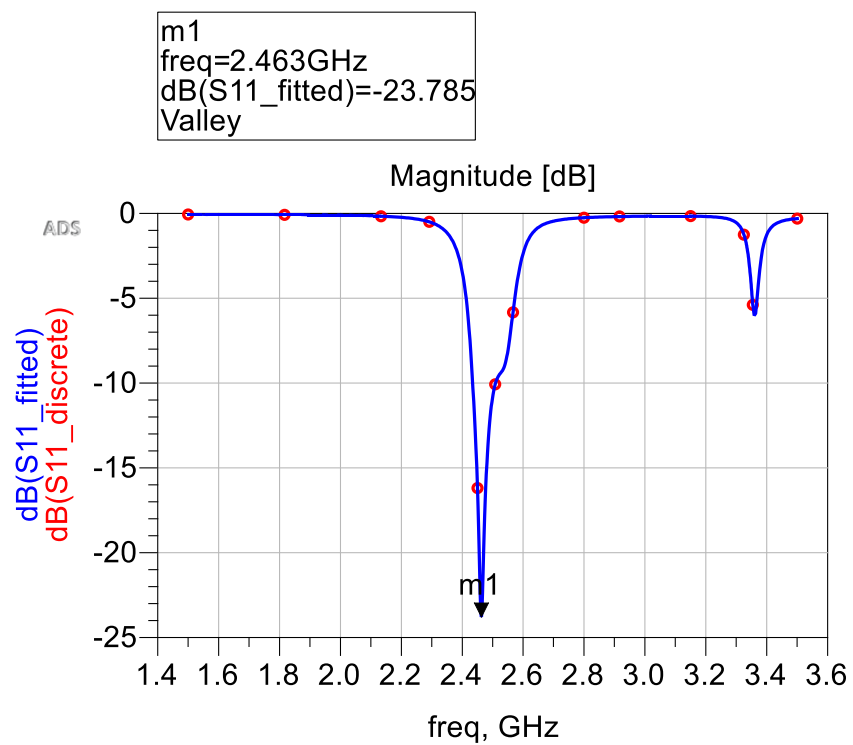


Figure 4.15 Return loss of antenna proposed in Figure 4.12

Figure 4.14 shows the proposed antenna in Figure 4.10 with an increased size of reflector elements. The two reflector elements in Figure 4.14 each have dimensions 23 mm × 12mm.

As shown in Figure 4.15, with the increased size of reflector elements, the resonant frequency shifts to 2.463 GHz from 2.460 GHz.

In conclusion, the frequency reconfigurability must be achieved by considering both the impact of parasitic elements and the slot. The frequency shift caused by the increased size of reflector and director is much smaller than frequency shift caused by slot.

(3) Our Method to Achieve Frequency Reconfigurable

Recall that in PASS theory, if the frequency ratio of two different working frequencies becomes larger, the PASS design may not get a good match for both modes, and slot implementations need to be carefully considered. For our proposed Yagi-Uda patch antenna, the two expected working frequencies are 1.9GHz and 2.4 GHz, and the frequency ratio is $2.4/1.9 = 1.26$. It is difficult to find a good match point for two modes by using only one slot. We chose to use two switchable slots in the antenna to obtain a good match for both modes and proved this is an effective method. The greatest challenge is finding a commonly matched position for both the switch's ON and OFF modes under the effect of parasitic elements. Because input impedance can be vary greatly with different modes, this method required many simulations.

A common good matching point is dependent on the dimensions of two slots and their positions. A great number of simulations have been carried out to find the proper parameters.

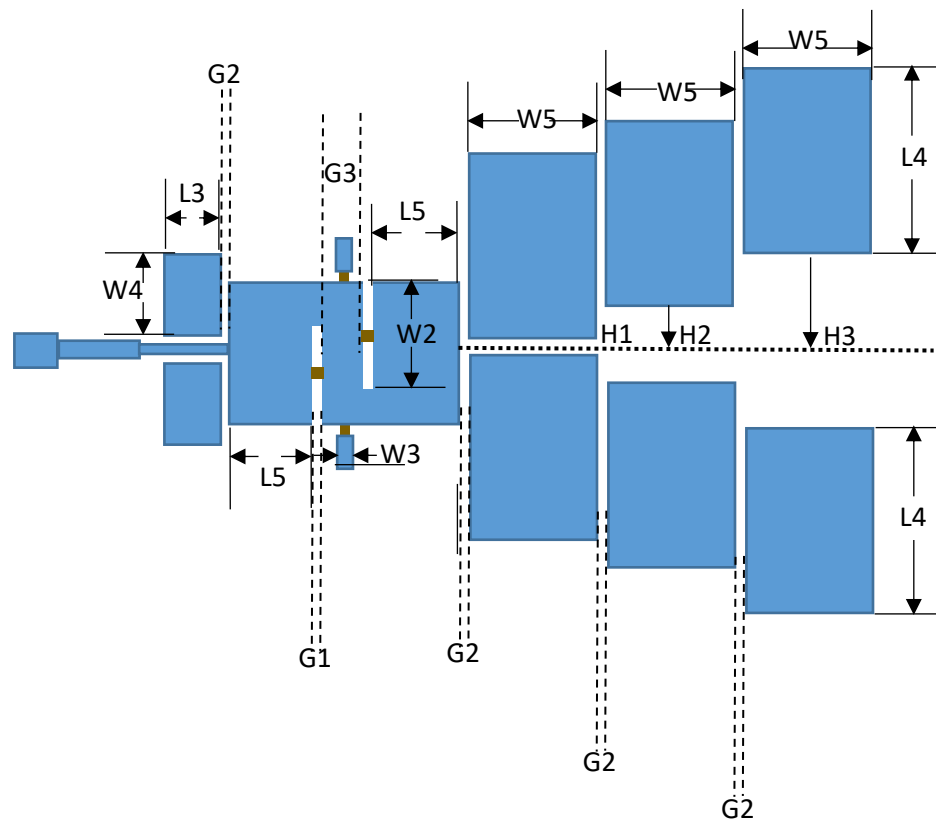


Figure 4.16 Geometry of Proposed Reconfigurable Yagi-Uda Patch Antenna

Figure 4.16 shows the final design for the proposed pattern and frequency reconfigurable Yagi-Uda patch antenna. Based on our simulations, the gap ($G3$) between two slots has been set to 10.5 mm, the distance ($L5$) between slot and radiation edge has been set to 18 mm. The corresponding parameters are shown in Figure 4.16. The size of the two slots has been set to $22.3\text{mm} \times 1\text{mm}$ ($W2 \times G1$). The size of the six director elements are set to be $30.5\text{mm} \times 40\text{mm}$ ($W5 \times L4$), and the size of two reflectors are be set to $18\text{mm} \times 10.5\text{mm}$ ($W4 \times L3$). The size of driven element has been adjusted to $48.5\text{mm} \times 29.5\text{mm}$.

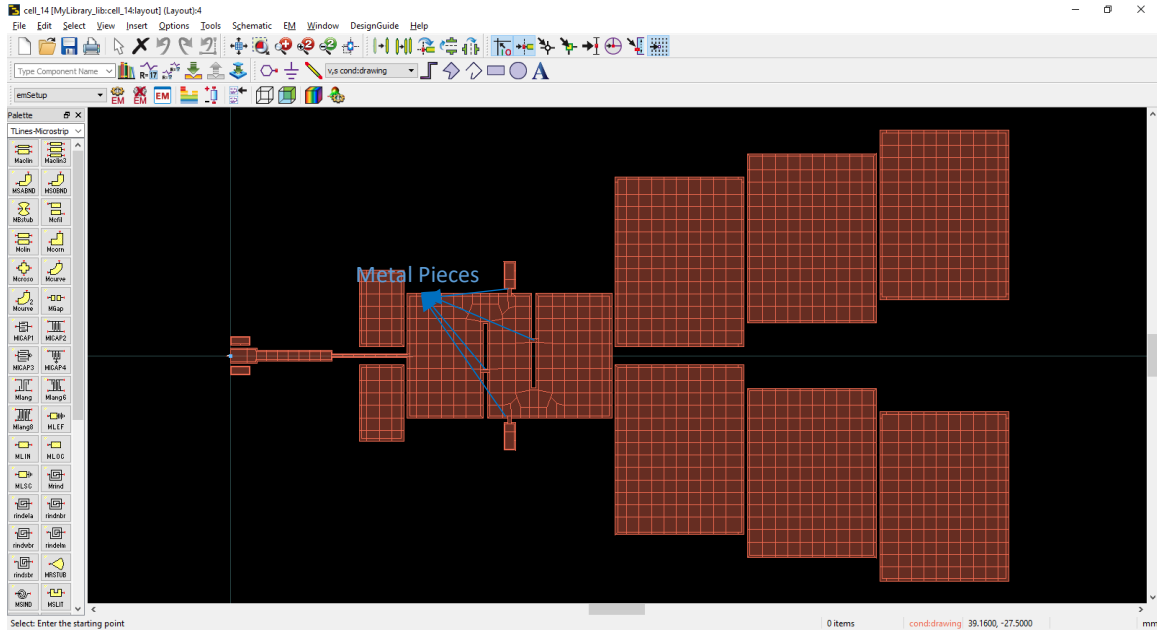


Figure 4.17 Layout simulation for proposed antenna with four metal pieces

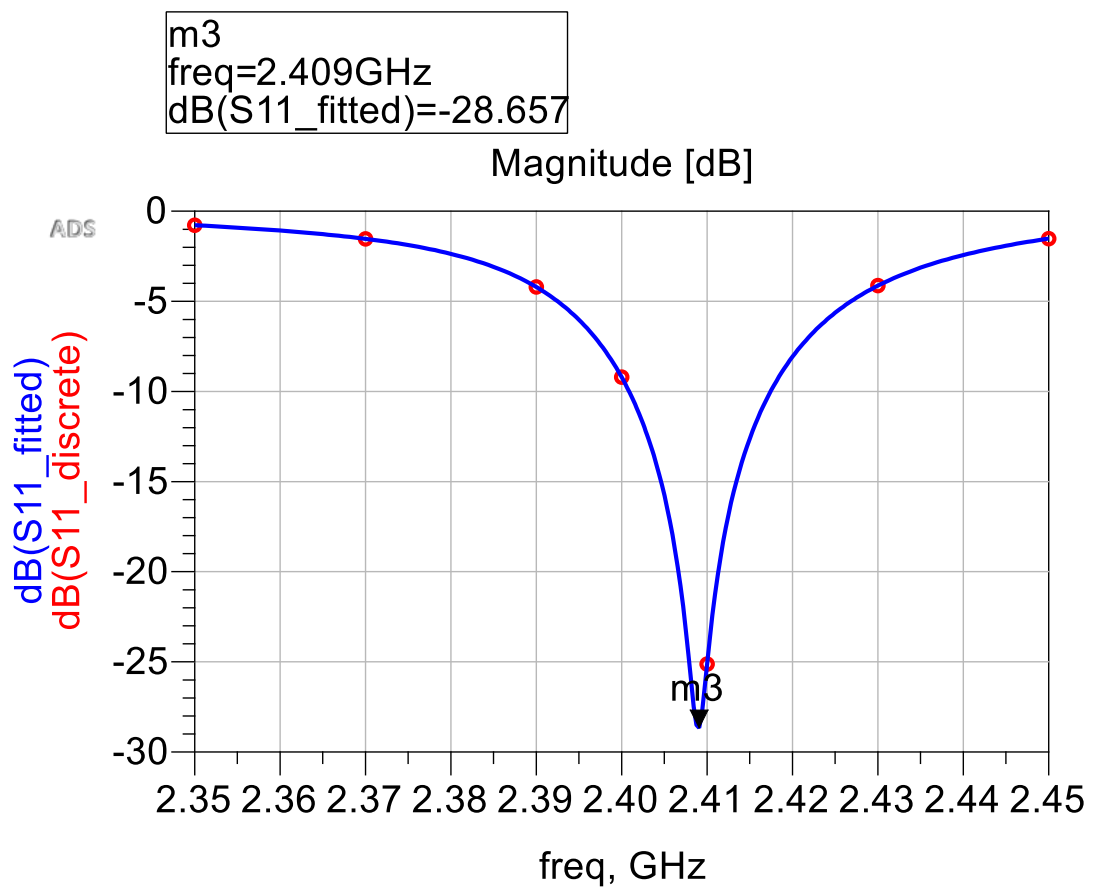


Figure 4.18 Simulated return loss for proposed antenna with four metal pieces

Figure 4.17 shows the 2.41GHz mode of proposed Yagi-Uda reconfigurable patch antenna (showing with all four metal pieces). Figure 4.18 shows the return loss performance for proposed antenna with four metal pieces. It can be observed that the band below-10 dB is about 20MHz, and at the resonant point 2.409 GHz, the return loss is -28.657dB.

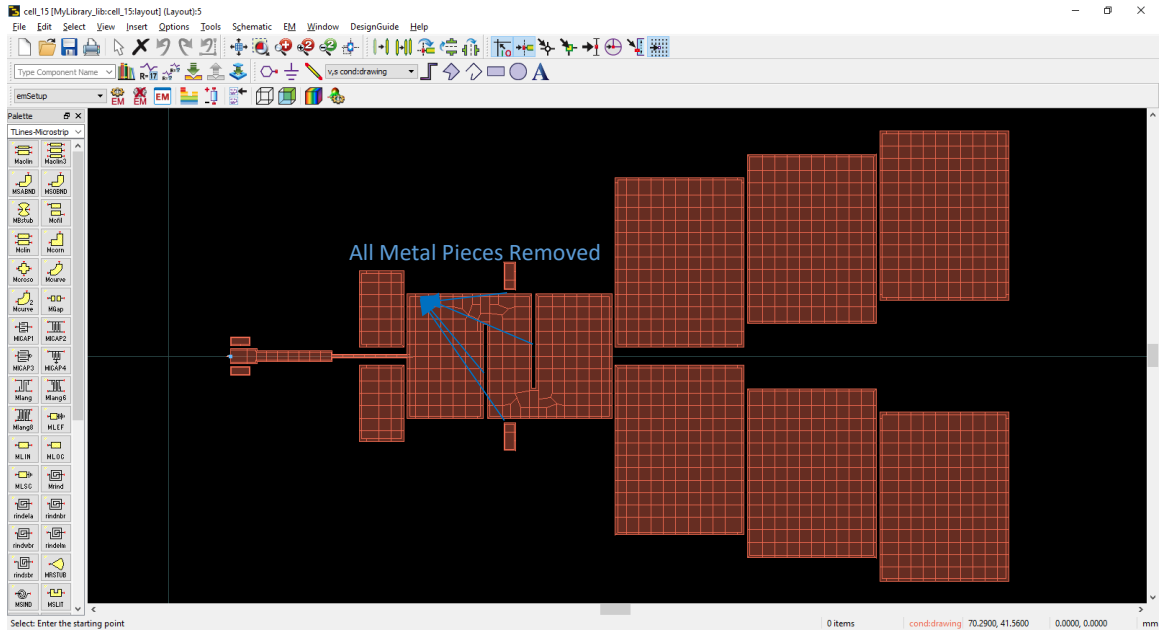


Figure 4.19 Layout simulation for proposed antenna without four metal pieces

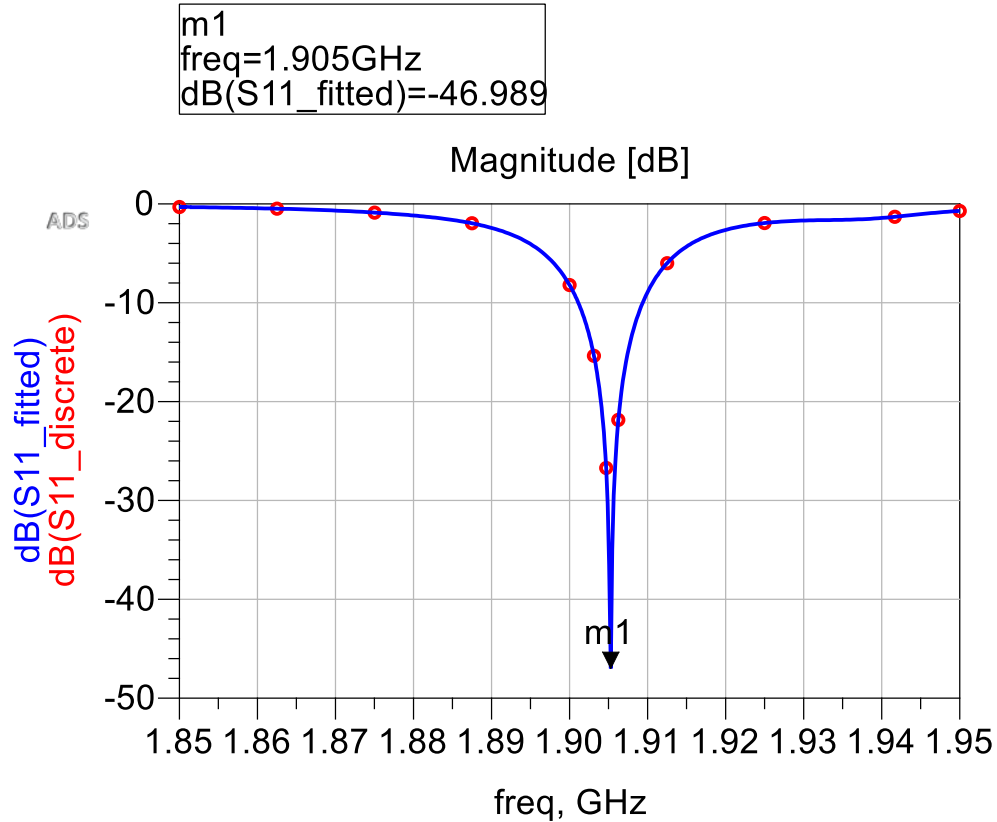


Figure 4.20 Simulated return loss for proposed antenna without four metal pieces

Figure 4.19 shows the 1.90 GHz mode of proposed Yagi-Uda reconfigurable patch antenna (showing without all four metal pieces). Figure 4.20 shows the return loss performance for proposed antenna with four metal pieces. It can be observed that the band below-10 dB is about 10 MHz, and at the resonant point 1.905 GHz, the return loss is -46.989 dB.

Compared to Figure 4.17, in Figure 4.19, all four metal pieces, which were used to replace PIN diodes, have been removed (equivalent to the off-state of all PIN diodes, meaning 1.90GHz mode of proposed antenna). Based on Figure 4.18 and 4.20, it can be observed that two resonance frequencies are at 2.409 GHz and 1.905GHz, with return loss are -28.657 dB and -46.989 dB, respectively. A very good commonly matching point has been found through multiple simulations. It also can be observed that the band below-10

dB is about 20MHz in Figure 4.18 and the band below-10 dB is about 10 MHz in Figure 4.20.

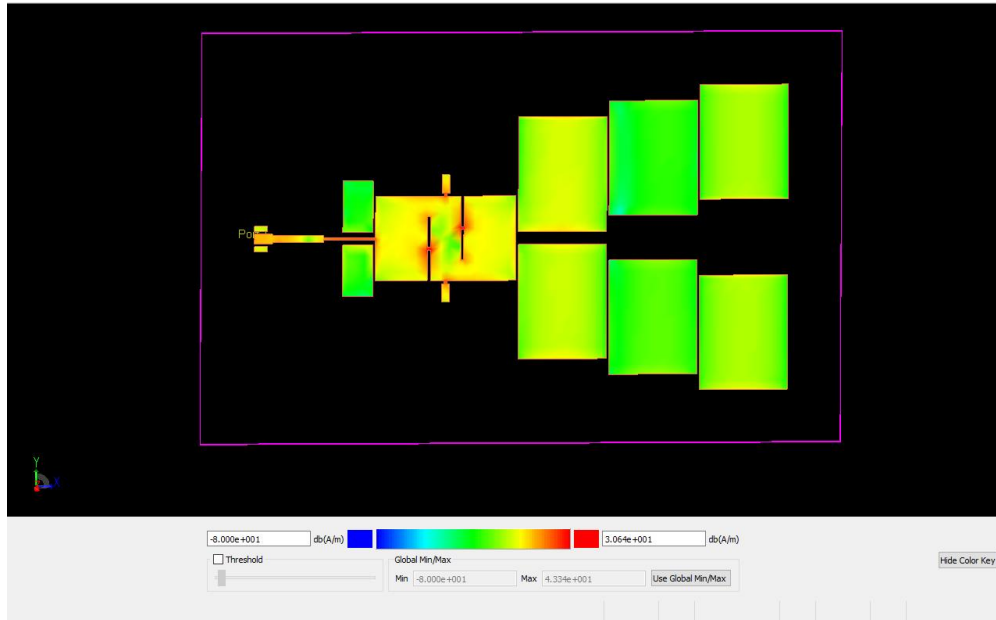


Figure 4.21 Surface Current Distribution for Antenna Working at 2.41GHz

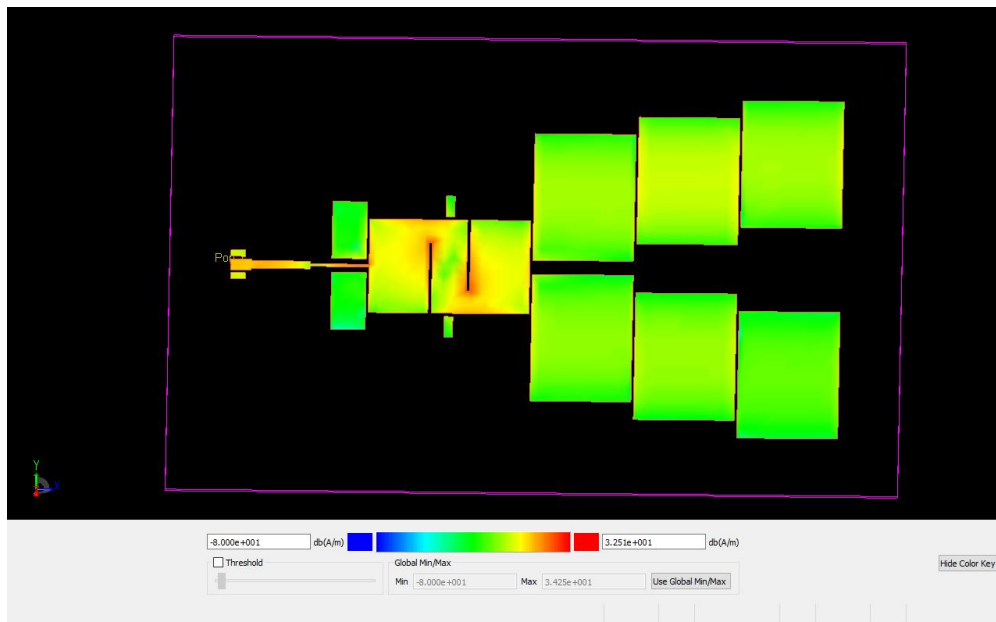


Figure 4.22 Surface Current Distribution for Antenna Working at 1.90GHz

Figure 4.21 and 4.22 show the surface current distribution for proposed antenna at two working frequencies. The effect of these slots and metal pieces can be observed from these two figures.

4.2.3 Pattern reconfigurable of proposed Yagi-Uda antenna

In early simulations, designs were found which worked at both required frequencies, as shown in Figures 4.23 and 4.26. However, the pattern and directivity for each of them were not good.

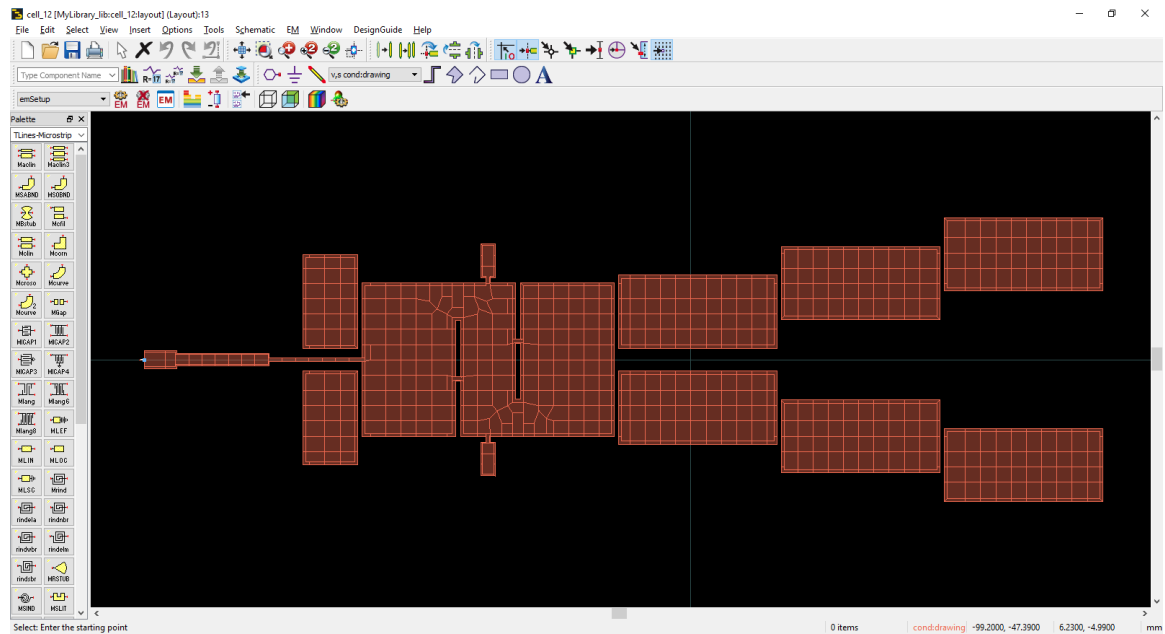


Figure 4.23 Early design of the proposed 2.41 GHz antenna

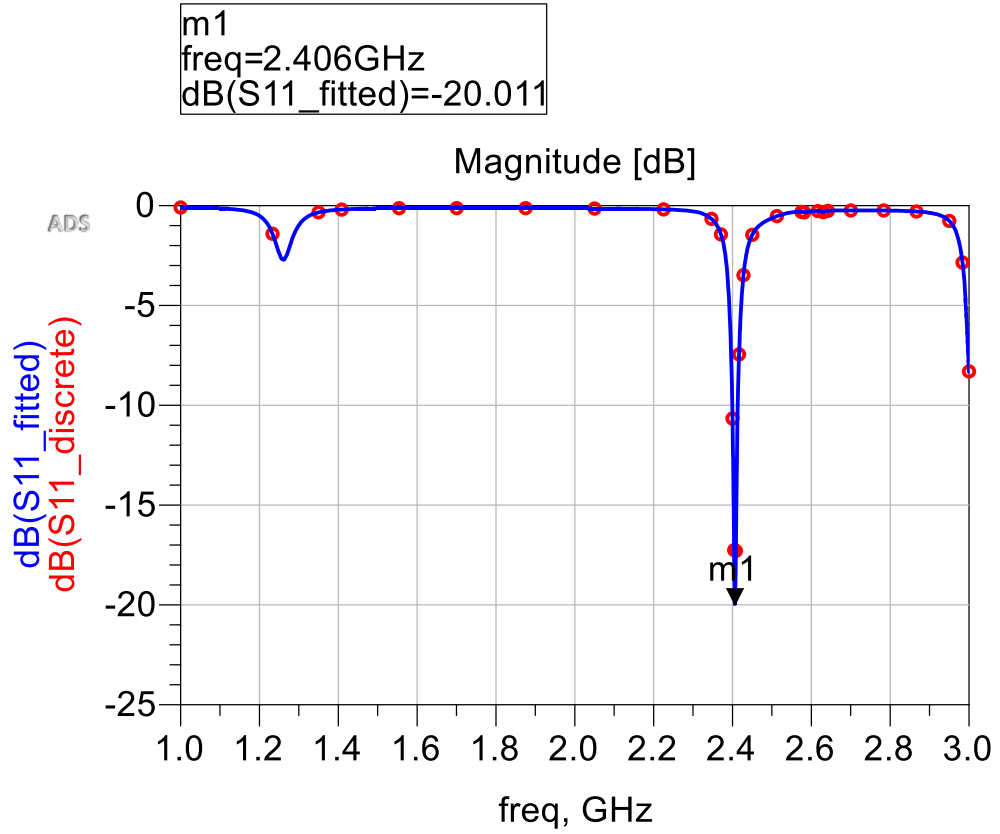


Figure 4.24 Return loss of early 2.41 GHz design

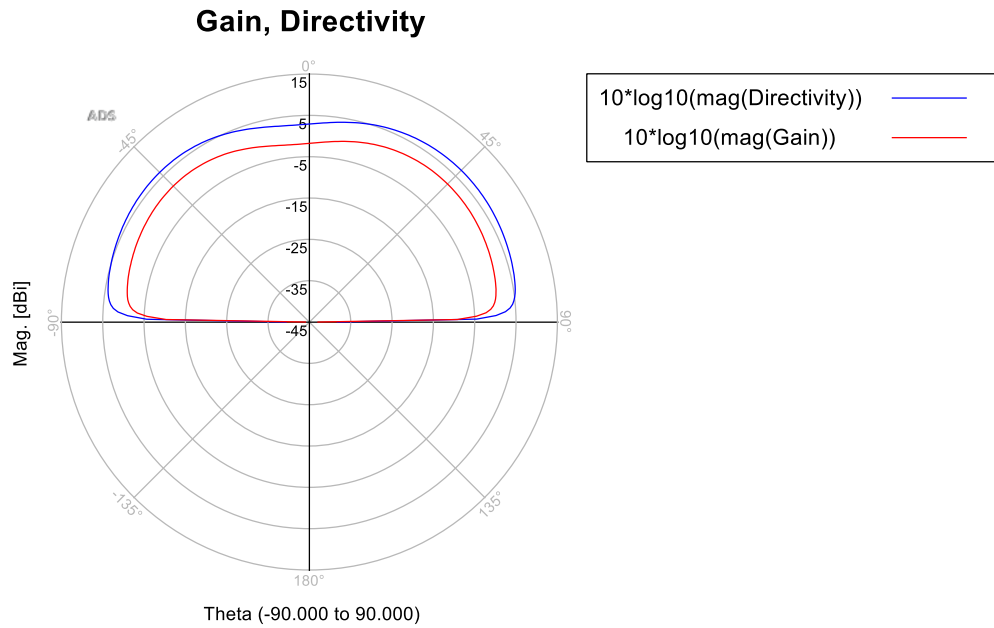


Figure 4.25 Pattern for the early 2.41 GHz design

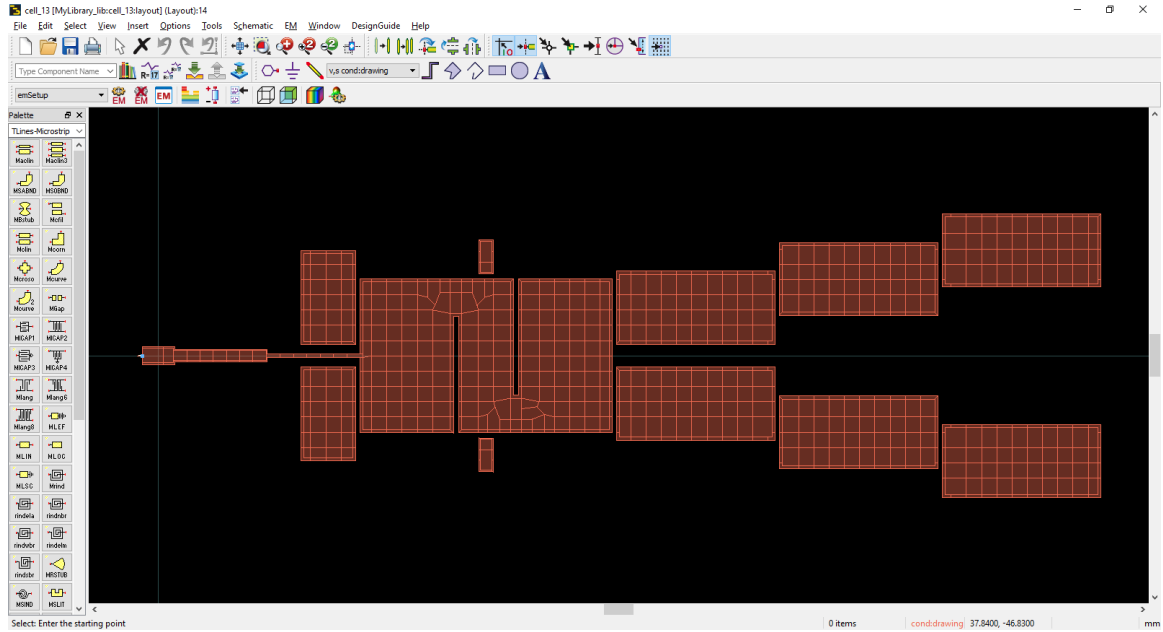


Figure 4.26 Early design of the proposed 1.90 GHz antenna

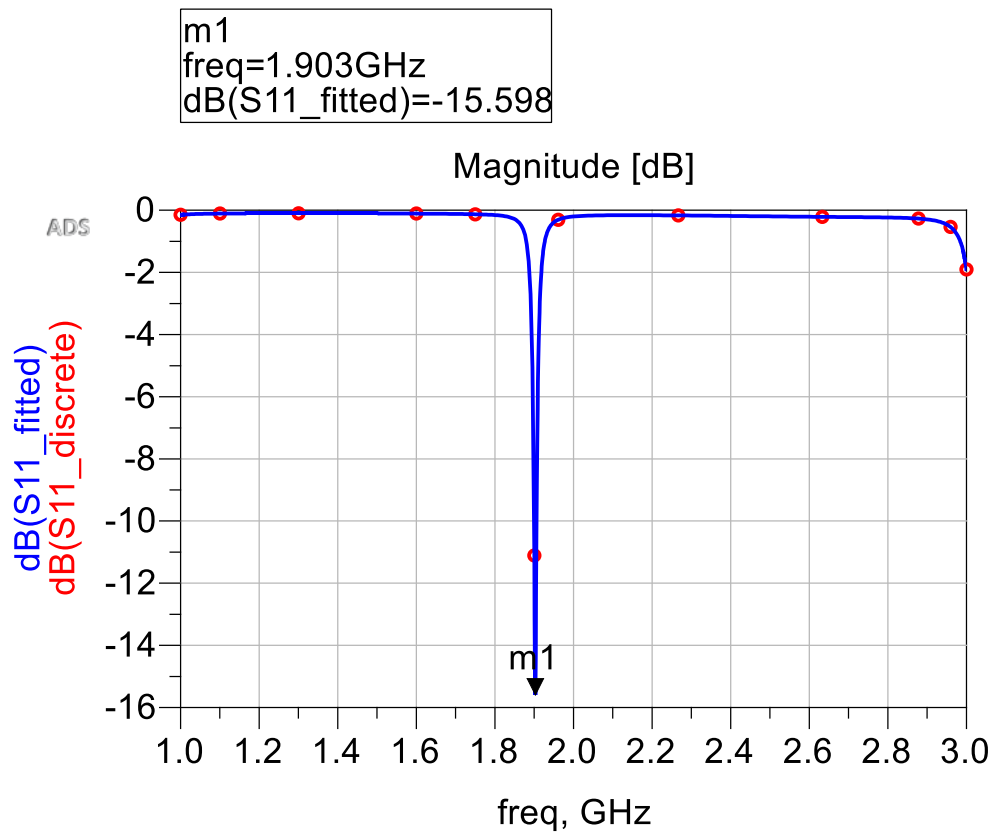


Figure 4.27 Return loss of early 1.90 GHz design

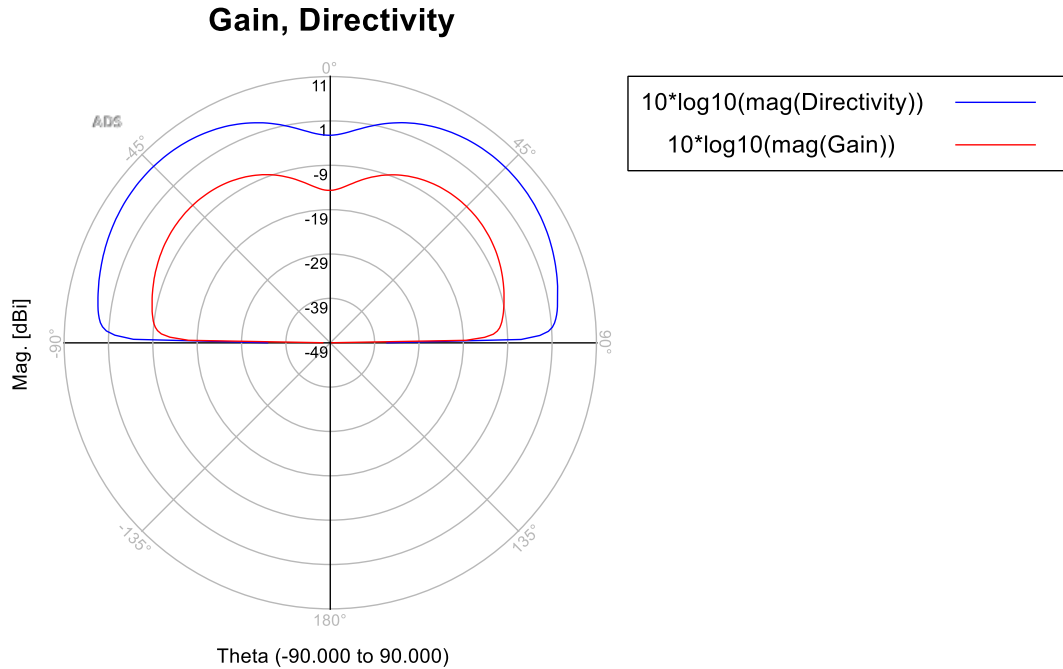


Figure 4.28 Pattern for the early 1.90 GHz design

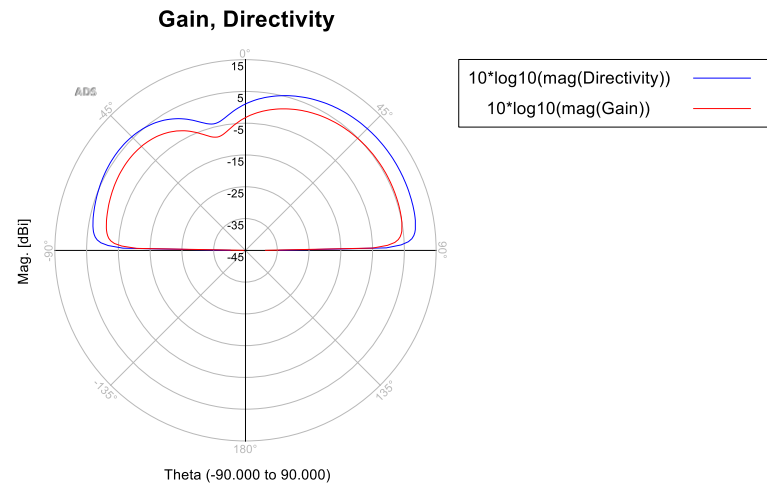
From the theory of Yagi-Uda antennas, the directors are responsible for increasing the directivity of antenna. Patterns in Figures 4.25 and 4.28 show that the directors did not work well. The size of six director elements were changed. After many simulations, we increased the size of each of six director elements from 30.5 mm × 14mm to 30.5 mm × 40 mm for the final Design, as shown in Figures 4.15 and 4.18.

Figure 4.29 (1) (2) shows the simulated radiation patterns of the final design at 2.41GHz and 1.90 GHz. Figure 4.30 shows the simulated intensity of the final design at 2.41GHz and 1.90 GHz . Radiation intensity in a given direction is defined as the power radiated from an antenna per unit solid angle. (The radiation intensity is a far-field parameter which can be obtained by simply multiplying the radiation density by the square of the distance: $U = R^2 \times W_{rad}$.) Table 4.2 shows all the related parameters at the two resonant frequencies of 2.41 GHz and 1.90 GHz in simulations . It can be seen from Figure 4.29 (1) (2) that the patterns of different working frequencies are different. From Table 4.2, we can see the

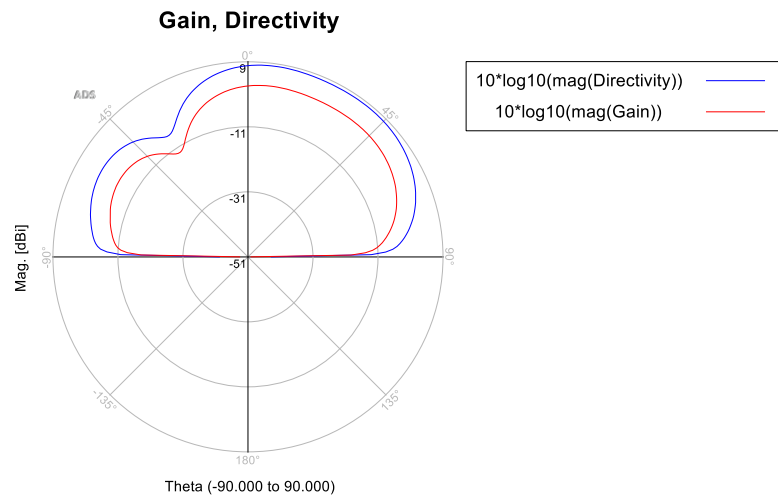
differece of main beam direction steering (azimuth angle- ϕ , elevation angle- θ) for different working frequencies.

TABLE 4.2 RADIATION PARAMETERS OF THE PROPOSED ANTENNA

Frequency	E_MAX(c/n)	Theta_Max(Degree)	Phi_Max(Degree)	Directivity_Max(dBi)
1.90GHz	0.482	10.000	354.000	8.159
2.41GHz	0.711	65.000	1.000	9.596



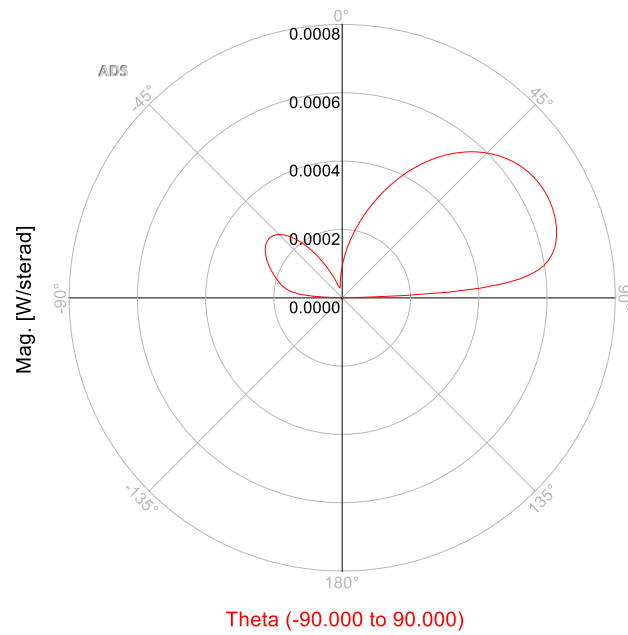
(1) Radiation pattern of 2.41GHz for proposed antenna



(2) Radiation pattern of 1.90 GHz for proposed antenna

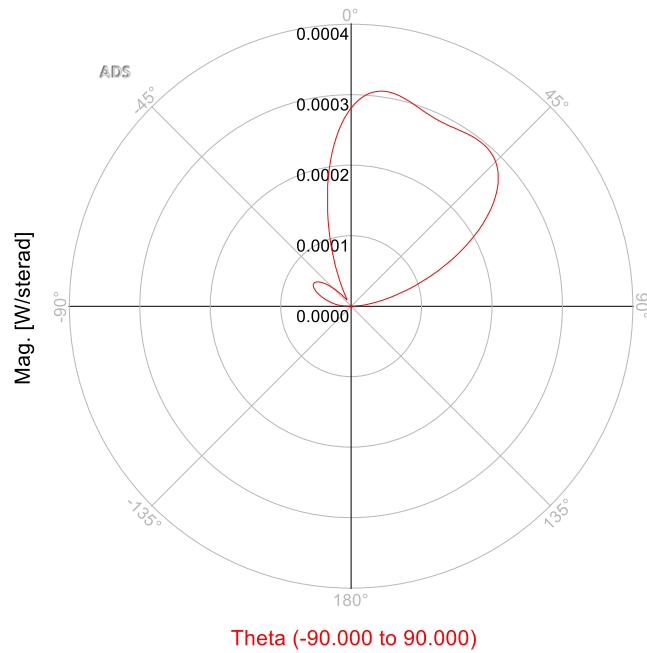
Figure 4.29 Radiation patterns of 2.41GHz and 1.90GHz for proposed antenna

Radiation Intensity



(1) Radiation Intensity for 2.41 GHz

Radiation Intensity



(2) Radiation intensity for 1.90 GHz

Figure 4.30 Radiation intensity for two working frequencies

4.2.4 Using of stubs for 2.41GHz

Narrow bandwidth is the serious limitation of microstrip antenna. An effective way of bandwidth enhancement is to load the surface patch by stubs. In [45], by attaching a pair of tuning stubs to the feedline to introduce an additional resonance in the high frequency range, bandwidth enhancement for broadband operation can be obtained. In [46], in order to further increase the BW, stub-loaded variations of a hexagonal patch was presented. In [47], a novel wideband aperture coupled microstrip antenna consists of radiating patch with stubs and a cross microstrip feed line is presented. The operating relative bandwidth of antenna of 41% is achieved with higher antenna efficiency and stable radiation patterns are realized also. By changing the dimension of the stub attached to the patch, the variable reactance may be realized. Usually, the capacitance of the open ended stub increases due to increase in the length. Short open-circuited stubs can also be used as load to adjust the operating frequency of patch antennas.

Two open-end stubs with optimized lengths and widths are involved to be loaded at the driven patch of the proposed Yagi-Uda patch antenna exclusively to adjust the impedance and bandwidths together, as shown in Figure 4.31. They were connected to the driven element by using metal pieces at 2.41GHz working frequency. Those metal pieces, used to replace PIN diodes in simulation, were removed when the proposed antenna was working at 1.90GHz (Shown in Figure 4.18). The dimensions of these two stubs are set to 2.72mm \times 6.5mm ($W_3 \times L_2$), based on our simulations.

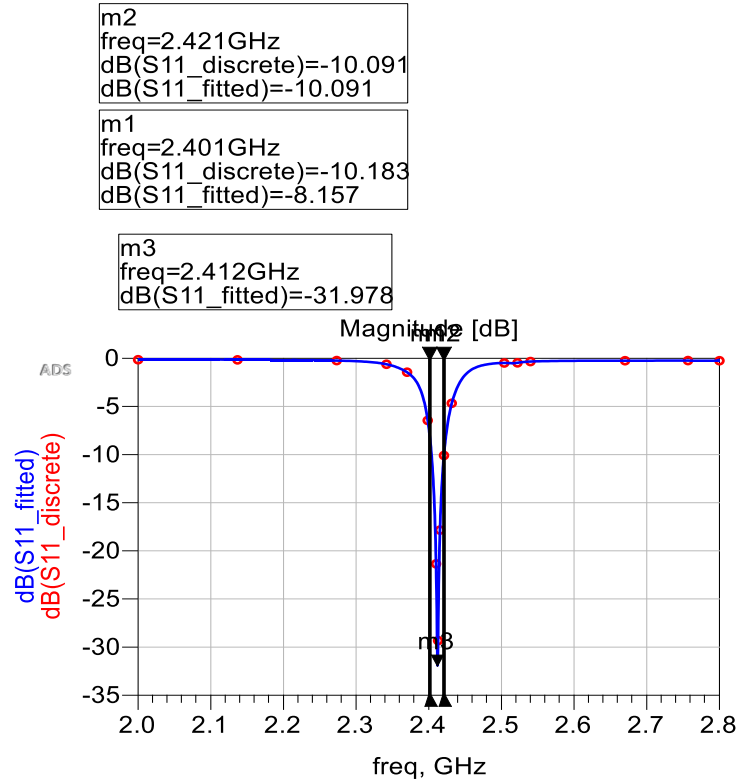


Figure 4.33 Return loss for proposed antenna working at 2.41GHz

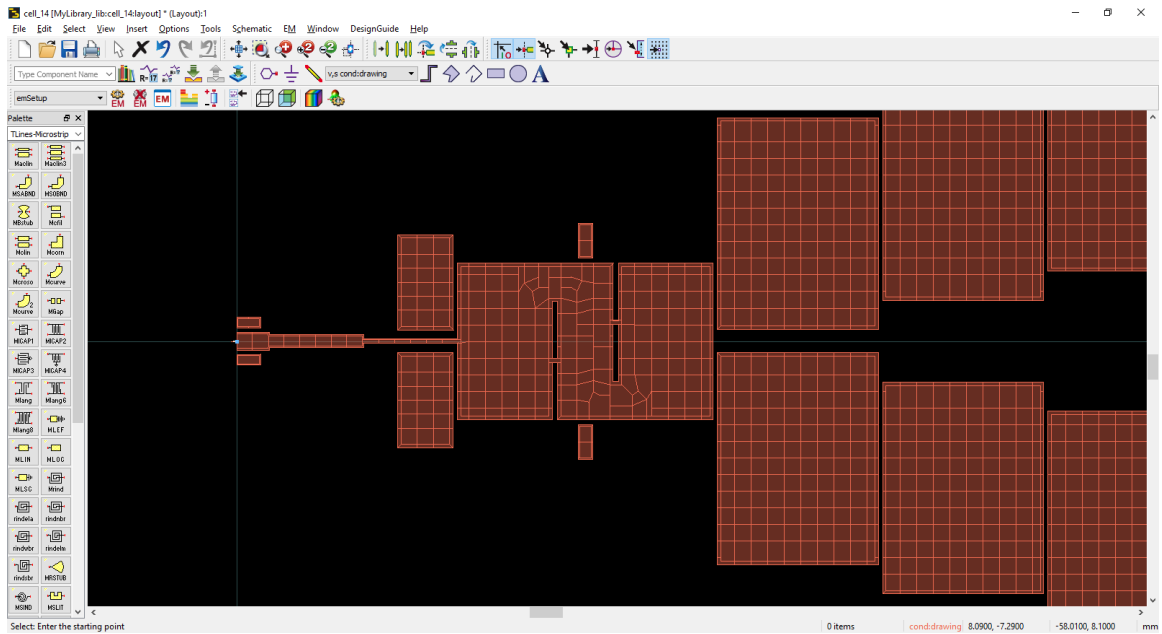


Figure 4.34 Without two pieces of metal used to connect stubs and driven element

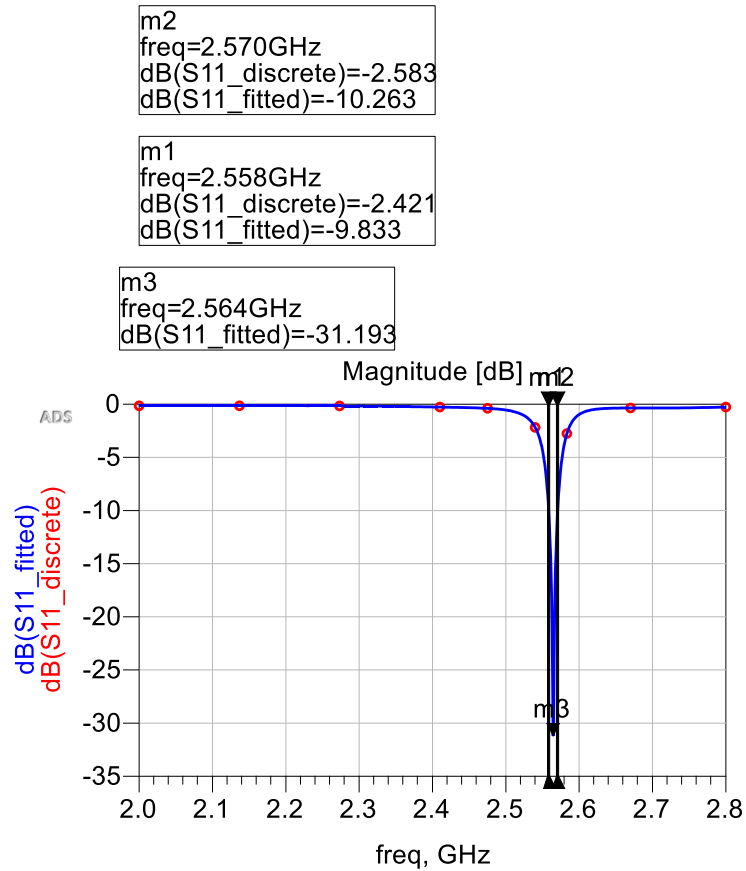


Figure 4.35 Return loss for proposed antenna with 2 metal pieces that used to connect stubs and driven pieces have been removed

For the antenna configuration which works in 2.41 GHz, if we remove those two stubs, the difference of return loss performance can be observed from Figure 4.33 and Figure 4.35. In figure 4.33, the bandwidth below -10 dB is about 20 MHz while the bandwidth below -10 dB is about 12 MHz in Figure 4.35. The stubs we used increased the bandwidth of the proposed antenna by about 67%. For the antenna working at 1.90 GHz, we did not use broadband technology. Future studies will investigate broadband technology, which can be used at both 2.14 GHz and 1.90 GHz.

4.3 Fabrications and Measurements of the Proposed Reconfigurable Yagi-Uda patch Antenna

We used a T Tech mill machine (Figures 4.36-4.38) to build our proposed reconfigurable Yagi-Uda patch antenna. The measurement works have been done by using Agilent E5062A Network Analyzer.



Figure 4.36 The T Tech mill machine used to build the proposed antenna



Figure 4.37 The T Tech mill machine controlled by a computer

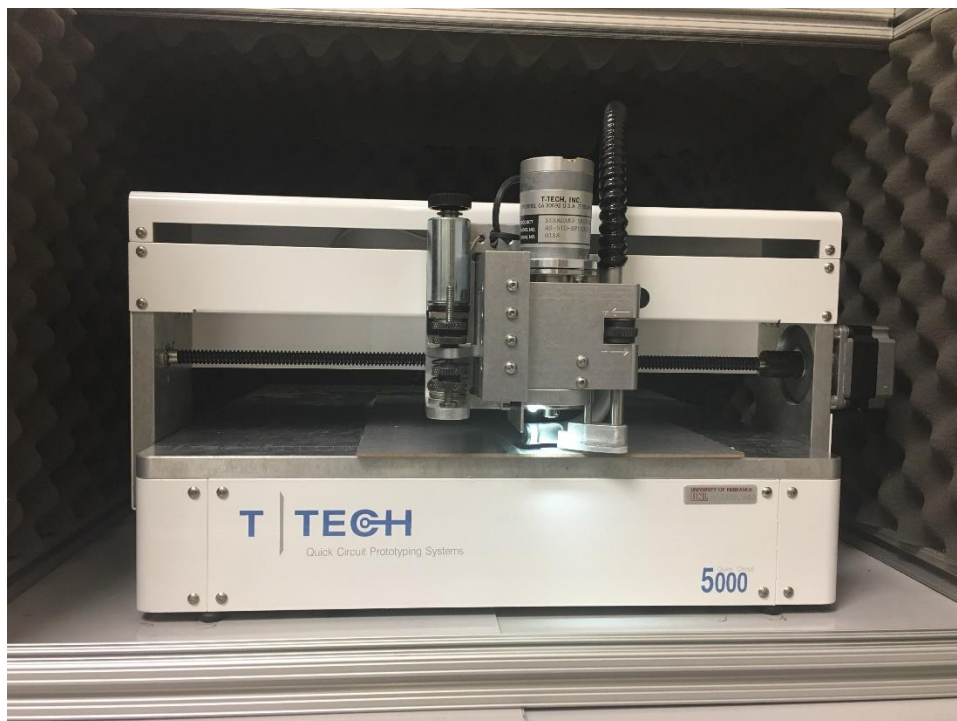


Figure 4.38 Milling device of T Tech Mill Machine

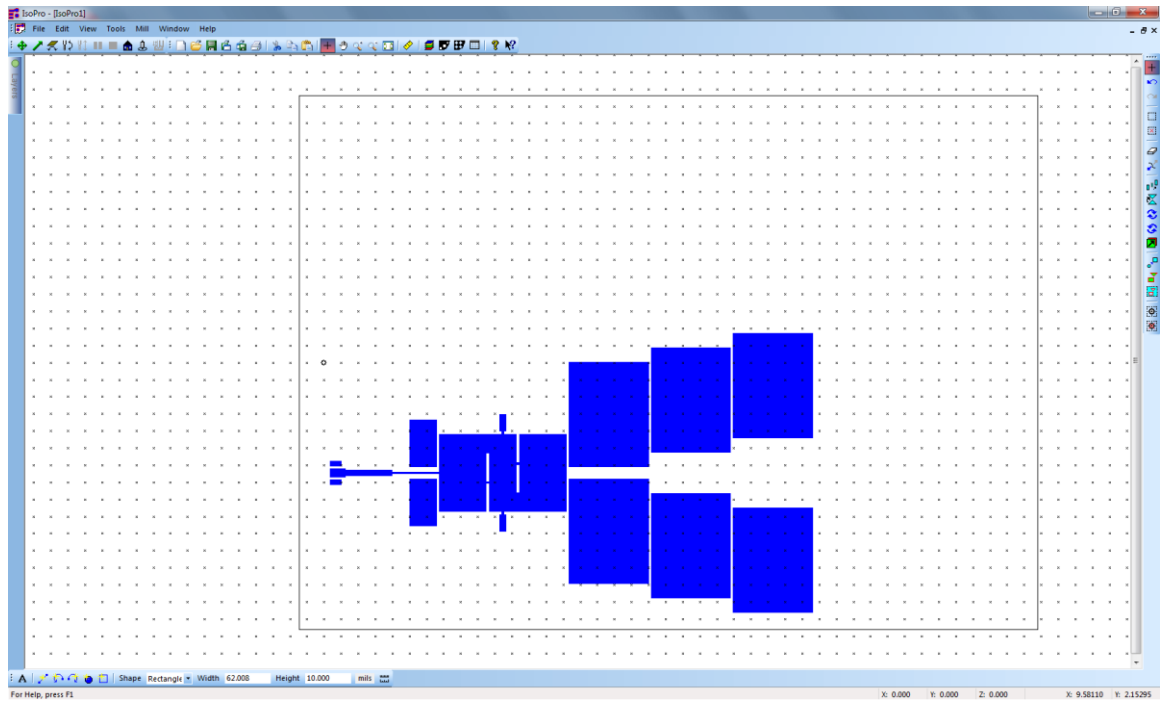


Figure 4.39 Antenna layout structure in control software of mill machine

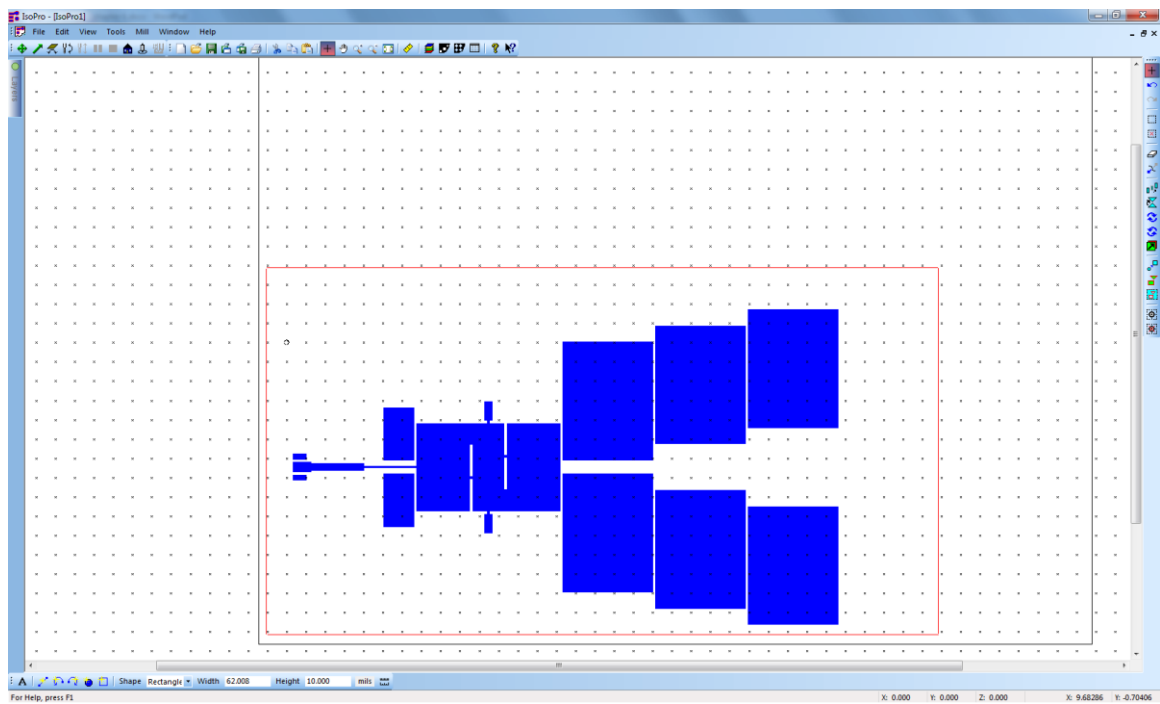


Figure 4.40 Antenna layout structure with a new added outline

Figure 4.39 shows the imported **cond.gbr** file in the control software of the mill machine. A gbr file can be generated in ADS based on our design work and can be easily recognized by mill machine. Before you build your structure you need to add the outline for your design as shown in Figure 4.40.

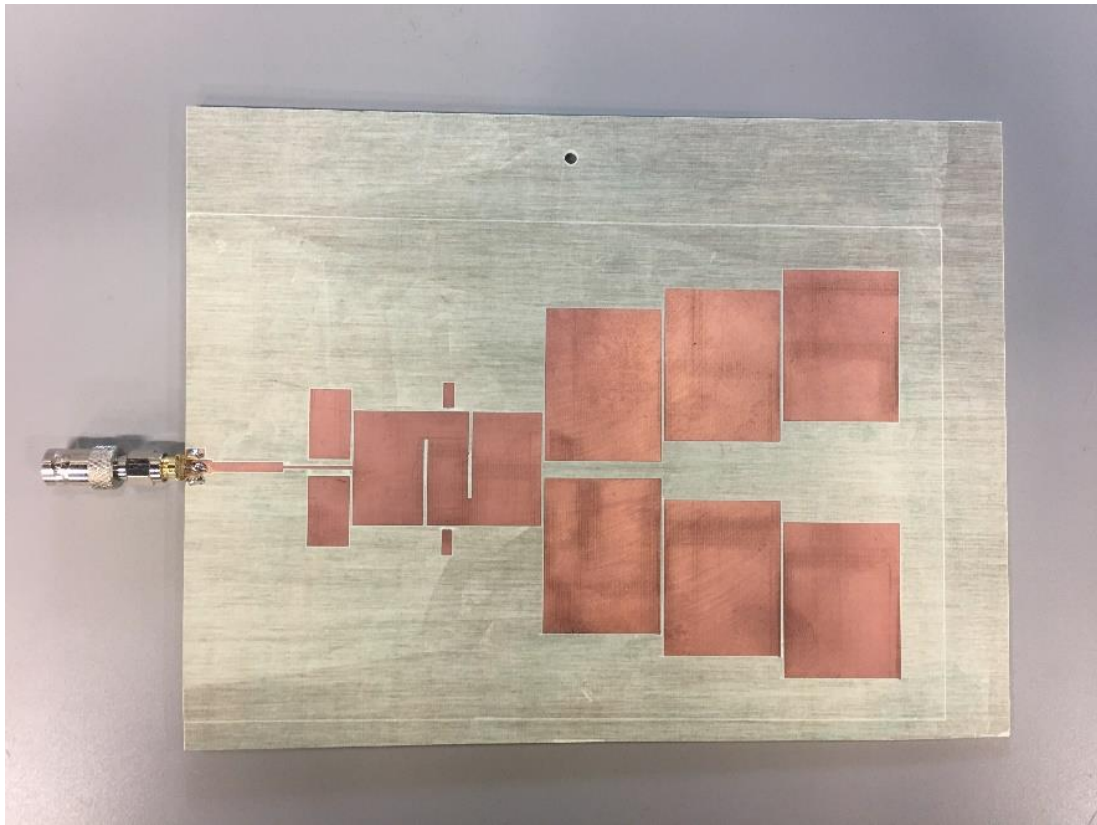


Figure 4.41 Prototype of the proposed 1.90GHz Yagi-Uda patch antenna

The fabricated antenna without all four metal pieces, which are used to imitate the antenna system with all four PIN diodes are in off-state, are shown in Figure 4.41. As before, the antenna was made on the RO4350b PCB board, with a thickness of 1.524mm.



Figure 4.42 Measurement of prototype 1.90GHz Yagi-Uda patch antenna (1)

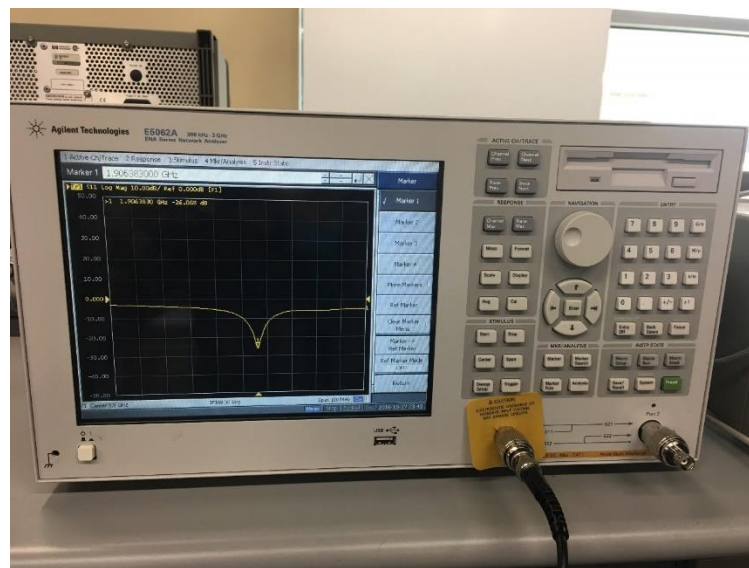


Figure 4.43 Measurement of prototype 1.90GHz Yagi-Uda patch antenna (2)

Figures 4.42 and 4.43 show the measuring process for the built 1.90 GHz mode antenna. The electronic device used in figure 4.42 and 4.43 is Agilent E5062A Network Analyzer.

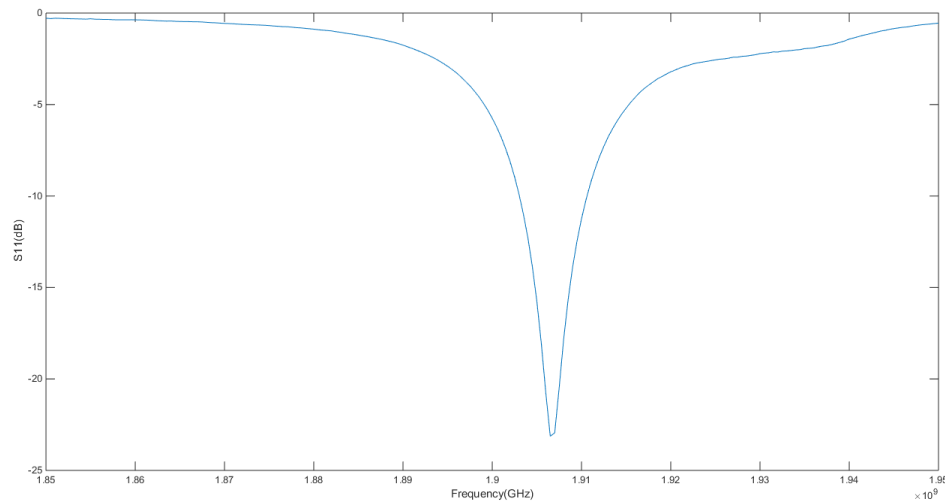


Figure 4.44 Measurement result for 1.90GHz Yagi-Uda patch antenna

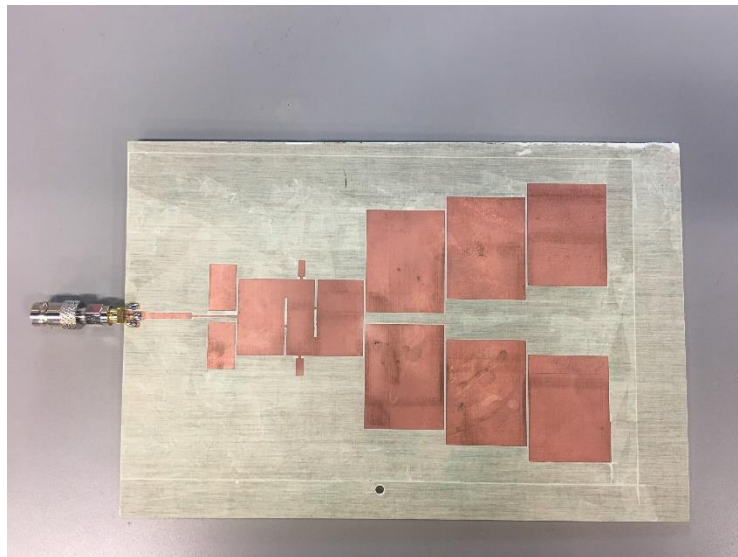


Figure 4.45 Prototype of the proposed 2.41GHz Yagi-Uda Patch Antenna

The fabricated antenna with all four metal pieces that were used to imitate the antenna system with all four PIN diodes in the ON state, is shown in Figure 4.45. It was also made on the RO4350b PCB board with the thickness of 1.524 mm.

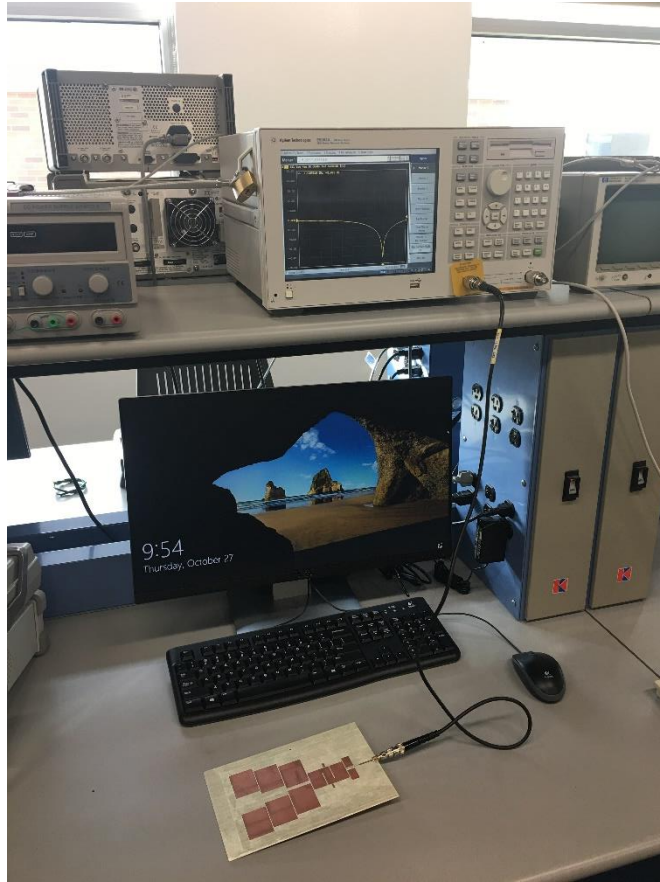


Figure 4.46 Measurement of the prototype 2.41GHz Yagi-Uda patch antenna (1)

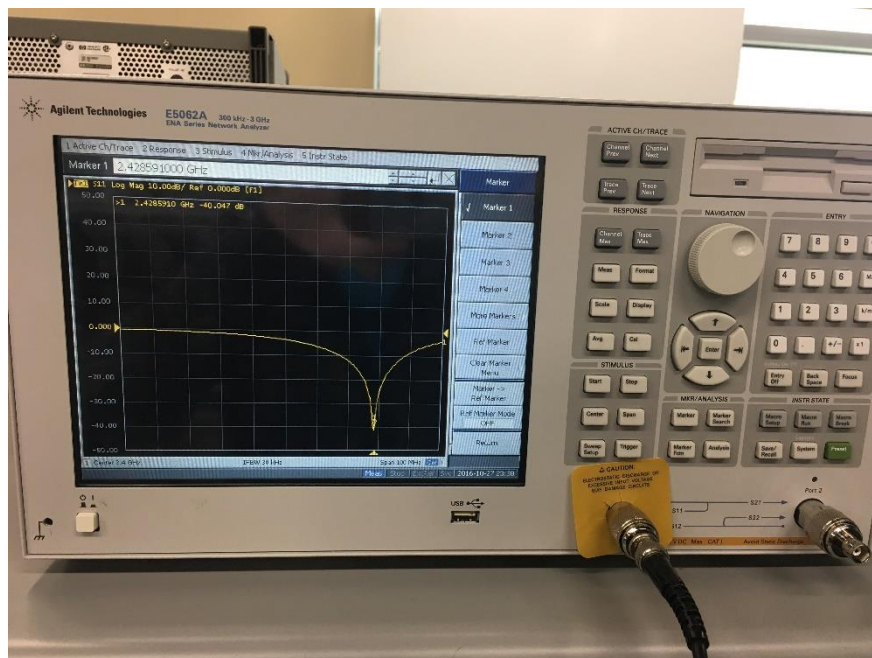


Figure 4.47 Measurement of the prototype 2.41GHz Yagi-Uda patch antenna (2)

Figure 4.46 and 4.47 show the measuring process for the built 2.41 GHz mode antenna. The electronic device used, shown in Figures 4.46 and 4.47, is also the Agilent E5062A Network Analyzer.

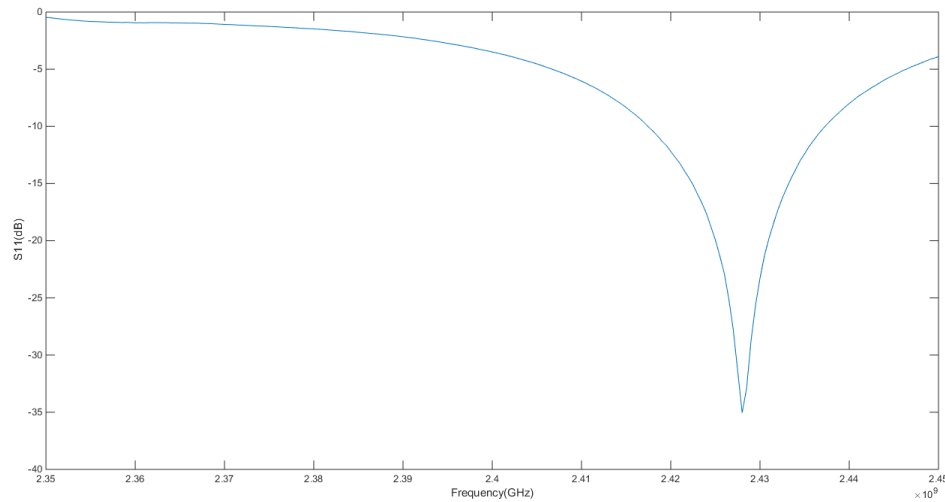


Figure 4.48 Measurement result for 2.41 GHz Yagi-Uda patch antenna

Based on Figures 4.44 and 4.48, the measured performance of return loss for two configurations of the proposed antenna can be observed. For antenna configuration which has been designed working at 2.41GHz, the resonant frequency of built antenna is 2.428 GHz, and the measured bandwidth below -10 dB is about 20 MHz. For the antenna configuration that was designed working at 1.90GHz, the measured return loss is about -23 dB at 1.908 GHz and the measured bandwidth below -10 dB is about 10 MHz. Because we did not apply broadband technology to this antenna configuration, the measured bandwidth below -10 dB is about 10 MHz.

4.4 Discussions

The comparisons of return loss performance between simulation and measurement are shown in Figures 4.49 and 4.50.

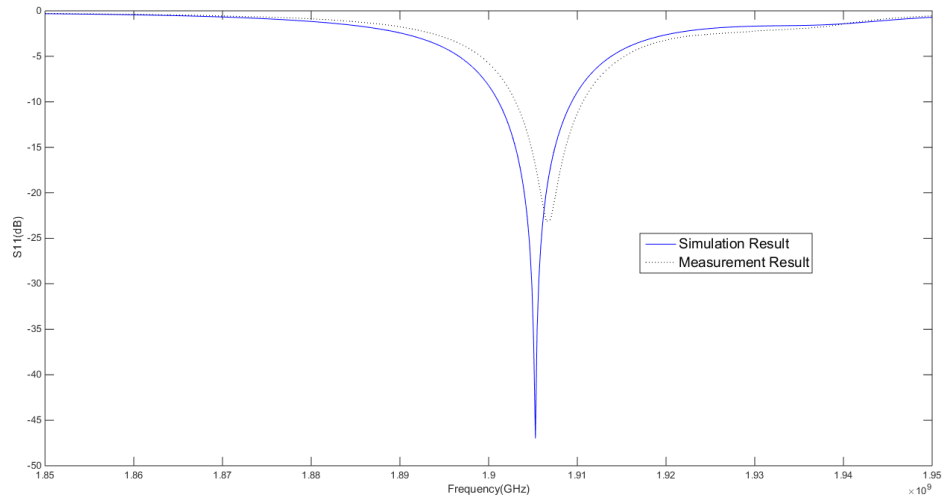


Figure 4.49 Simulation and Measurement results for proposed antenna without all four metal pieces (Design working frequency is 1.90 GHz)

It can be observed from Figure 4.49 that the frequency shift between simulation and measurement for the proposed antenna without four metal pieces is very small (within 3 MHz). The measured return loss is about -23 dB at 1.908 GHz and the measured bandwidth below -10 dB is about 10 MHz.

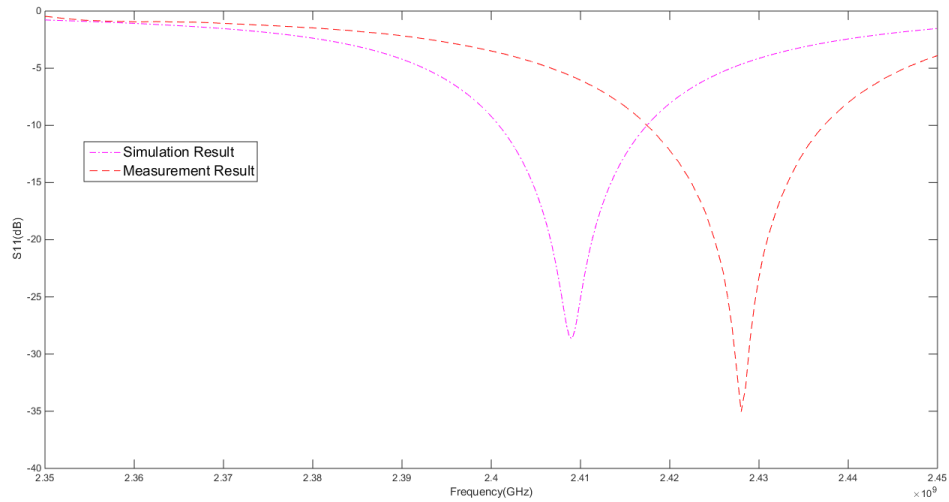


Figure 4.50 Simulation and Measurement results for proposed antenna with all four metal pieces (Design working frequency is 2.41 GHz)

It can be observed from Figure 4.50 that the frequency shift between simulation and measurement for the proposed antenna with four metal pieces is about 18 MHz. The measured return loss is about -35 dB at 2.428 GHz and the measured bandwidth below -10 dB is about 20 MHz.

The reason for 18 MHz frequency shift in 2.41 GHz design has been analyzed by follows:

- (1) For the 2.41 GHz design simulation, the positions of two metal pieces which have been loaded in two slots must be very accurate. As can be observed from Figure 4.51, the distance (As H in Figure 4.51) from each of those two metal pieces to top border and bottom border of the slot was set to be 10.7 mm. And the positions of those two metal pieces have been got based on a lot of simulations.
- (2) If we move the metal piece which loaded in the right slot of the driven element up for 1mm (As shown in Figure 4.52), the resonant point will shift to 2.434 GHz (As shown in Figure 4.53).

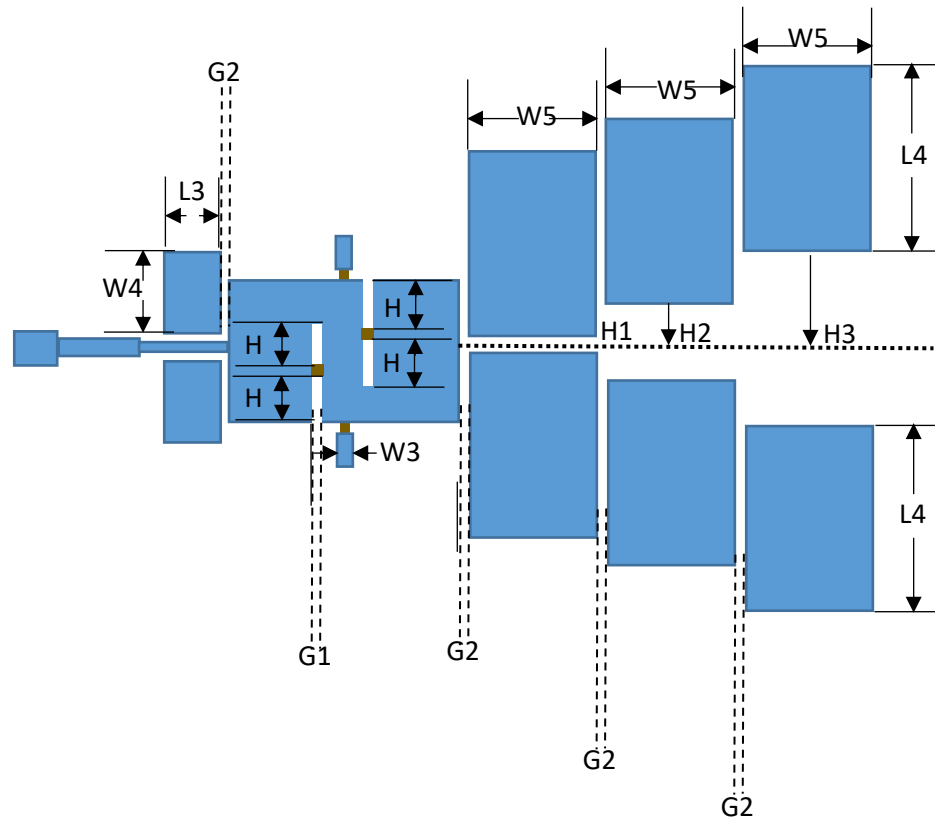


Figure 4.51 The layout structure for proposed antenna

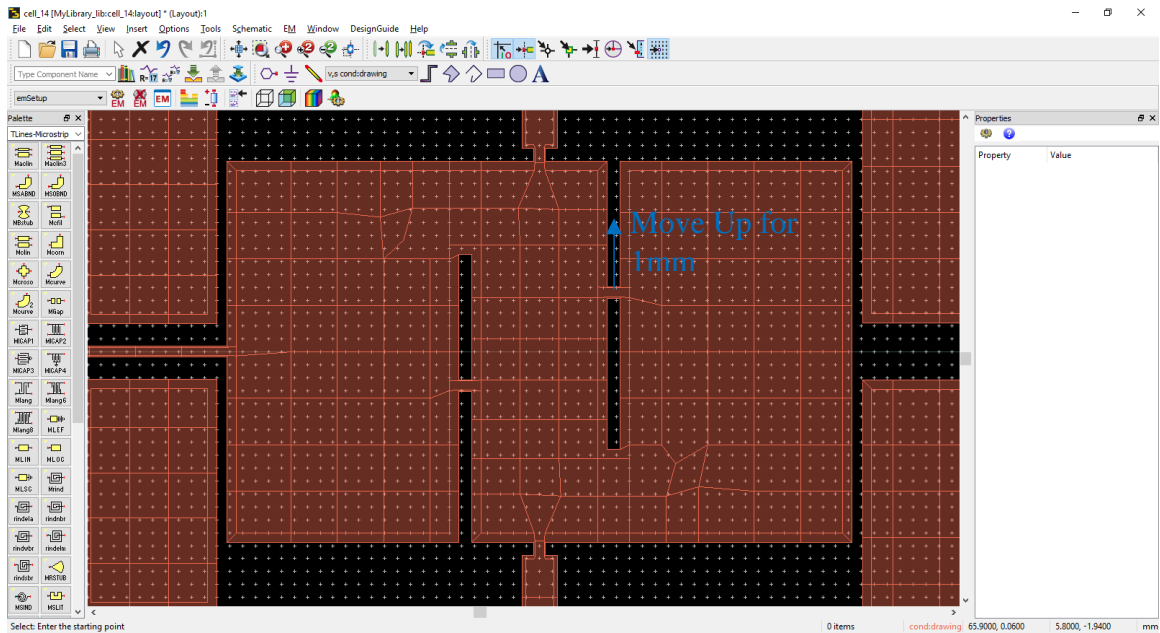


Figure 4.52 The proposed antenna with the metal piece loaded in the right slot has been moved up 1mm

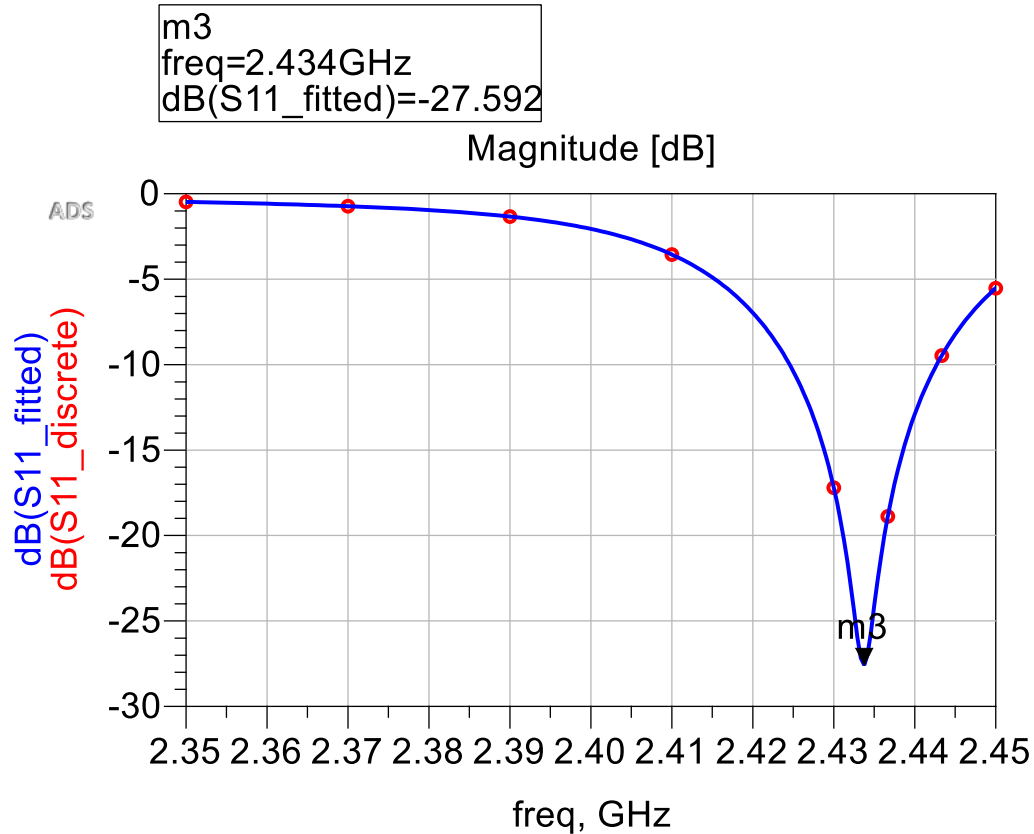


Figure 4.53 The resonant point shift to 2.434 GHz based on the change has been made in figure 4.52

- (3) If we move the metal piece which loaded in the right slot of the driven element down for 1mm (As shown in Figure 4.54), the resonant point will shift to 2.385 GHz (As shown in Figure 4.55).
- (4) The resonant point of this antenna is very sensitive to the dimension of those two metal pieces loaded in two slots. Based on simulation works, we made the dimension of all four metal pieces as 0.9mm (height) \times 1mm (width). If we increase the height of those two pieces which loaded in two slots by 0.2 mm (As shown in Figure 4.56), the resonant point will shift to 2.424GHz. If we decrease the height of those two pieces which loaded in two slots by 0.2 mm (As shown in Figure 4.58), the resonant point will shift to 2.393 GHz.

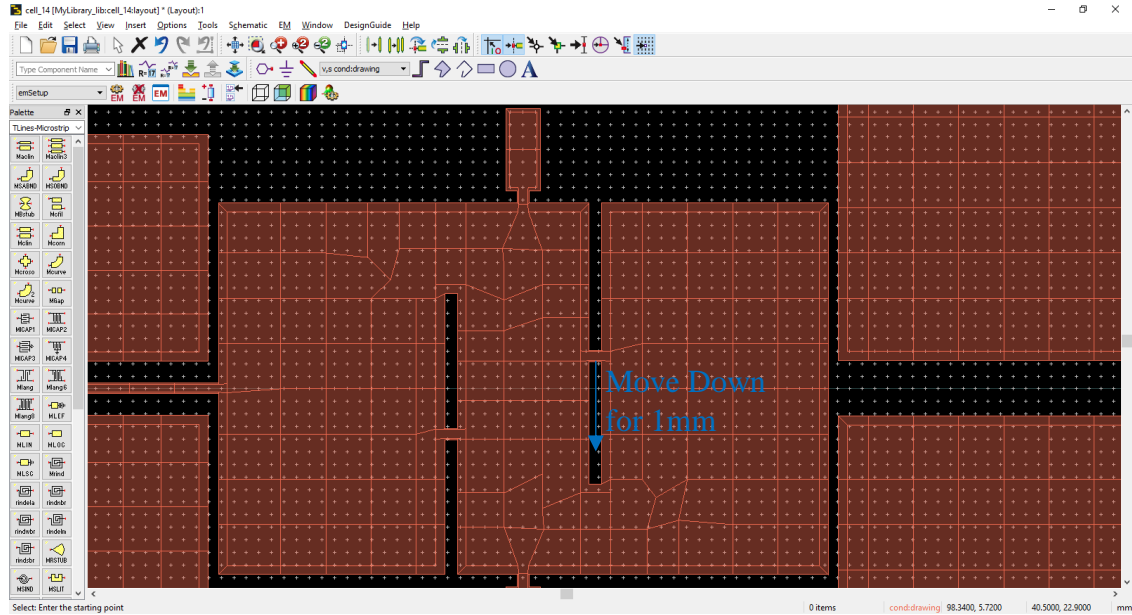


Figure 4.54 The proposed antenna with the metal piece loaded in the right slot has been moved down for 1mm

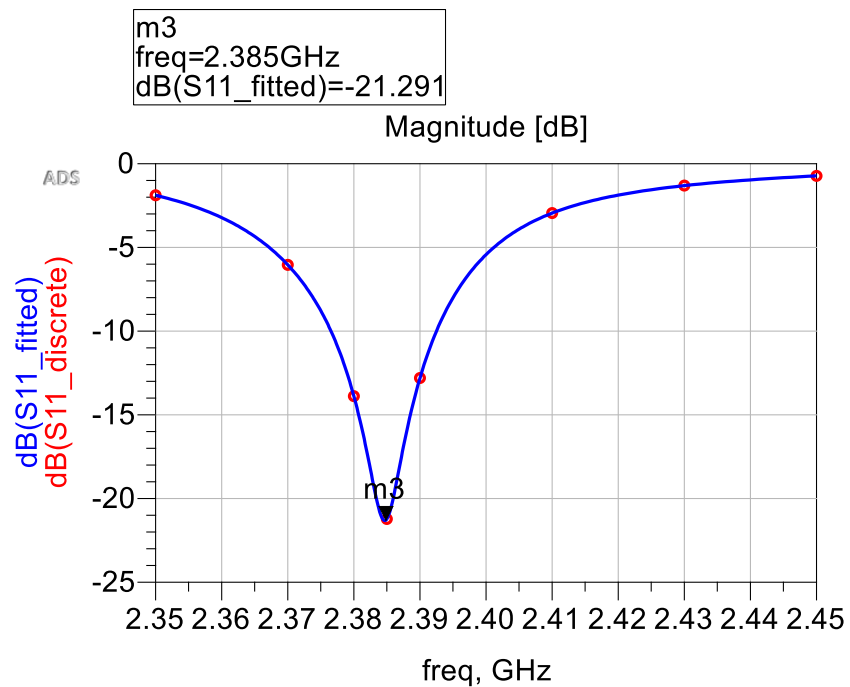


Figure 4.55 The resonant point shift to 2.385 GHz based on the change has been made in figure 4.54

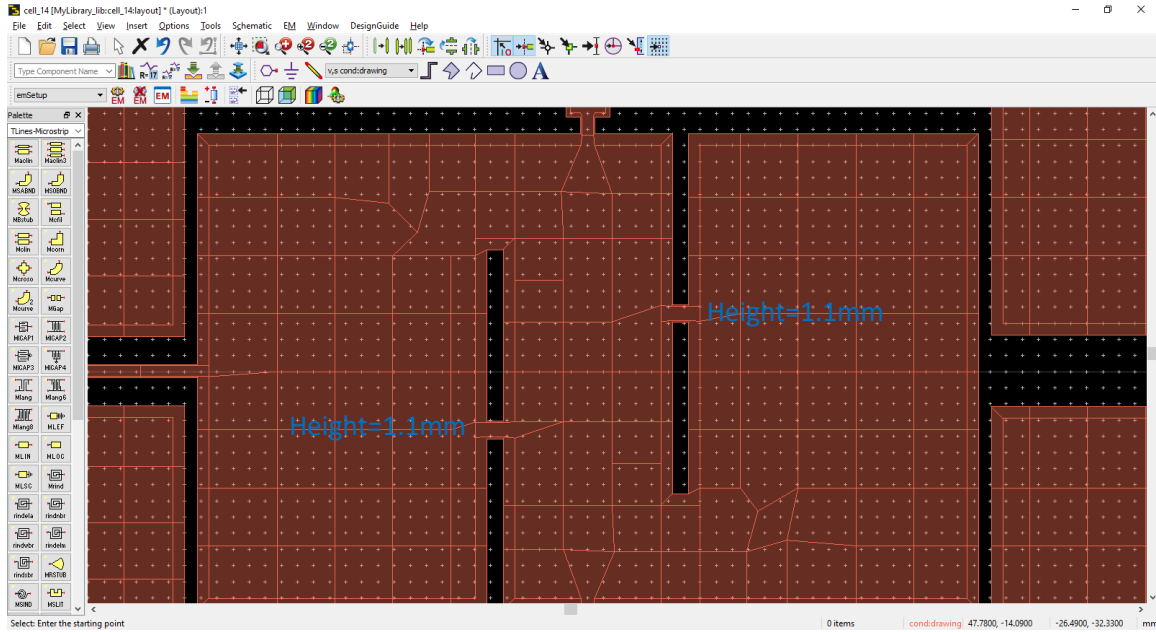


Figure 4.56 The proposed antenna with the height of metal pieces loaded in slots has been increased by 0.2 mm

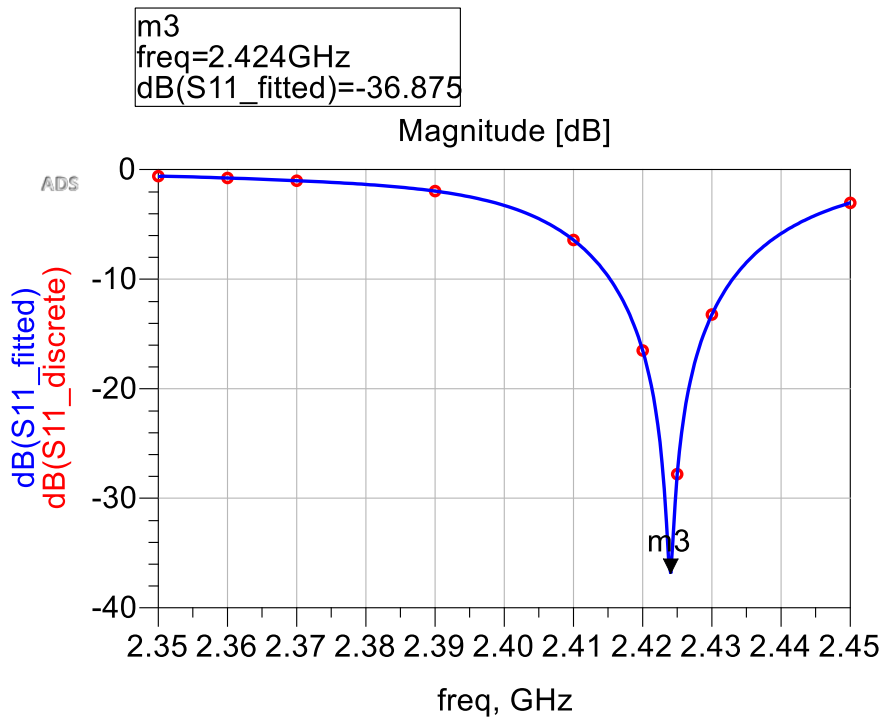


Figure 4.57 The resonant point shift to 2.424 GHz based on the change has been made in figure 4.56

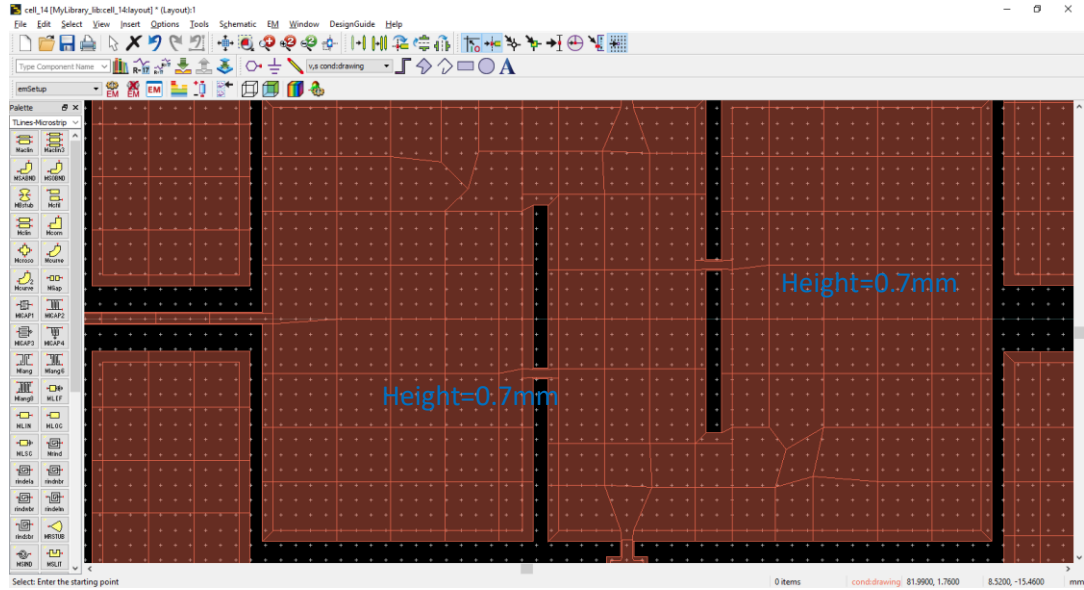


Figure 4.58 The proposed antenna with the height of metal pieces loaded in slots has been decreased by 0.2 mm

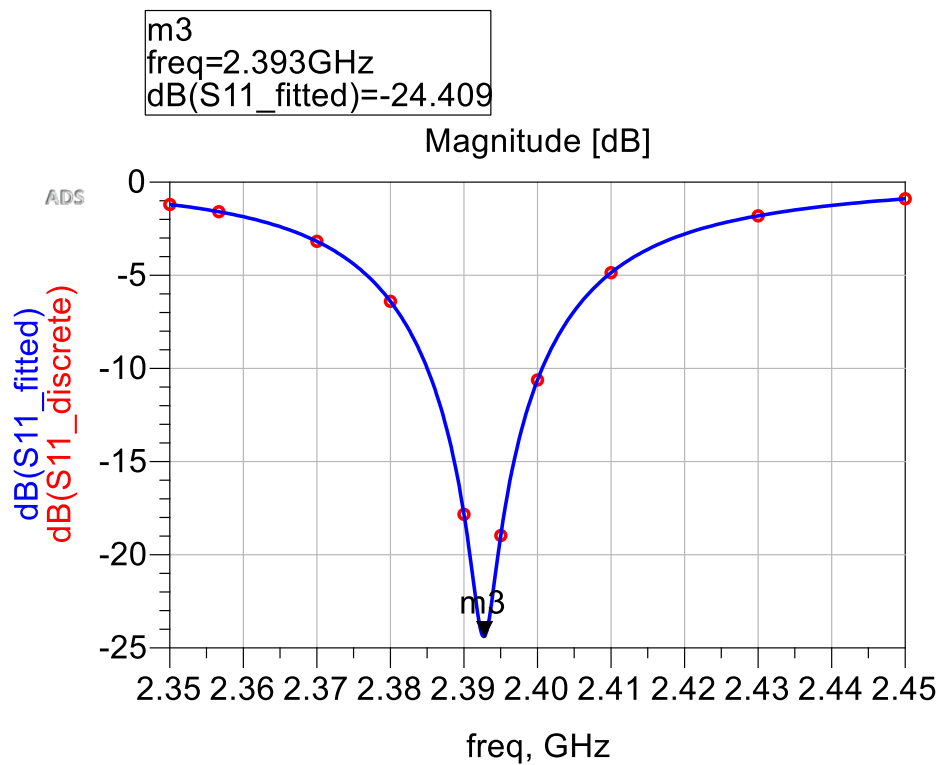


Figure 4.59 The resonant point shift to 2.393 GHz based on the change has been made in figure 4.58

We used a T Tech Mill machine to build the proposed antenna. During the fabrication process, there has to be error of metal pieces, and the resonant point is very sensitive to the position and dimension of those two metal pieces which are loaded in the slots. This can explain the 18 MHz frequency shift for 2.41 GHz design. For 1.90 GHz design, because there are no metal pieces loaded in the slots, the frequency shift is very small (around 3 MHz). Despite the frequency, this antenna can still be used for Wi-Fi systems (Band 4 or Band 5 of the 2.4 GHz band channel). Considering our fabrication conditions, our results were quite successful.

4.5 Summary of the Proposed Yagi-Uda Antenna

In this chapter, a novel Yagi-Uda reconfigurable patch antenna was proposed. Two slots have been used on the driven element of this antenna system to create frequency and pattern reconfigurability and we use metal pieces to replace PIN diodes in the simulation and measurement. Pattern reconfigurability and directivities with all over 8.1 dBi in both main radiation directions have been found on two different working frequencies in simulation. The measured bandwidth of the return loss below -10dB for 2.41GHz working mode is about 20 MHz and for the 1.90 GHz working mode is 10 MHz. The simulation and measurement for return loss results closely agree. The slight frequency shifts are due to fabrication error. This pattern and frequency reconfigurable Yagi-Uda patch antenna array can be applied for both LTE and Wi-Fi systems.

Chapter 5. Conclusions

In chapter 3, a novel dual-frequency antenna array with multiple pattern selectivities is proposed. We used a single-feed switchable network as a basic beam pattern reconfigurability structure for this dual-frequency antenna array. The slotted corners on the patch together with the states of PIN diodes gave this antenna array more freedom of pattern changeability. The measured bandwidth of the return loss below -10dB for the on-state is about 25 MHz and for the off-state is also nearly 25 MHz at two different working frequencies, respectively. We have validated this structure is effective to introduce more pattern selectivity. This pattern reconfigurable patch antenna array can be applied in the wideband code division multiple access system.

In chapter 4, a novel Yagi-Uda patch antenna with frequency and pattern selectivity was proposed. Our proposed antenna consists of two reflector elements, a driven element and six director elements. Two open-end stubs, which were used to improve the return loss performance and adjust working frequency, were connected to the driven element when it was working at 2.41 GHz. In order to easily validate our design, we used four metal pieces to imitate different states of PIN diodes in simulation and measurement. We built two proposed Yagi-Uda patch antennas, one with and one without, metal pieces. For the built antenna without metal pieces, the measured return loss is about -23 dB at 1.908 GHz and the measured bandwidth below -10 dB is about 10 MHz. For the built antenna with four metal pieces, the measured return loss is about -35 dB at 2.428 GHz and the measured bandwidth below -10 dB is about 20 MHz. The frequency shifts are mainly attributed to the fabrication error. Basically, the simulation and measurement results agreed well. The pattern of the proposed antenna is different between two working frequencies but with the

directivity all above 8 dBi. The effectiveness of this kind of antenna structure has been validated by this study. It can be both frequency and pattern reconfigurable. This proposed Yagi-Uda reconfigurable patch antenna can be used in both LTE and Wi-Fi systems.

References

- [1] Wenquan Cao, Bangning Zhang, Aijun Liu, Tongbin Yu, Daosheng Guo, and Kegang Pan, "A reconfigurable microstrip antenna with radiation pattern selectivity and polarization diversity," *IEEE Antenna and Wireless Propagation Letters*, Vol.11, pp. 453-456, 2012.
- [2] H. M. Lee, "Pattern reconfigurable micro-strip patch array antenna using switchable feed-network," *Proceedings of Asia-Pacific Microwave Conference 2010*, FREG-12.
- [3] S. L. S. Yang and K. M. Luk, "Design a wide-band L-probe patch antenna for pattern reconfigurable or diversity applications," *IEEE Trans. Antennas Propag.*, vol. 54, no. 2, pp. 433–438, Feb. 2006.
- [4] L. Low and R. J. Langley, "Single-feed antenna with radiation pattern diversity," *Electron. Lett*, vol. 40, No.16, Aug. 5, 2004.
- [5] L. Petit, L. Dussopt, and J.-M. Laheurte, "MEMS-switched parasitic antenna array for radiation-pattern diversity," *IEEE Trans. Antennas Propag.*, vol. 54, no. 9, pp. 2624–2631, Sep. 2006.
- [6] D.kornek, J.Meyer, C.Orlob, I. Rolfes, "Reconfigurable triangular patch antenna for pattern diversity," *EuCAP 2009. 3rd European Conference on Antennas and Propagation*, pp 3744-3747.
- [7] Yan-Ying Bai, Shaoqiu Xiao, Changrong Liu, Xiang Shuai, and Bing-Zhong Wang, "Design of pattern reconfigurable antennas based on a two-element dipole array model," *IEEE Transactions on Antennas and Propagation*, vol.61, Issue.9, Pages: 4867 – 4871, 2013.

- [8] Hai Liang Zhu, Sing Wai Cheung, Tong Ip Yuk, “Mechanically pattern reconfigurable antenna using metasurface,” *IET Microwaves, Antenna and Propagation*, Volume.9, Issue.12,Pages: 1331 – 1336,2015.
- [9] Mei Li, Shaoqiu Xiao, Bingzhong Wang, “Compact, low-profile, HIS-based pattern reconfigurable antenna for wide-angle scanning,” *The 8th European Conference on Antennas and Propagation (EuCAP 2014)*, Pages: 1541 – 1544.
- [10] Dwi Andi Nurmantris, Heroe Wijanto, Bambang Setia Nugroho, “A pattern reconfigurable of circular short-circuited patch antenna based on Genetic Algorithm,” *2014 2nd International Conference on Information and Communication Technology (ICoICT)*, pp 351-355.
- [11] Jeen-Sheen Row and Jia-Fu Tsai, “Frequency-reconfigurable microstrip patch antennas with circular polarization,” *IEEE Antennas And Wireless Propagation Letters*,VOL.13, pp 1112-1115, 2014.
- [12] Qiang Liu, Naizhi Wang, Qingsheng Zeng, Changying Wu, Gao Wei, “A frequency reconfigurable patch antenna with reed switches,” *2014 IEEE International Wireless Symposium (IWS)*.
- [13] Chao Sun, Huili Zheng, Lingfei Zhang, and Ying Liu, “A compact frequency-reconfigurable patch antenna for beidou (COMPASS) navigation system,” *IEEE Antennas And Wireless Propagation Letters*,VOL.13, pp 967-970, 2014.
- [14] I.Rouissi, J.M.Floc’h, H.Rmili, H.Trabelsi, “Design of a frequency reconfigurable patch antenna using capacitive loading and varactor diode,” *2015 9th European Conference on Antennas and Propagation (EuCAP)*.

- [15] M. A. Aris, M. T. Ali, N. H. Abd. Rahman, N. Ramli, "Frequency reconfigurable aperture-coupled microstrip patch antenna using defected ground structure," 2015 IEEE International RF and Microwave Conference (RFM 2015), pp 200-204.
- [16] R. Kanimozhi, P. Jothilakshmi, "A high frequency-reconfigurable multilayer microstrip patch antenna (HFRMPA)," International Conference on Communication and Signal Processing, pp 480-484, April 3-5, 2014, India.
- [17] Lei Ge, and Kwai-Man Luk, "Frequency-reconfigurable low-profile circular monopolar patch antenna," IEEE Transaction Antennas and Propagation, Vol.62, No.7, pp 3443-3449, July 2014.
- [18] N. Ramli, M. T. Ali, A. L. Yusof, S. Muhamud - Kayat, and A. A. A. Aziz, "PIN diode switches for frequency-reconfigurable stacked patch microstrip array antenna using aperture-coupled technique," 2013 Asia-Pacific Microwave Conference Proceedings, pp 1052-1054.
- [19] Ratnesh Kumari, Mithilesh Kumar, "Compact tri band frequency reconfigurable L-slot octagonal shape patch antenna," 2013 5th International Conference on Computational Intelligence and Communication Networks, pp 64-69.
- [20] Jeen-Sheen Row and Ting-Yi Lin, "Frequency-reconfigurable coplanar patch antenna with conical radiation," IEEE Antennas And Wireless Propagation Letters, VOL. 9, pp 1088-1091, 2010.
- [21] Zi-Xian Yang, Hong-Chun Yang, Jing-Song Hong, and Yang Li, "Bandwidth enhancement of a polarization-reconfigurable patch antenna with stair-slots on the ground," IEEE Antennas And Wireless Propagation Letters, VOL. 13, pp 579-582, 2014.

- [22] Xue-Xia Yang, Bing-Cheng Shao, Fan Yang, Atef Z. Elsherbeni, and Bo Gong, "A polarization reconfigurable patch antenna with loop slots on the ground plane," *IEEE Antennas And Wireless Propagation Letters*, VOL. 11, pp 69-72, 2012.
- [23] Hucheng Sun, Sheng Sun, "A polarization-agile aperture-coupled patch antenna using quad-mode reconfigurable feeding network," 2016 IEEE MTT-S International Microwave Workshop Series on Advanced Materials and Processes for RF and THz Applications (IMWS-AMP).
- [24] Hui Gu, Jianpeng Wang, Lei Ge, and Chow-Yen-Desmond Sim, "A new quadri-polarization reconfigurable circular patch antenna," *IEEE Access*, Digital Object Identifier 10.1109/ACCESS.2016.2600250.
- [25] Nghia Nguyen-Trong, Leonard Hall, and Christophe Fumeaux, "A frequency- and polarization-reconfigurable stub-loaded microstrip patch antenna," *IEEE Transaction On Antennas And Propagation*, Vol. 63, No. 11, pp 5235-5240, November 2015.
- [26] Xue-Xia Yang, Bo Gong, Fang Yang, Atef Z. Elsherbeni, "A reconfigurable patch antenna with quadri-polarization states using dual feed ports," 978-1-4673-0462-7/12, 2012 IEEE.
- [27] Constantine A. Balanis, "Antenna Theory: Analysis And Design," Second Edition, John Wiley&Sons, INC.
- [28] D. Orban and G.J.K Moernaut, "The Basics of Patch Antennas, Updated," Orban Microwave Products, www.orbanmicrowave.com.
- [29] D. M. Pozar, "Microstrip Antennas," *Proc. IEEE*, Vol. 80, NO. 1, pp. 79-81, January 1992.

- [30] N. K. Uzunoglu, N. G. Alexopoulos, and J. G. Fikioris, "Radiation properties of microstrip dipoles," *IEEE Transaction and Propagation*, Vol. AP-27, NO. 6, pp. 853-858, November 1979.
- [31] I. E. Rana and N. G. Alexopoulos, "Current distribution and input impedance of printed dipoles," *IEEE Transaction. Antenna And Propagation*, Vol. AP-29, No. 1, pp. 99-105, January 1981.
- [32] P. B. Katehi and N. G. Alexopoulos, "On the modeling of electromagnetically coupled microstrip antenna-the printed strip dipole," *IEEE Transaction. Antenna And Propagation*, Vol. AP-32, No. 11, pp. 1179-1186, November 1984.
- [33] D. M. Pozar, "Analysis of finite phased arrays of printed dipoles," *IEEE Transaction. Antenna And Propagation*, Vol. AP-33, No. 10, pp. 1045-1053, October 1985.
- [34] C. A. Balanis, "Advanced Engineering Electromagnetics," John Wiley & Sons, New York, 1989.
- [35] E. O. Hammerstad, "Equations for microstrip circuit design," *Proc. Fifth European Microwave Conference*, pp. 268-272, September 1975.
- [36] I. J. Bahl and P. Bhartia, "Microstrip Antennas," Artech House, Dedham, MA, 1980.
- [37] J. Huang; "Planar microstrip Yagi array antenna," *IEEE AP-S symposium Digest* June 1989, pp 894-897.
- [38] Chen, C. A. and D. K Cheng, "Optimum element lengths for Yagi-Uda arrays," *IEEE Trans. Antennas and Propagation*, Vol. 23, Jan. 1975.

- [39] M. Bemani and S. Nikmehr, "A novel wide-band microstrip Yagi-Uda array antenna for WLAN applications," *Progress In Electromagnetics Research B*, Vol. 16, 389–406, 2009.
- [40] Xue-Song Yang, Bing-Zhong Wang, Weixia Wu, and Shaoqiu Xiao, "Yagi patch antenna with dual-band and pattern reconfigurable characteristics," *IEEE Antennas and Wireless Propagation Letters*, Vol. 6, pp 168-171, 2007.
- [41] T. Sabapathy, R.B. Ahmad, M. Jusoh, M. R. Kamarudin, "The effect of shorting pin locations on the performance of a pattern reconfigurable Yagi-Uda patch antenna," 2014 2nd International Conference on Electronic Design (ICED), August 19-21, 2014, Penang, Malaysia.
- [42] Jian Zhang, Xue-Song Yang, Jia-Lin Li, and Bing-Zhong Wang, "A linear phased array with reconfigurable dynamic Yagi-Uda patch antenna elements," 2012 International Workshop on Microwave and Millimeter Wave Circuits and System Technology (MMWCST).
- [43] Thennarasan Sabapathy, Muzammil Jusoh, R. Badlishah Ahmad, Muhammad Ramlee Kamarudin, and Ping Jack Soh, "A ground-plane-truncated, broadly steerable Yagi-Uda patch array antenna," *IEEE Antennas and Wireless Propagation Letters*, Vol.15, pp 1069-1072, 2016.
- [44] Fan Yang and Yahya Rahmat-Samii, "Patch antennas with switch slots (PASS) in wireless communications: concepts, designs, and applications," *IEEE Antennas and Propagation Magazine*, Vol. 47, No. 2, pp13-29, April 2005.

- [45] Oteng Gyasi Kwame, Wen Guangjun, Xue Xiao Lin, Muhammad Abdul Basit, “Bandwidth enhancement of a microstrip-line-fed printed rotated wide slot antenna with tuning stubs,” 2016 IEEE MTT-S International Wireless Symposium (IWS).
- [46] Amit Deshmukh, Sudesh Agrawal, Kshitij Lele, K. P. Ray, “Broadband CPW fed stub loaded hexagonal slot backed hexagonal microstrip antenna,” 2015 International Conference on Microwave and Photonics (ICMAP).
- [47] Youbao Wang , Yaming Bo and De Ben, “Wideband aperture coupled microstrip antenna with stubs,” The 2006 4th Asia-Pacific Conference on Environmental Electromagnetics, pp 682-684.